MACPISA-CANDU: INLET FEEDER STAGNATION BREAK IN CANDU 6

MACPISA-CANDU:

MULITI-STEP APPROACH TO CODE-COUPLING FOR PROGRESSION INDUCED SEVERE ACCIDENTS IN CANDU NUCLEAR POWER PLANTS

By

DANIEL J. POHL, B.A.Sc.

A Thesis

Submitted to the School of Graduate Studies

in Partial Fulfillment of the Requirements

for the Degree

Master of Applied Science

McMaster University

MASTER OF APPLIED SCIENCE (2009) McMaster University

(Engineering Physics) Hamilton, Ontario

TITLE: MACPISA-CANDU: Multi-step Approach to Code-coupling for Progression Induced Severe Accidents in CANDU Nuclear Power Plants

AUTHOR: Daniel J. Pohl, B.A.Sc. (University of Toronto)

SUPERVISOR: Professor J.C. Luxat

NUMBER OF PAGES: xiii, 179

Abstract

A methodology called the Multi-step Approach to Code-coupling for Progression Induced Severe Accidents in CANDU nuclear power plants (MACPISA-CANDU) was developed and applied. MACPISA-CANDU was used to couple a MATLAB single fuel channel model with a primary heat transport system model developed in MELCOR (MELCOR 1.8.5) to model a small break loss of coolant accident (SBLOCA) in conjunction with a loss of emergency coolant injection (LOECI) in a CANDU 6 nuclear power plant. The specific type of SBLOCA modelled was an individual reactor inlet feeder stagnation break ($8.03cm^2$). The early stages of the SBLOCA-LOECI event were the focus of this thesis. 13 seconds after the initiation of the break it was predicted that the pressure tube would heat up to 1473 K and rupture. It is assumed that the calandria tube ruptures along with the pressure tube causing coolant to return to the fuel channel and flow out of the rupture into the calandria vessel. It predicted that the moderator within the calandria vessel would be able to act as an ultimate heat sink and end the transient at 298 seconds. In addition, the MATLAB single fuel channel model was replaced by a single fuel channel model created in SCDAP/RELAP5 (RELAP/SCDAPSIM Mod 3.4 (bi7)). The coupled SCDAP/RELAP5-MELCOR simulation predicted that the pressure tube would rupture at 23 seconds and subsequently the transient would end at 403 seconds.

The results from both code-coupled simulations are shown to be in reasonable agreement with the results of other validated computer models.

Acknowledgements

I am very thankful to those who have supported me over the past two years while this work was completed. First and foremost, I greatly appreciate my supervisor Dr. John Luxat for his guidance and for believing that I would eventually find my way.

Much of this work would not have been possible without the mentoring of Dr. Walter Giannotti. In addition, I would like to thank Dr. David Novog and Dr Alessandro Petruzzi for graciously giving me the opportunity to travel to the University of Pisa in Italy where I conducted part of this research with the San Piero a Grado Nuclear Research Group.

I would also like to acknowledge "the boys in the lab": Andy B., Matt, Fiend, Fang, Ken, Ricardo, Brad, Adam, Kurt, Hummel, Ken, Justin, Ryan, and Jack. Whether it was squash, barbequing, adjusting the electric water heater to III, afternoon sunshine, 10 p.m. coffee, carrying a couch down Broadway or just plain-old conversation, you made McMaster feel like home.

Finally, and most importantly, I would like to thank my family for all their love and support. Thank you Uncle Keith for teaching me that it's okay to ask for help when I need it. Thank you Uncle Jay for showing me that no one can ever or will ever keep us down. Thank you Erika for being everything I ever wanted you to be. You are a constant source of inspiration. Thank you Mom for showing me that wherever life takes me I should always keep my chin up.

Table of Contents

List of Figures

List of Tables

Nomenclature

Alphanumeric Characters	Description	SI Units
A	Flow area	m^2
Cp	Specific heat capacity	J/kg/°C
D	Hydraulic diameter	m
e	Total enthalpy	kJ/kg
h	Enthalpy or Heat transfer coefficient	J/kg or J/s/m^2/°C
h_{fg}	Latent heat	kJ/kg
h_{fg} or h_{lv}	Latent heat	J/kg
$(\Delta i_{SUB})_i$	Enthalpy inlet subcooling	J/kg
f	Friction factor	dimensionless
g	Acceleration due to gravity	m/s^2
G	Mass flux	kg/m^2/s
k	Thermal conductivity	J/s/kg/°C
M	Mass flow rate	kg/s
P	Pressure	Pa
Pe	Peclet number	dimensionless
q''_H	Heat flux	J/s/m^2
r	Relaxation factor	dimensionless
Re	Reynolds number	dimensionless
S_H	Heated perimeter	m
S_W	Wetted perimeter	m
t	Time	s
Δt	Time difference	s
u	Velocity	m/s
x or x_m	True mass quality	dimensionless
x_{th}	Thermodynamic equilibrium quality	dimensionless
x_{OSV}	Saha-Zuber quality	dimensionless
z	Distance	m
Δz	Distance difference	m

Greek Characters	Description	SI Units
A	Void fraction	dimensionless
ε	Surface roughness	m
ε_u	Velocity stop criterion	dimensionless
ε_p	Pressure correction stop criterion	dimensionless
ε_e	Energy stop criterion	dimensionless
ε_d	Density stop criterion	dimensionless
ν	Specific Volume	m^3/kg
μ	Viscosity	Pa·s
Φ_{CRIT}	Critical heat flux	J/s/m^2
ρ	Density	kg/m^3
σ	Surface tension	N/m
τ	Shear stress	kg/m/s^2

Superscripts	Description
t	Evaluate at current time step
$t+\Delta t$	Evaluate at next time step
*	Guessed value
'	Corrected value

Subscripts	Description
av	Average value
w	West face of control volume
e	East face of control volume
p	At node center point
n	n^{th} node
old	Old value
new	New value
H	Heated or Hydraulic
j	j^{th} node
L, or l or f	Liquid
m	Mixture
o	One phase or Initial value
p	At node center point
t or total	Total
Sat or SAT	Saturation value
TP	Two-phase
V or v or g	Vapour
W	Wall

1. Introduction

1.1 Objective

This work outlines and applies a modern approach to modelling the progression of severe accidents in CANDU nuclear power plants using computer codes. The method is called the Multi-step Approach to Code-coupling for Progression Induced Severe Accidents in CANDU nuclear power plants (MACPISA-CANDU). In an application of this method, a single fuel channel model that was developed in MATLAB was coupled with a primary heat transport system model developed in the U.S. NRC computer code MELCOR (MELCOR 1.8.5) (MELCOR Manuals). This was done in order to simulate a small break loss of coolant accident (SBLOCA) in conjunction with a loss of emergency coolant injection (LOECI) in a CANDU 6 nuclear power plant. The specific type of SBLOCA analyzed was a stagnation break (8.03 cm^2) in an individual reactor inlet feeder that is attached to a high powered fuel channel (7.3 MW). As a validation of MACPISA-CANDU methodology, the aforementioned SBLOCA-LOECI event was also modelled with a single fuel channel model developed in SCDAP/RELAP5 (RELAP/SCDAPSIM Mod 3.4 (bi7)) (RELAP Manuals) which was also coupled with the MELCOR primary heat transport system model in an effort to improve the results of the simulation.

1.2 Motivation for Severe Accident Analysis

Modelling of severe accidents is an increasingly important part of reactor safety analysis that conforms to modern international standards (IAEA SRS No. 23, 2001). Severe accidents have a very low frequency of occurrence, but may have significant consequences resulting from degradation in cooling of nuclear fuel. The infrequent nature of some severe accident sequences has led the nuclear industry to use overly conservative analysis guidelines in some scenarios. Nevertheless, in the recent past the Canadian nuclear industry has moved towards risk-informed decision making and towards best estimate code development (Luxat et al., 2000).

Computer codes are essential tools for understanding how a nuclear reactor and its containment might respond under severe accident conditions. Codes are used to support engineering judgment and mitigation features in the event of severe accidents. With the progress in computer technology and advancement of severe accident codes, accident analysis has increasingly been focused on the following (Nguyen et al., 2008) (IAEA-TECDOC-1594, 2008):

1. Support for probabilistic safety assessment (PSA)
2. Resolution of severe accident issues/severe accident research
3. Development of training programs
4. Analytical support for accident management programs
5. Use of computer codes in simulators for severe accidents
6. Support for new designs

Support for PSA activities was one of the earliest uses of the integral severe accident computer codes (IAEA SRS No. 50-P-8, 1996). Calculations were performed using codes for representative groups of sequences of events in order to establish:

1. Results for important variables as a function of time
2. Timing for major events
3. Source terms for high frequency release sequences or sequences expected to have large releases of fission products (i.e. high consequence)

The results of these calculations were supported by sensitivity studies, expert opinion and sometimes by mechanistic code calculations in order to estimate the overall uncertainties of the results. These results were then used to generate accident progression event trees and the associated probabilities for different branch points. These results were used as a part of a level 2 PSA (IAEA-TECDOC-1594, 2008). The present thesis is of value to level 2 PSA in that it outlines the important variables as functions of time as well as the timing for major events. In the current analysis, it was determined that no fission products were released for the single reactor inlet feeder stagnation break event in conjunction with a loss of emergency coolant injection for the period of time considered. However, the worst case scenario for fission product release is considered.

Computer codes have been used to design and analyze severe accident experiments and to resolve technical issues. These uses often result in additional

modelling insights and improvements and lead to the release of new versions of the severe accident codes (IAEA-TECDOC-1594, 2008). In particular, little work has been done to qualify the LWR (light water reactor) codes SCDAP/RELAP5 and MELCOR for the purpose of analyzing CANDU type reactors. The limited qualification can be attributed to the difficulty in modelling the horizontal fuel channels. Nonetheless it is possible to derive results using the MACPISA-CANDU methodology and to analyze the progression of a severe accident. The value in doing such an analysis is that it provides a valuable independent check of experimental work and results from current CANDU validated severe accident computer codes. In addition, such an analysis highlights the possible areas for model improvements within the MATLAB, SCDAP/RELAP5 and MELCOR codes for modelling the progression of severe accidents in CANDU nuclear power plants.

Combining code specific user training along with generalized training of severe accident phenomena and research is also an effective way to train engineering analysts and other technical staff. Specifically, engineering analysts familiar with system thermalhydraulic codes used for design basis analysis can be trained quickly to use mechanistic codes for severe accident conditions. Plant models developed for system thermalhydraulic design basis accident analysis can be extended by use of the mechanistic codes, and thus convenient conversion can take place between data used for design basis accident calculations and data used for severe accident calculations (IAEA-TECDOC-1594, 2008).

One of the most frequent applications of severe accident analysis is the development of accident management programs (Nguyen et al., 2008) (IAEA-TECDOC-1594, 2008). Clearly, the primary purpose of reactor safety is to prevent any accident from occurring in order to achieve extremely low core melt probabilities. This fact aside, should an accident become severe, then the priority is to stop or at least slow the accident progression in order to mitigate releases of radioactive material by exploiting all means of accident management available at the nuclear power plant site. Accident analysis related to mitigation is important because it is required to understand the plant's response to beyond design basis accidents and severe accidents, to understand which accident phenomena are important for the specific plant, to understand and rank challenges to fission product boundaries, and to provide a basis for the investigation of preventive and mitigation measures of the accident management program. There are specific IAEA reports devoted to accident management programs and to their review (IAEA SRS No. 32, 2004) (IAEA SRS No. 56, 2008). These reports highlight the motivation for three categories of analysis needed to support preparation, development and implementation of accident management programs. These three categories of analysis are (IAEA SRS No. 32, 2004):

- Preliminary analyses – provide an understanding of the response of the plant to various types of accidents and basis for selection of recovery strategies

- Procedure and guideline development analyses – detailed confirmation of the choice of recovery strategies adopted, to provide necessary input to set-point calculations and to resolve any other open items identified during the previous step
- Validation analyses for procedures and guidelines – demonstrate the capabilities and choice of appropriate strategies and optimize some aspects of these

The current work falls in the preliminary analyses category. It is informative in nature and provides basis for selection of recovery strategies in that it provides an understanding of the response of the plant to the early stages of a SBLOCA-LOECI event.

The application of severe accident analysis and computer codes to simulators and simulation techniques in general accident management training is described in the IAEA report SRS No. 56 (2008). In the report, a simulator is characterized as:

'A computer based assembly of software and hardware, which is capable of presenting the physical behaviour of the whole nuclear power plant or the part of it during various operational states and malfunctions. The simulators are typically equipped with an advanced user interface (graphical or hardware interface) suitable for interactive operation and particularly suitable for training purposes.'

Generally, the simulators are subdivided into engineering simulators (i.e. used for design purposes and in particular for justification of the design) and training

simulators. Given the robustness of both the LWR codes SCDAP/RELAP5 and MELCOR it is possible that either or both codes could possibly be employed as engineering simulators.

For new reactor designs, developing mitigation measures specifically to cope with severe accidents has started to be considered. Such measures have been the focus of many international research programs (IAEA-TECDOC-1594, 2008). Activities are being carried out to understand the main phenomenological aspects and to develop the most suitable preventative and mitigating measures. Some of the generation III+ reactor designs have incorporated severe accidents into their design and licensing approach. A combination of calculations using mechanistic system codes is typically needed. Calculations often have to be complemented by special experiments. To account for large uncertainties in calculations, compensation is required to make the design more robust. Given that there are relatively few severe accident codes qualified to model CANDU nuclear power plants, namely MAAP4-CANDU and ISAAC, providing cross code validation with internationally recognized codes, such as SCDAP/RELAP5 and MELCOR, would provide further support for the robustness of a given reactor design.

1.3 Scope of the Problems Addressed

There are very few fully-integrated severe accident codes for analyzing CANDU nuclear power plants. Namely these codes are MAAP4-CANDU and ISAAC. MAAP4-CANDU is used within the Canadian nuclear industry whereas ISAAC was developed for the South Korean nuclear industry. For

intercomparison and validation purposes alone, more diversity is needed for the modelling of severe accidents in CANDU nuclear power plants. Moreover, although these codes have been seen to yield successful predictions (Brown, Petoukhov and Mathew, 2009) they have limitations associated with their nature of being fully-integrated codes. The computational time of a large fully-integrated code is not as easy to optimize as smaller individual mechanistic models. In addition, when using fully-integrated codes the user is limited to the models provided with the code itself. New versions of these codes are only released when they are altered with major changes. Hence, incremental updating with the latest research and experimental results is not possible. A clear solution to these problems is to use a multi-step approach in which codes are coupled in order to incorporate the latest research, optimize computational time, and to specify individual step requirements as needed. Hence, a generalized methodology for code-coupling is required in order to simulate the sequential nature of CANDU severe accidents.

Secondly, there are benefits in using codes that have not specifically been qualified for CANDU nuclear power plants. Often mechanistic codes specifically qualified for CANDU nuclear reactors are not available for an individual analyst, as these codes are often proprietary in nature. Even if they are available, using other codes for the same purpose allows for cross code validation. SCDAP/RELAP5 and MELCOR are two LWR codes that have generally not been qualified for CANDU nuclear power plants to any great extent. Nonetheless,

these codes are in wide use internationally and have various advantages. SCDAP/RELAP5 is a best-estimate computer code and offers the ability to model horizontal fuel channels. On the other hand, MELCOR is a fast fully-integrated, parametric severe accident code capable of simulating a full reactor core and containment.

Finally, SBLOCA-LOECI events are a very important type of accident to study. This category of accident usually terminates as a limited core damage accident (LCDA) and falls at the boundary between the design basis accident (DBA) and beyond design basis accident (BDBA) categories in terms of frequency of occurrence and fuel damage. Whether the accident is a DBA or BDBA depends on the moderator system acting as ultimate heat sink (Luxat, 2007). The relevance of SBLOCA-LOECI with regards to severe accident analysis is that LCDAs are usually precursors to severe core damage accidents (SCDAs) and thus provide valuable information for the progression of severe accidents. The specific event analyzed in this report is a stagnation break in a single reactor inlet feeder attached to a high powered channel in conjunction with a loss of emergency coolant injection. The specific focus of the accident analysis within this thesis will be on the early stages of this event, with particular attention on how the fuel channel experiencing flow stagnation affects the moderator.

1.4 Structure of Report

Section 2 of this thesis presents a background for severe accident progression within CANDU nuclear power plants. It also outlines current

computer codes and approaches used in modelling severe accidents for CANDU nuclear power plants. Section 3 presents the generalized methodology used in the multi-step code-coupling for the purposes of analyzing severe accidents within CANDU nuclear power plants. It also presents how this method was specifically applied to coupling the single channel models in MATLAB and SCDAP/RELAP5 with the primary heat transport system model in MELCOR. In addition, Section 3 outlines the details of the single fuel channel model created in MATLAB and SCDAP/RELAP5 and the details of the full figure-of-eight primary heat transport system model created in MELCOR. Section 4 presents a detailed description of the stagnation break in a single reactor inlet feeder attached to a high powered fuel channel. It also presents the results and analysis of the event in addition to the validation and intercomparison of the computer models. Section 5 presents the limitations of the present analysis and recommendations for further work. Section 6 outlines the conclusions of the thesis.

2. Background

2.1 Severe Accidents and Definition of Event Classes

The term 'severe accident' is often referred to in different ways. For instance, it sometimes refers to beyond design basis accidents, or accidents that fall below a certain cut-off frequency. In other instances, severe accidents are accidents that involve fuel damage or core damage. The current IAEA definitions are used within this thesis and are as follows (IAEA-TECDOC-1594, 2008):

- Beyond Design Basis Accidents (BDBAs) – Accident conditions more severe than a design basis accident and may or may not involve reactor core degradation
- Severe Accidents (SAs) – Accident conditions more severe than a design basis accident and involve significant reactor core degradation

Severe accidents involve very complex physical phenomena that take place sequentially during various stages of the accident progression. For a CANDU nuclear reactor, accidents that result in damage to the reactor core fall naturally into two classes (IAEA-TECDOC-1594, 2008):

- Limited Core Damage Accidents (LCDAs) – An accident where the reactor core geometry is preserved
- Severe Core Damage Accidents (SCDAs) – An accident where the reactor core geometry is lost

SCDAs are within the above definition of a severe accident. On the other hand, LCDAs are typically considered as part of the design basis for CANDU nuclear reactors. As such, there are provisions for their prevention and mitigation, and severe accident management is not required. However, LCDAs are typically precursors to SCDAs. A SBLOCA-LOECI event is usually within the category of a LCDA. This type of event may be at the boundary between DBA and BDBA depending on the integrity of the moderator system to act as an ultimate heat sink (Luxat, 2007). Therefore, a SBLOCA-LOECI is a relevant event class for analysis because it could well be a precursor to a SCDA. However, the specific focus of the accident analysis within this thesis will be on the early stages of this event. Particular attention will be paid to how the fuel channel experiencing flow stagnation affects the moderator.

2.2 Characteristics of a CANDU 6 Nuclear Power Plant

A CANDU 6 nuclear power plant incorporates special safety systems with the primary intent of mitigating severe accidents. These special safety systems include:

- Emergency Core Cooling System (ECCS)
- Shutdown Safety System 1 – Shutdown Rods
- Shutdown Safety System 2 – Poison Injection
- Containment

Besides these special safety systems, other plant features can affect the progression to a severe accident. Table 1 below lists some of the main CANDU 6 nuclear power plant design features and their characteristics with respect to severe accident prevention and mitigation.

Table 1: CANDU 6 design features-severe accident prevention and mitigation characteristics

Plant Feature	Design Description	Severe Accident Prevention and Mitigation Characteristics
Fuel and Fuel Channels	• 380 horizontal fuel channels • Zirconium/niobium alloy pressure tube surrounded by zircaloy-2 calandria tube with CO_2 gap in between • Each channel has 12 fuel bundles • Fuel bundles have 37-elements • Each element is made of zircaloy-4 tube with UO_2 pellets	• Fuel channels maintain integrity and fuel is below melting even when heat removal by flowing coolant is not available
Calandria	• Calandria shell is a horizontal cylinder made of austenitic stainless steel • Ends of shell enclosed by stainless steel tubesheets • Cover gas system maintains a pressure of less than 27.6kPa above moderator • Over pressure protection is provided by rupture discs at upper ends of four pressure relief pipes	• Adequate discharge area for heavy water flow to containment for simultaneous pressure tube/ calandria tube rupture at full system pressure
Calandria Vault	• Made of concrete and filled with light water for biological shield under normal operating conditions • Reactor building ventilation system provides venting of calandria vault, end shields, and delay tanks • Rupture discs are provided on the combined vent lines to relieve over pressure caused by boiling of the vault water or failure of cover gas system	• Passive heat sink under severe accident conditions • Will inherently remove decay heat from calandria through the calandria wall • Vault floor has large spreading area for potential core debris • Two layers of concrete under vault floor provides large amount of time for ablation by molten debris
Primary Heat Transport System	• Comprised of 2 figure-of-8 loops • Each loop serves 190 of the 380 fuel channels • Each loop divided by the vertical center plane of the reactor • Each loop contains 2 pumps, 2 steam generators, 2 inlet header and 2 outlet headers • Feeders connect the inlet and outlet headers to the fuel channels • Pressurized heavy water circulates through the fuel channels to remove heat produced by fission of natural uranium fuel • Heat is transported by the reactor coolant to steam generators where it is transferred to light water to generate steam, which drives the turbine • Steam generators, PHTS pumps and header are located above the reactor • Reactor outlet headers at one end of the reactor are connected to a common pressurizer	• Loops can be isolated from each other, which reduces reactor coolant loss in the event of a loss of coolant accident • Steam generators, PHTS pumps and headers are located above the reactor to facilitate thermosyphoning (natural circulation) when the PHTS pumps are unavailable and the reactor is shut down
Moderator System	• Heavy water moderator thermalizes fast neutrons produced by fission • Operating pressure at the moderator is maintained slightly above atmospheric pressure • Fully independent of heat transport system • Includes 2 100% pumps and 2 100% tube and shell heat exchangers • Level controlled by moderator system head tank	• Low temperature and pressure D_2O moderator provides effective heat sink under some accident scenarios

2.3 Severe Accident Progression in a CANDU

There is significant commonality in how severe accidents progress in CANDU nuclear power plants. A convenient way to represent severe accident progression is to define a small number of core damage states (CDSs). A CDS is a quasi-steady state during which the decay heat is absorbed into its surrounding environment. Although the timing of progression from one state to the next can be affected by the initiating event, the detailed design and operator actions, CDSs are independent of the initiating event and generally independent of station design (IAEA-TECDOC-1594, 2008). There are five such typical CDSs for CANDU nuclear power plants that are listed in Table 2 below.

Table 2: 5 Core Damage States (CDSs) for a CANDU NPP and brief description of events (IAEA-TECDOC-1594, 2008)

Core Damage State	Description of Events
CDS1	• Fuel channels have lost water inventory, dried out and heated up • Fuel sheath is oxidized and pressure tubes have ballooned or sagged into contact with calandria tubes • Moderator removes most of decay heat • Terminal state of a LOCA plus loss of ECI • Sustainable as long as the moderator level can be maintained
CDS2	• Moderator level has dropped exposing several upper channels (due to moderator rupture disk bursting due to boiling or in-core LOCA) • Exposed channels have heated up, sagged, oxidized and broken apart collapsing onto lower submerged channels or dropping to bottom of calandria vessel • Most of decay heat is removed from submerged channels as well as some of decay heat of the collapsed fuel channels that are now submerged • Adding water to calandria vessel can prolong this state
CDS3	• Moderator inventory is gone (moderator boiled off slowly or drained quickly due to type and location of break) • All channels have heated up, sagged, oxidized and broken apart leaving a rubble pile of 'corium' (mix of fuel and core structural materials) at bottom of the calandria vessel • Steel calandria vessel and surrounding biological shielding materials (water and steel in the shield tank, or concrete) remove some of decay heat • Structure is not capable of removing all decay heat and corium will eventually melt through; however, adding water to calandria vessel can prolong this state
CDS4	• Corium has penetrated through calandria vessel, biological shield and is on concrete floor • Accumulated water will quench molten corium
CDS5	• Due to lack of water or insufficient contact area for boiling, or due to formation of an upper crust, corium attacks concrete referred to as molten core concrete interaction • Ablation of concrete produces steam, H_2, CO and CO_2 • Degree to which the molten core concrete interaction can be terminated depends on decay heat (diminishes with time), surface area of the melt (affects rate of cooling by a water layer, limited by critical heat flux) and availability of water • Rate of ablation is slow (about 2 cm/hour with decay power at 1%) and the basemat is thick (>1m), and decay power diminishes with time, basemat penetration is unlikely

2.4 Single Channel Events

As mentioned above, the CANDU nuclear reactor accidents that could result in damage to the reactor core fall naturally into two classes: LCDAs and SCDAs. The former can involve single channels or the whole reactor core. For

instance, a feeder break can result in overheating of the fuel in the affected channel. On the other hand, a large break loss of coolant accident with a loss of emergency coolant injection (LBLOCA-LOECI) could lead to widespread fuel damage. However, in both cases the presence of the moderator with sufficient subcooling as a secondary heat sink prevents failure of the fuel channels and core degradation. In this sense, the LCDAs are distinct from the accident sequences for a light water reactor (LWR) as they can involve fuel damage without core relocation.

2.4.1 Description of System Behaviour

The focus of this section will be on the system behaviour as it pertains to single channel events. A stagnation break in a reactor inlet feeder attached to a high powered channel in conjunction with a loss of emergency coolant injection falls into this category.

2.4.1.1 Thermalhydraulic Behaviour

When the coolant flow in a single fuel channel is reduced, the remaining flow will increasingly be converted to steam. Nonetheless, the lessened flow is still capable of removing heat from the fuel. High reductions in mass flow are required before the fuel, sheath and pressure tube temperatures experience any significant increases. In fact, it is reported that the flow would have to reduce by a corresponding amount to blockages greater than 90% of the flow area of the fuel channel for them to experience large temperature increases (IAEA-TECDOC-

1594, 2008). Events that could potentially lead to core damage are those that result in a severe reduction in coolant flow with subsequent temperature excursions for the fuel and fuel channel. The limiting case is flow stagnation, during which there is no net flow in the fuel channel. The primary thermal and hydraulic phenomena of interest are:

- Heat transfer within the fuel
- Heat transfer from fuel to coolant
- Heat transfer from coolant to pressure tube
- Thermal radiation
- Phase separation of the coolant in the channel
- Feedback of phase separation on thermal behaviour

The fuel channel experiencing a severe reduction in coolant flow will eventually rupture due to thermal-mechanical deformation allowing the reintroduction of coolant from the reactor headers.

2.4.1.2 Fuel Behaviour

For severe reductions in coolant flow in an individual fuel channel, the fuel undergoes a rapid temperature excursion. The phenomena of primary interest are those that can lead to fuel bundle deformation and to failure of the fuel cladding. These phenomena include:

- Fuel element bowing
- Zircaloy oxidation

- Be-braze penetration

The high coolant pressure tends to prevent clad ballooning. If the pressure tube does not fail due to circumferential temperature gradients, there can be clad melting and relocation onto the pressure tube, which is predicted to cause failure. However, if delayed failure is assumed, there can be fuel melting (IAEA-TECDOC-1594, 2008).

2.4.1.3 Fuel Channel Behaviour

The temperature of the pressure tube will rise as heat is transferred to it from the fuel. As its temperature starts to increase, material deformation can occur due to the highly pressurized coolant in the primary heat transport system. Stratification of the coolant in the fuel channel will keep fuel temperatures lower in the bottom of the fuel channel. The stratification of coolant will lead to a circumferential temperature gradient which in turn causes the top of the pressure tube to deform more quickly and fail. On the other hand, if the fuel channel becomes rapidly devoid of coolant a more uniform temperature will persist around the circumference of the pressure tube. In this case, the pressure tube will balloon (i.e. expand uniformly) into contact with the calandria tube (IAEA-TECDOC-1594, 2008). Calandria tubes are thinner than the pressure tubes. If the pressure tube fails prior to ballooning into contact with the calandria tube, the annulus between the tubes will become pressurized causing the calandria tube to fail as well (AECL, 2002).

2.4.1.4 Reactor Core Behaviour

A primary reason for analyzing single channel events is the possibility for propagation of the event to additional channels. The mechanisms for this are shown in Figure 1. The three means of propagation are:

- Failure of the initiating channel leading to failure of the calandria vessel
- Propagation of the initiating failure to neighbouring channels
- Ability to shutdown could be impaired by damage to control and shutoff rods and by displacement of poisoned moderator by heavy water coolant

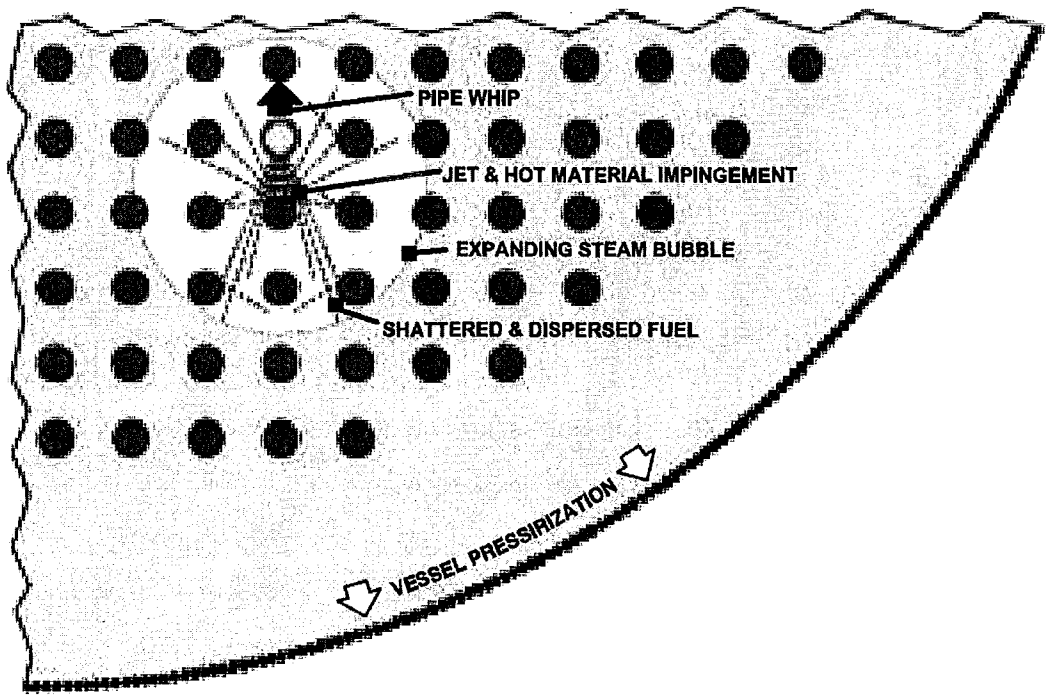

Figure 1: Core behaviour phenomena in single channel events (IAEA-TECDOC-1594, 2008)

When a fuel channel fails, coolant discharging into the calandria vessel can form a large steam bubble that displaces the liquid moderator and pressurizes

the calandria vessel. In addition, ejection of hot fuel materials can deposit additional energy into the moderator, producing more steam (Figure 2).

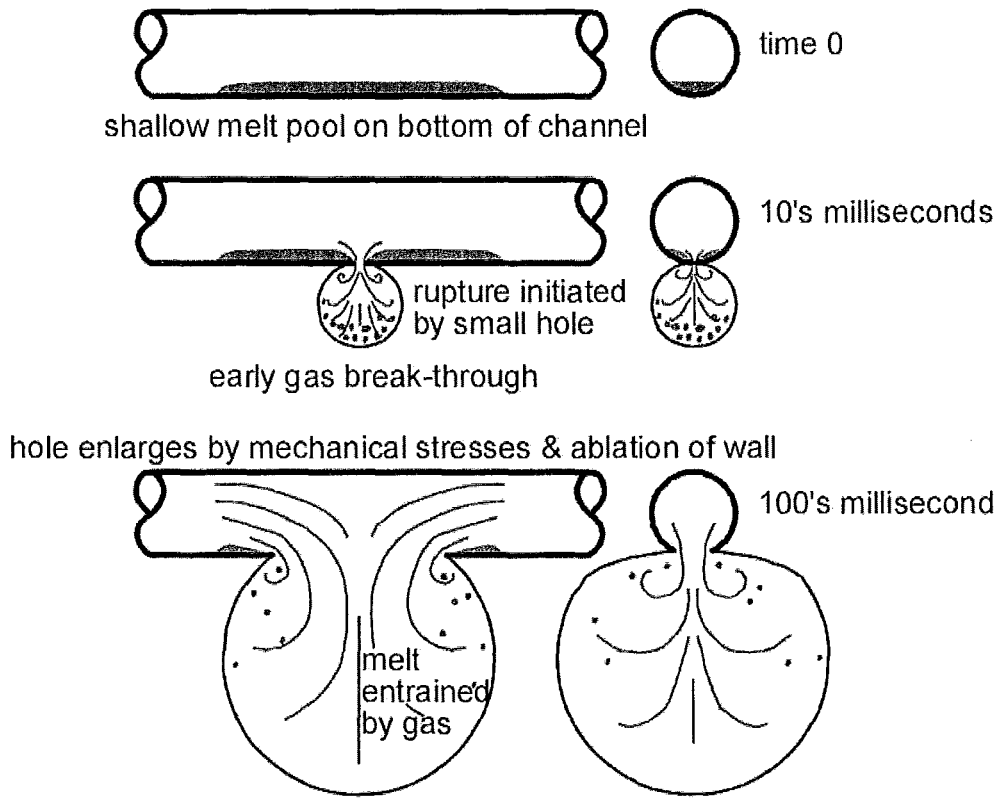

Figure 2: Conceptual schematic of forced melt/water interaction

(IAEA-TECDOC-1594, 2008)

If there is liquid material in the effluent, the possibility of a steam explosion should be considered even though it is believed to be unlikely for high pressure ejection (IAEA-TECDOC-1594, 2008).

Pressure relief ducts are attached to the calandria vessel, which are designed to accommodate sustained coolant discharge from the primary heat transport system. However, there is an initial pressure spike in the calandria

vessel, when the rapidly growing steam bubble displaces the incompressible liquid. The effect of the pressure spike is dampened by the collapse of neighbouring calandria tubes onto their pressure tubes. The resulting early loads on the walls of the calandria vessel are approximately the value of the calandria tube collapse pressure, and the vessels of CANDU reactors have been shown to be able to withstand these loads (IAEA-TECDOC-1594, 2008).

The discharge of high enthalpy coolant into the calandria vessel also produces strong jet impingement loads onto the surrounding channels as well as in core devices. Surrounding components can also be struck by the ruptured channel (i.e. pipe whip) and by projectiles consisting of fuel bundles or fragments of fuel bundles. These phenomena have been assessed and there is no damage propagation to the adjacent fuel channels and enough shut-off rod guide tubes are undistorted to maintain adequate shutdown capability (IAEA SRS No. 29, 2003). In addition, the poison inventory of the second shutdown system is adequate to ensure shutdown even if poisoned moderator is displaced by primary coolant (IAEA-TECDOC-1594, 2008).

2.4.1.5 Fission Product Behaviour

For a single channel event, the maximum fission product release is the complete inventory of the fuel channel. For a severe reduction in channel flow, the release could occur very rapidly. With the wide range of possible conditions, it is simplest to evaluate the fuel releases parametrically, assuming varying magnitudes of release up to the total channel inventory and release rates up to an

essentially instantaneous release of the volatile fission products. While some fission products could remain dissolved in the primary heat transport system or in the moderator, such retention is not typically credited. Fission product behaviour in containment is determined by wet aerosol phenomena and the complex chemistry of radioiodine (Wren, 2001).

2.4.1.6 Containment Behaviour

There are significant safety issues related to containment behaviour for single channel events. Some hydrogen could be produced during the transient (up to the amount equivalent to all zircaloy in the fuel bundles of one fuel channel), but the maximum amount is too small to cause flammable concentrations in the containment (IAEA-TECDOC-1594, 2008).

2.4.2 Initiating Events

Single channel events are a particular subset of SBLOCAs affecting only one reactor fuel channel. They consist of the following SBLOCA accidents (IAEA SRS No. 29, 2003):

1. A 'spontaneous' pressure tube rupture, assumed for the purpose of analysis to result also in rupture of the calandria tube.
2. A break in an individual feeder pipe. A special case is a break in an inlet feeder of exactly the correct size to temporarily cause the flow in the channel to stagnate. This can then result in channel overheating and failure.

3. Failure of the end-fitting attached to the pressure tube, and assumed ejection of the fuel.
4. Blockage of the flow in a channel, assumed to be complete enough to cause channel overheating and failure.

2.4.3 Acceptance Criteria

Table 3 below lists the acceptance criteria as applied to single channel events in CANDU reactor safety analysis (IAEA SRS No. 29, 2003). However, the criteria regarding fuel and fuel channel damage do not apply to the affected channel.

Table 3: Acceptance criteria for single channel events

Criteria #	Description of Acceptance Criteria
1	Dose to the most exposed individual in the critical group is below the Event Class 2 limit.
2	There should be no systematic fuel failures. Systematic fuel failures mean that some fuel elements initially operating within the allowed operating limits are predicted to have a high probability of failure when subject to the event transient. This does not include fuel with an incipient defect that might fail due to the stresses caused by the event. Prevention of significant fuel failure is sufficient but not necessary to meet the dose limit; it also reduces the economic risk of a small LOCA. There are two periods of interest: at high power (before reactor trip) and at low power (due to prolonged dry-out at low flows). The fuel sheath will remain intact if: i. There is no fuel centreline melting (centreline temperature lower than 2840°C). ii. There is no excessive strain (uniform sheath strain less than 5% for temperatures lower than 1000°C). iii. There are no significant cracks in the surface oxide (uniform sheath strain less than 2% for temperatures higher than 1000°C). iv. There is no oxygen embrittlement (oxygen concentration less than 0.5% by weight over half the sheath thickness). v. There is no penetration by the beryllium braze at spacer and bearing pad locations. vi. Various times at the temperature limits can be used as a conservative surrogate for these physical requirements.
3	The channel geometry must remain coolable. There are two sufficient criteria: i. The amount of fuel sheath oxidation must not embrittle the sheath on rewet to maintain fuel integrity. ii. The amount of sheath strain must be limited so that coolant can flow through the channel.
4	Channel integrity is maintained. Sufficient conditions include: i. There is no fuel melting. ii. There is no sheath melting. iii. There is no constrained axial expansion of the fuel string. iv. For cases where the pressure tube strains or sags, it is sufficient if: v. The pressure tube does not fail prior to contacting the calandria tube. This criterion is satisfied if the pressure tube local strain is less than 100% at any location. vi. The calandria tube remains intact after pressure tube contact. This criterion is satisfied if the calandria tube outer surface does not go into prolonged film boiling.
5	Pressure within the containment is below the design pressure.
6	Pressure within containment compartments does not cause internal structural failures.
7	A safe shutdown state is maintained. Manual action may be credited in the long term to supplement the shutdown system reactivity.
8	The failure does not propagate to other reactor fuel channels.
9	The calandria vessel pressure transient does not cause vessel failure or loss of moderator (other than through the relief pipes), and any vessel deformation does not prevent operation of the shutdown systems.

2.4.4 Relevant Event Combinations

Single channel events are also combined with the impairments of containment, Class IV power and emergency core cooling system (ECCS). For a single channel event the requirement on the integrity of the fuel channels and their fuel applies to all fuel channels except the affected fuel channel. Particular attention is paid to moderator temperature for in core breaks, which will undergo an initial excursion due to the flow of high temperature coolant into the moderator. If an in core break is combined with an impairment in ECCS, some of the other channels may sag or strain (eventually) into contact with their calandria tubes. This means that the moderator temperature must be kept low enough to prevent prolonged dryout of the calandria tube (IAEA SRS No. 29, 2003).

The specific focus of the accident analysis within this thesis will be on the early stages of a reactor inlet feeder stagnation break in conjunction with a loss of ECI event. Particular attention will be paid on how the fuel channel experiencing flow stagnation affects the moderator. Given that the ECI could be seen to trip on low system pressure, the effect of ECI do not come into play within the time frame of interest.

2.5 Approaches to Modelling Severe Accidents

2.5.1 MAAP4-CANDU

The MAAP4-CANDU (Modular Accident Analysis Program for CANDU Nuclear Generating Station) code was developed from the MAAP4 code used for PWRs (pressurized water reactors) and BWRs (boiling water reactors).

For the CANDU 6 model developed in MAAP4-CANDU a simplified fuel channel model was used in the core. The 22 rows by 22 columns of a CANDU 6 were divided into 6 vertical nodes and 6 horizontal nodes. The 3 horizontal on left are one loop and the 3 horizontal nodes on the right are the other loop. Therefore, the 380 fuel channels have been reduced to 36 representative channels and 18 representative channel groups for each loop. As for the 12 fuel bundles, they are divided into 5 axial nodes. Thus, each loop is modelled as 90 nodes in 3-dimensions as seen in Figure 3.

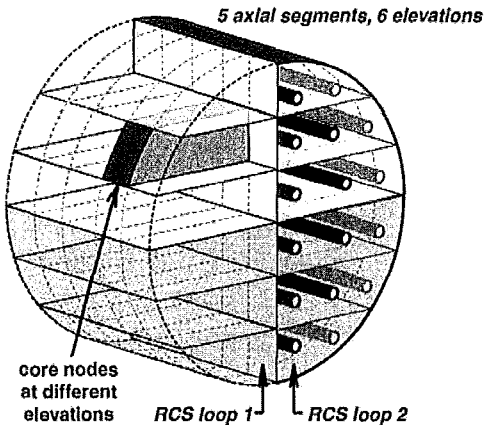

Figure 3: Nodalization of CANDU 6 core in MAAP4-CANDU (Mathew et al., 2008)

The fuel channel, which consists of a calandria tube, pressure tube and 37-element fuel bundle was converted into elements arranged in 4 rings (central, inner, intermediate and outer rings) and is shown in Figure 4 below.

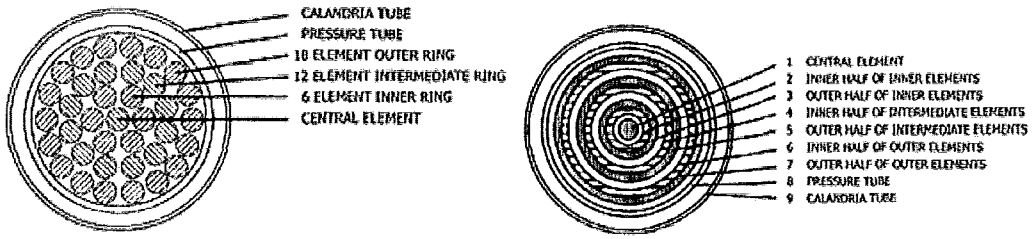

Figure 4: Nodalization of fuel channel in MAAP4-CANDU (IAEA-TECDOC-1594, 2008)

The primary heat transport system (Figure 5) was modelled to contain two steam generators, two pumps, two reactor inlet headers, and two reactor outlet headers. The feeders connect the inlet and outlet end of fuel channels to inlet and outlet headers respectively. The flow through one loop follows the shape of figure-of-eight with some channels carrying the flow inward and others outward from the reactor face.

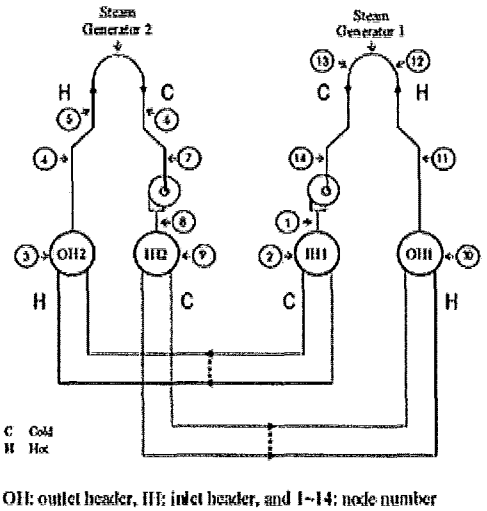

Figure 5: Primary heat transport system as modelled in MAAP4-CANDU (IAEA-TECDOC-1594, 2008)

2.5.2 ISAAC

The ISAAC (Integrated Severe Accident Analysis code for CANDU plants) code was developed from MAAP and it employs most of the MAAP models for severe accident phenomena in general. The use of ISAAC allows the simulation of accident scenarios that could lead to a damaged core and eventually to containment failure at the Wolsong nuclear power plants of the Republic of Korea, which contain CANDU 6 type reactors.

For the CANDU 6 model developed in ISAAC a simplified fuel channel model was used in the core. The 380 fuel channels were reduced to 28 (up to 74) representative fuel channels or 14 (up to 37) representative channel groups for each loop (Figure 6). As for the 12 fuel bundles, they are divided into 12 axial nodes.

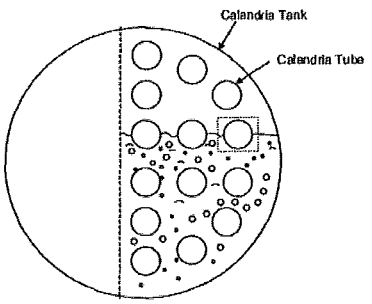

Figure 6: Nodalization of CANDU 6 core in ISAAC (IAEA-TECDOC-1594, 2008)

The fuel channel, which consists of the calandria tube, pressure tube and 37-element fuel bundle was converted into a single fuel pin surrounded by the pressure tube and calandria tube (Figure 7).

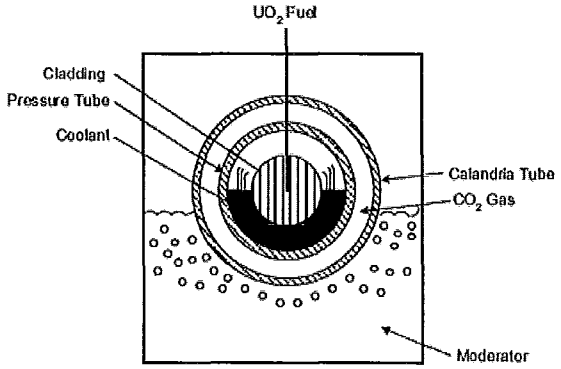

Figure 7: Nodalization of fuel channel in ISAAC (IAEA-TECDOC-1594, 2008)

The primary heat transport system has been modelled with two independent figure-of-eight loops. Both loops and all four steam generators/pumps are modelled individually. The arrows in Figure 8 below indicate the direction of coolant flow in the figure-of-eight loop.

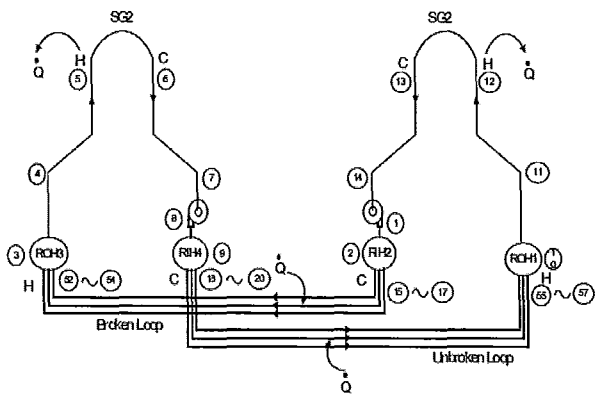

ROH: reactor outlet header; RIH: reactor inlet header; SG: steam generator;
H: hot; C: cold, Q: heat flux, and 1 ~ 57: node number

Figure 8: Primary heat transport system as modelled in ISAAC (IAEA-TECDOC-1594, 2008)

2.5.3 Multi-step Code-coupling Approach

Recently a multi-step approach to code-coupling has been employed to analyze the core damage of pressurized heavy water reactors (PHWRs). In the multi-step approach, computed data in one step is used as a boundary condition for the next step. In turn, each step addresses specific phenomena. This procedure helps to reduce computational time and numerical problems, while increasing the ability to select specific requirements for each step (IAEA-TECDOC-1594, 2008). This fits well with the sequential nature of CDSs in that each code can sequentially be employed. Recently the codes SCDAP/RELAP5, ASTEC and ANSYS have been used in this manner to analysis severe accidents (IAEA-TECDOC-1594, 2008).

Mladin et al. (2008, 2009) have made the most current attempts at modelling a CANDU 6 fuel channel in SCDAP/RELAP5. They used a standard 5.94-m long CANDU 6 fuel channel, containing twelve 37-element fuel bundles. Using RELAP/SCDAPSIM Mod 3.4 (bi7) they modelled fuel as depicted in Figure 9 below.

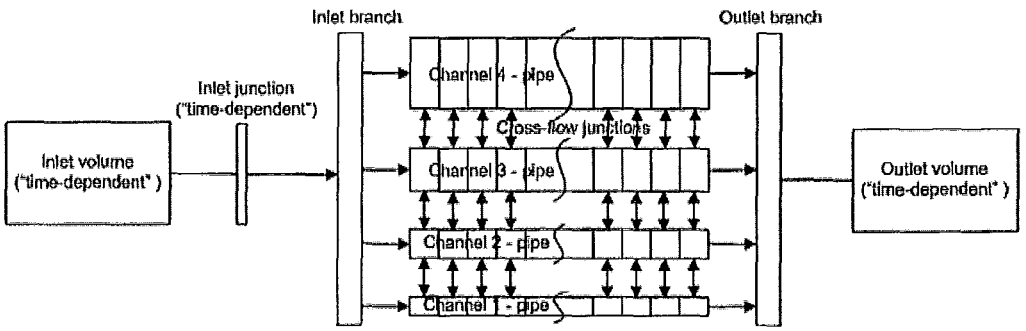

Figure 9: Hydrodynamic representation of the CANDU 6 fuel channel (Mladin et al., 2009)

There are many techniques for coupling advanced codes. In essence, the coupling may be either loose (meaning the codes only communicate after a number of time steps) or tight such that the codes update one another time step to time step. Whether a loose coupling or a tight coupling is required depends on the phenomena that are being modelled and analysed. During a relatively slow transient, close coupling of codes in not required and thus the codes of interest do not have to communicate time step by time step. In contrast, the behaviour of fluid moving through the core region, where a portion of the core is modelled in great detail using a CFD code while the remainder of the core is modelled using a system analysis code, would require tight coupling if the two codes were linked, since dramatic changes may occur during a nuclear power plant transient (IAEA SRS No 32, 2008).

3. Methodology and Models

The Multi-step Approach to Code-coupling for Progression Induced Severe Accidents in CANDU nuclear power plants (MACPISA-CANDU) is a generalized methodology for modelling severe accidents in a CANDU nuclear power plant. The logic for this methodology as applied to coupling different codes is presented as a flow chart in Figure 10. Based on the characteristics of a given CANDU reactor design, there are a number of phenomena that can occur. The computer codes selected to analyze a particular sequence depends on the type of phenomena that are encountered in that sequence. Within the computer codes there may be more than one model available for simulating a particular phenomenon. The model selection is based on the progression of a severe accident. In the case of severe accident progression in a CANDU nuclear power plant, these phenomena can be seen to take place sequentially in the 5 quasi-static core damage states (CDSs) shown in Table 1. This allows each phenomenon to be modelled in sequence with separate codes. The results from one code are the boundary conditions for another until a terminal core state is reached. The terminal state is reached when there is no further deterioration in the state of the plant.

As a partial validation of this methodology, two distinct code-coupling simulations were performed. First, a single fuel channel model programmed in MATLAB was coupled with a primary heat transport system model in MELCOR.

This is shown in Figure 11 below. Second, a single fuel channel model in SCDAP/RELAP5 was coupled with a primary heat transport system model in MELCOR. This is shown in Figure 12 below. Each of these simulations has been chosen to model a small break loss of coolant accident with loss of emergency coolant injection (SBLOCA-LOECI) in a CANDU 6 nuclear power plant. Based on the characteristics of the CANDU 6 reactor design, there are a number of phenomena that occur for this event. The capabilities of the MATLAB, SCDAP/RELAP5 and MELOCR codes to model these phenomena that occur for SBLOCA-LOECI are listed in Table 4. The input data for the models was taken from a report comparing the primary heat transport systems and components between Darlington NGS, Bruce 'B' and CANDU 6 done by Atomic Energy of Canada Limited (AECL, 1991).

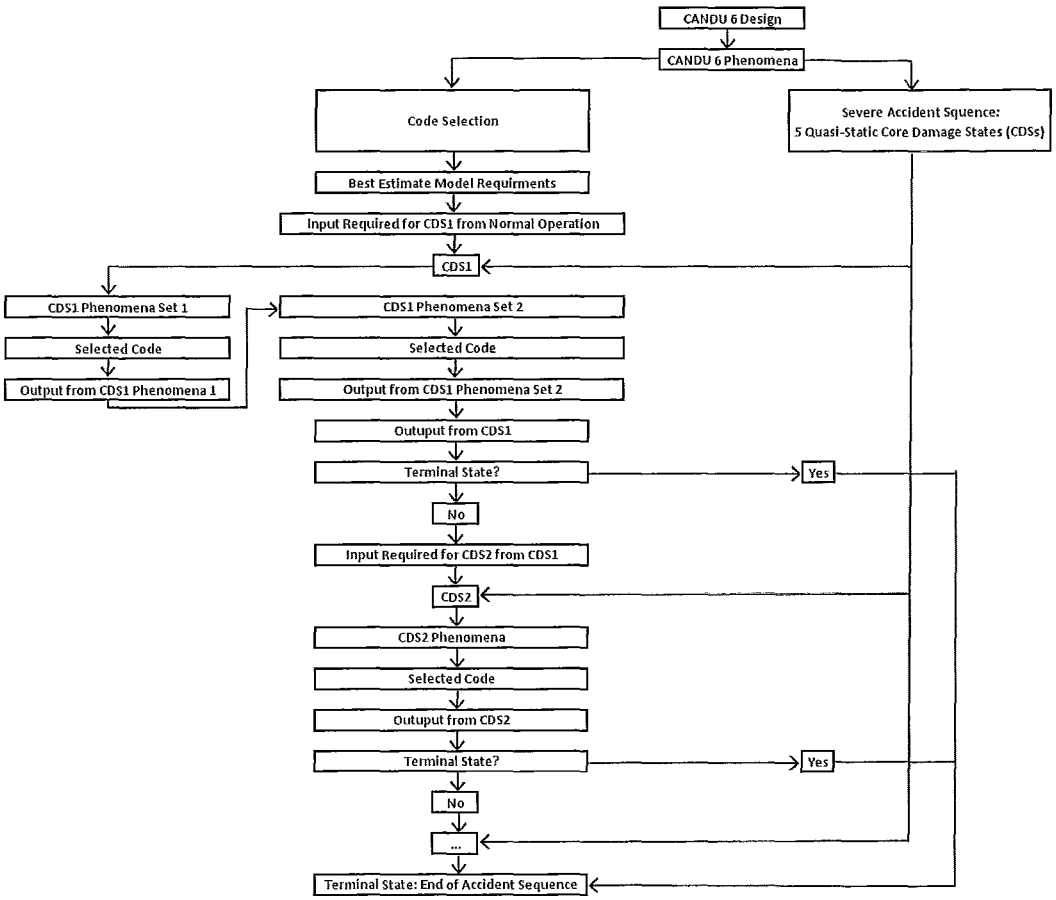

Figure 10: Multi-step Approach to Code-coupling for Progression Induced Severe Accidents in CANDU nuclear power plants (MACPISA-CANDU)

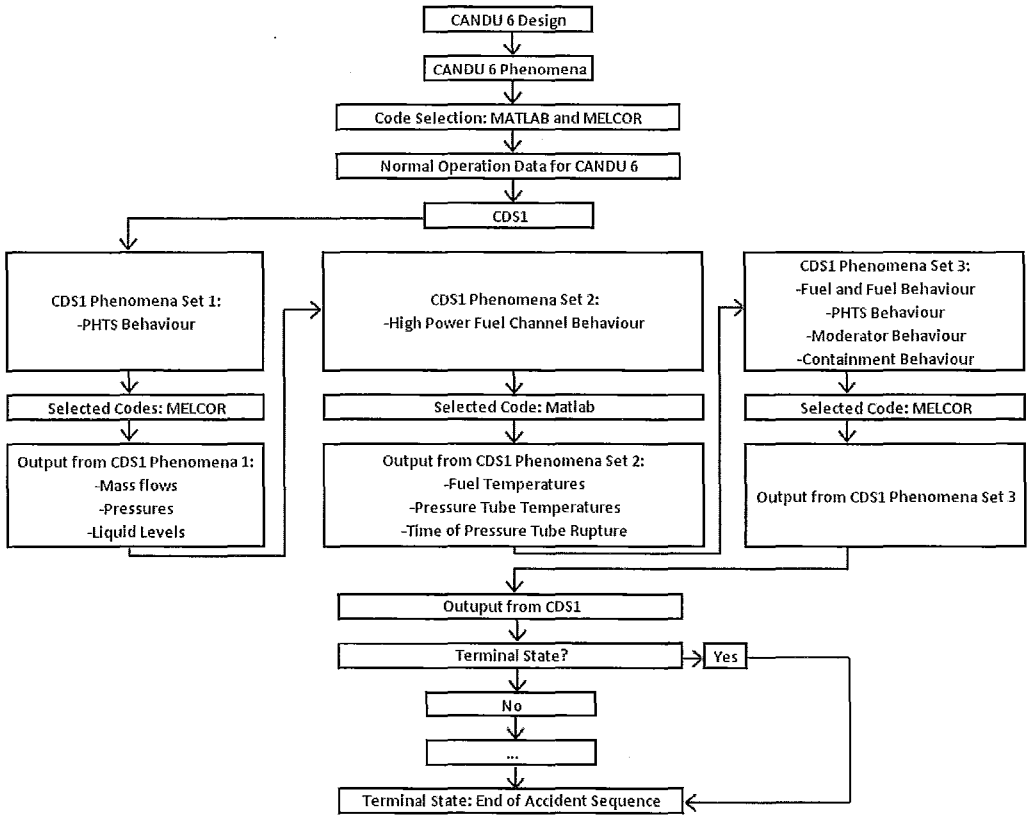

Figure 11: Coupling MATLAB and MELCOR for SBLOCA-LOECI event

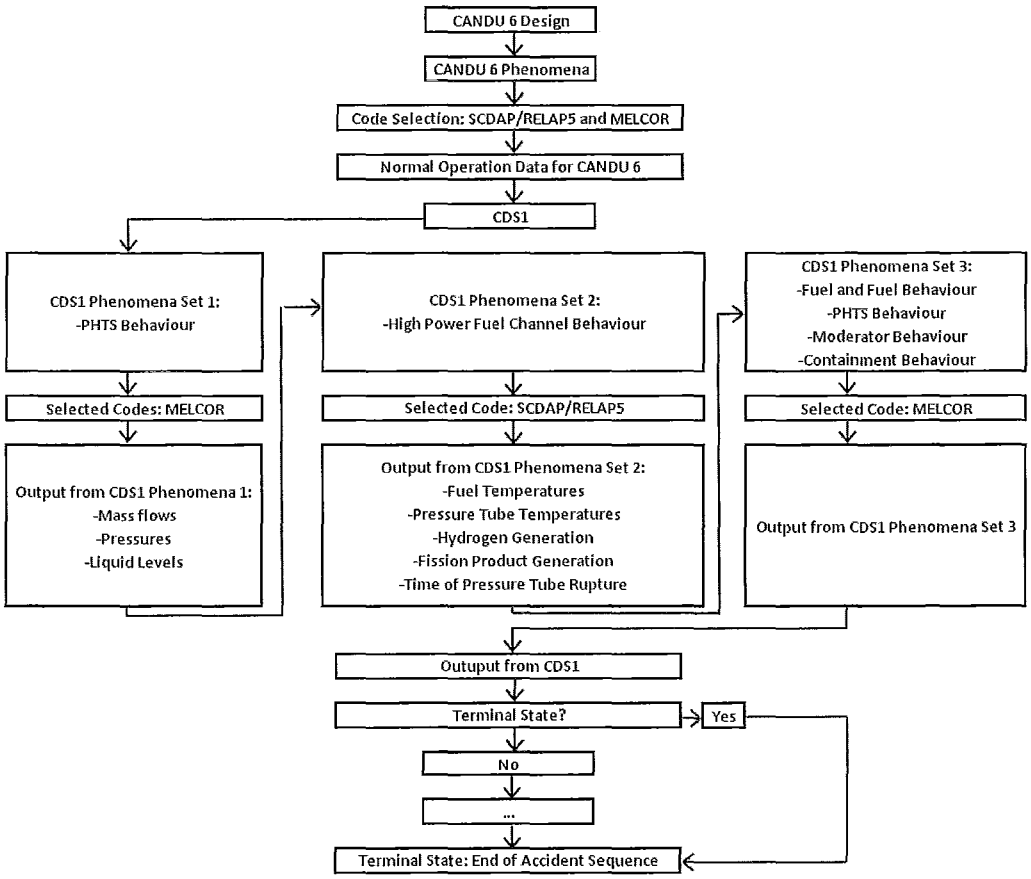

Figure 12: Coupling SCDAP/RELAP5 and MELCOR for SBLOCA-LOECI event

Table 4: Code capabilities for modelling SBLOCA-LOECI phenomena

Phenomena for SBLOCA-LOECI in CANDU 6	MATLAB Model	SCDAP/RELAP5 Model	MELCOR Model
• Single phase and two phase thermalhydraulics in the PHTS and containment thermalhydraulics	Yes	Yes	Yes
• Reactor header flow stratification	No	Yes	Yes
• Channel flow stratification	No	Yes	Yes
• Radiation heat transfer among the fuel pins, pins to the pressure tube and also from pressure tube to the calandria tube	No	Yes	No
• Pressure tube deformation by sagging or by symmetric/asymmetric ballooning	No	No	No
• Calandria Tube outer surface boiling heat transfer	Yes	Yes	Yes
• Fuel element metallurgical deformations and release of fission gas from fuel matrix	No	Yes	Yes
• Sagging of the fuel bundle	Yes	Yes	Yes
• Bundle behaviour during asymmetric fuel pin heating	No	No	No
• Steam-zircaloy-UO2 reaction and formation of the eutectic of U-Zr alloy and hydrogen generation	No	Yes	No
• Transportation of the radioactive material in the PHTS	No	No	No
• Ex-channel molten fuel-coolant (moderator) interaction	No	No	No
• Debris bed–molten pool behaviour	No	No	No

3.1. MATLAB Single Fuel Channel Model

3.1.1 Types of Thermalhydraulic Models

Generally there are three types of models used within nuclear thermalhydraulic system codes. These formulations of the mass, momentum and energy conservation equations are the homogenous equilibrium mixture (HEM) model, the drift-flux model and the two-fluid model.

The homogeneous equilibrium mixture (HEM) model is the simplest of the two-phase fluid transport models. The HEM transport equations are derived from the two-phase mixture equations by assuming that the velocity of each fluid phase is equal (homogenous) and that both phases are at saturated conditions. The assumption of equilibrium means that the thermodynamic properties of each fluid phase can be expressed as a function of saturation pressure (Reyes, 2009).

The most widely employed version of the drift-flux model uses four field equations from the elimination of one energy and one momentum equation from the original six field equations of the two-fluid model. Hence, the relative motion and energy difference between the phases should be expressed by additional constitutive equations. These effects are taken in to consideration by using a continuity equation for one of the phases and supplementing it with kinematic and phase-change constitutive equations (Chexal and Lellouche, 1985).

The two-fluid model is the most detailed and accurate formulation of the thermalhydraulic behaviour of two-phase systems. The mathematical equations for the two-fluid model are expressed by the six conservation equations consisting

of mass, momentum and energy equations for both phases (Ishii and Hibiki, 2006).

The HEM is a straightforward model to formulate and solve hence it was the model used in the development of the single fuel channel model developed in MATLAB. Although, two phase flow always involves some relative motions of one phase with respect to the other, the HEM model is assumed to be appropriate for the reactor inlet feeder stagnation break because the coolant is no longer flowing within the fuel channel. However for comparison with this HEM model, a SCDAP/RELAP5 single fuel channel model was also used to model the event since it uses the more rigorous two-fluid model.

3.1.2 Conservation Equations

The flow chart for the derivation of the general balance equation is shown in the diagram below.

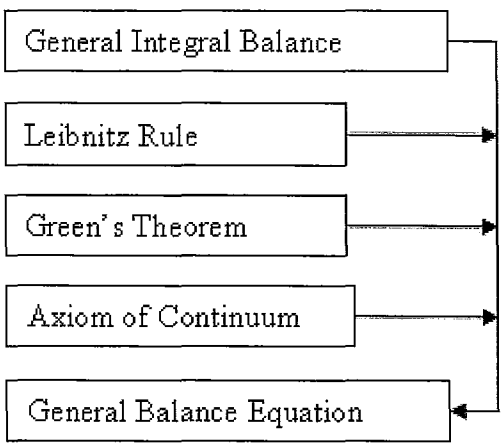

Figure 13: Derivation of general balance equation (Ishii & Hibiki, 2005, p. 14)

The general integral balance for each phase, designated by k, can be written using the fluid density ρ_k, the efflux J_k, and the body source $\square_k$ of any quantity ψ_k which is defined for a unit mass. This is expressed as the following equation:

$$\frac{d}{dt}\int_{V_m}\rho_k\psi_k dV = -\oint_{A_m} n_k \cdot J_k dA + \int_{V_m}\rho_k\phi_k dV$$

Equation 1

In this equation, V_m is a material volume with a material surface A_m. It states that the time rate of change of $\rho_k\psi_k$ in V_m is equal to the influx through A_m plus the generation with the V_m. As alluded to above, the subscript k refers to the k^{th}-phase. If the functions appearing in equation above are sufficiently smooth such that the Jacobian transformation between the material and the spatial coordinates exists, then the differential form of the balance equation can be obtained by using the Reynolds transport theorem (Ishii & Hibiki, 2005, p. 14). This is expressed as the following equation:

$$\frac{d}{dt}\int_{V_m} F_k dV = \int_{V_m}\frac{\partial F_k}{\partial t}dV + \oint_{A_m} F_k v_k \cdot n\, dA$$

Equation 2

In this equation, F_k is a general function associated with phase k and v_k represents the velocity of a fluid particle in phase k. Green's theorem gives a transformation between a certain volume and surface integral:

$$\int_V \nabla \cdot F_k dV = \oint_A n \cdot F_k dA$$

Equation 3

Hence from Equations 2 and 3 we obtain:

$$\frac{d}{dt}\int_{V_m} F_k dV = \int_{V_m}\left[\frac{\partial F_k}{\partial t} + \nabla\cdot\left(v_k F_k\right)\right]dV$$

Equation 4

Reynolds transport theorem is also sometimes called the 'Leibnitz-Reynolds transport theorem' given that it is a three dimensional generalization of the Leibnitz integral rule. The Leibnitz integral rule is given by:

$$\frac{d}{dt}\int_{V} F_k dV = \int_{V}\frac{\partial F_k}{\partial t}dV + \oint_{A} F_k u\cdot n\, dA$$

Equation 5

In this equation, V(t) is an arbitrary volume bounded by A(t) and u·n is the surface displacement velocity of A(t). Substituting Equations 3 and 4 into Equation 1 we obtain the general differential transport theorem for phase k (Ishii & Hibiki, 2005, p. 15).

$$\frac{\partial \rho_k \psi_k}{\partial t} + \nabla\cdot\left(v_k \rho_k \psi_k\right) = -\nabla\cdot J_k + \rho_k \phi_k$$

Equation 6

The first term on the left hand side of the equation above is the time rate of change of the quantity per unit volume. The second term on the left hand side of the equation is the rate of convection per unit volume. The first term on the right hand side of the equation is the surface flux. The second term on the right of the equation is the volume source. By replacing the quantity ψ_k, the efflux J_k, and the body source $\square_k$ with appropriate terms the conservation equations for mass, momentum and energy are obtained. These terms are listed in Table 5 below.

Table 5: Variable definitions for different conservation equations (Ishii & Hibiki, 2005)

Conservation Equation	ψ_k	J_k	$\square_k$
Mass	1	0	0
Momentum	u_k	$p_k I - \tau_k$	g_k
Energy	$i_k + u_k^2/2$	$q_k - T \cdot u_k$	$g_k \cdot u_k + q_k/\rho_k$

System thermalhydraulic codes are usually one dimensionally averaged. In addition, another common simplification is to consider the fluid in a two phase system as a mixture. Given that the mixture is usually contained within a structure, such as pipe, other source terms may need to be considered as well. The one dimensional mixture general balance equation is:

$$\frac{\partial \rho_k \psi_k}{\partial t} + \frac{\partial (v_k \rho_k \psi_k)}{\partial z} = -\frac{\partial J_k}{\partial z} + \rho_k \phi_k + I_m + I_w$$

Equation 7

After inserting the variables in Table 5 into Equation 7 we obtain the following conservation of mass, momentum and energy conservation equations:

$$\frac{\partial (\rho_m)}{\partial t} = -\frac{\partial (\rho_m u_m)}{\partial z}$$

Equation 8

$$\frac{\partial}{\partial t}(\rho_m u_m) = -\frac{\partial}{\partial z}\left(u_m^{\,2} \rho_m\right) - \frac{\partial P}{\partial z} - \frac{1}{A}\left[\tau_{m,W} S_{m,W}\right]$$

Equation 9

$$\frac{\partial}{\partial t}\left[A(\rho_m e_m - P)\right] = -\frac{\partial}{\partial z}(A \rho_m u_m e_m) - 2PA\frac{\partial \alpha}{\partial t} + q''_H S_H$$

Equation 10

Where,

$\rho_m, u_m, \tau_{m,W}, S_{m,W}, e_m$ are the mixture properties.

The assumptions made in deriving these there equations are:

- The flow is horizontal and one dimensional
- Internal generation of mass, momentum and energy can be neglected
- Mean values of velocity and density are assumed to exist across an area normal to flow
- The flow area is constant along the length of the channel, z
- Pressure across an area normal to the flow is uniform
- There is no removal or addition of mass through the channel walls
- Viscous dissipation of energy can be neglected
- Surface tension can be neglected
- Turbulence can be neglected
- Axial heat conduction heat transfer can be neglected
- The mechanical terms of the total enthalpy, e, are relatively small compared to the value of the specific enthalpy, h

It is worth reiterating that in obtaining the general differential transport theorem we are also assuming that a continuum exits; otherwise known as the 'continuum hypothesis'. This is a fundamental principle in thermalhydraulics. It is often impractical and unimportant to study fluid behavior on a molecular basis. Therefore, we use a macroscopic approach and define a differential volume to

represent a point in a given fluid. This involves using the average values for fluid properties at each point in space thus allowing the fluid properties to vary continuously throughout the fluid. In other words, by ignoring the behavior of individual molecules of the fluid and assuming that the fluid consists of continuous matter we can define unique values for the flow variables: P, T, V, τ, ρ, etc. For example, for statistical averages to become meaningful we must define density at a point for fluid as a continuum according to:

$$\rho = \lim_{\delta V \to \delta V'} \left(\frac{\delta m}{\delta V} \right)$$

Equation 11

Where $\delta V'$ is a differential volume that contains a sufficient number of molecules. For all liquids and for gases at atmospheric pressure, the limiting volume is about 10^{-9} mm^3 (Massoud, 2005, p. 225).

Having defined flow field variables at a point, we use partial derivatives to determine the change in such variables between two points separated by elements of length. For example, if pressure, P, is located at point x, y, z in the Cartesian coordinate system, then the pressure at a point located some distance dx, dy, and dz away is P+dP. Where,

$$dP = \left(\frac{\partial P}{\partial x} \right) dx + \left(\frac{\partial P}{\partial y} \right) dy + \left(\frac{\partial P}{\partial z} \right) dz$$

Equation 12

3.1.3 Correlations

In order to solve the mass, momentum and energy conservation equations empirical correlations are required. The required correlations to solve the equations are the single phase friction factor, fluid mixture properties or two-phase frictional multiplier, onset of significant void (OSV), void fraction, mass quality, mixture viscosity, critical heat flux (CHF) heat transfer, and post dryout (PDO) heat transfer. All thermalhydraulic correlations that are available for used within the MATLAB single fuel channel computer code are detailed in the following sections.

3.1.3.1 Single Phase Friction Factor

Two correlations were required for the single phase friction factor in order to cover the range of Reynolds numbers that could be obtained while running the computer code. A good approximation for laminar flow (Re<2300) is the Darcy friction factor (Shaughnessy, Katz, and Schaffer, 2004).

$$f = \frac{64}{\mathrm{Re}}$$

Equation 13

This correlation was also used as a rough estimate of the friction factor for Reynolds numbers between 2300 and 4000. For turbulent flow (Re>4000) the friction factor can be obtained by using the Haaland correlation (1983):

$$\frac{1}{\sqrt{f}} = -1.8\log\left[\left(\frac{(\varepsilon/D)}{3.7}\right)^{1.11} + \frac{6.9}{\mathrm{Re}}\right]$$

Equation 14

This correlation is in ± 1.5% agreement with the Colebrook-White equation (Haaland, 1983). It is beneficial to use the Haaland correlation because it is simple and quick given its explicit nature. Moreover, it is accurate given that it reduces to the appropriate limiting equations for the smooth regime and the fully rough regime. Alternatively, if we chose to iterate the Colebrook-White equation, the results would still have an error of 3-5% as compared to the experimental data (Haaland, 1983). Furthermore, unlike the Haaland correlation, Colebrook-White equation takes a large amount of time to compute. Hence, to aid functionality of the code the Haaland correlation was chosen over the Colebrook-White equation.

3.1.3.2 Mixture Fluid Properties and Two-Phase Frictional Multiplier

Generally, there are two methods that can be employed to account for two-phase friction pressure loss. One method is to define mixture fluid properties and use them to evaluate the single-phase friction factor. The second method is to use single-phase fluid properties to evaluate the friction factor and then adjust the single-phase friction factor with a two-phase frictional multiplier. Both approaches are outlined in the following sections.

3.1.3.3 Mixture Fluid Properties Approach

In the mixture fluid properties approach, mixture properties are defined in order to evaluate the conservation equations. One of these mixture properties is

the mixture density which is a weighted fraction of the saturated liquid and vapour densities using the void fraction.

$$\rho_m = \rho_l(1-\alpha) + \rho_v(\alpha)$$

Equation 15

A direct result of the HEM assumptions is that the mixture velocity is the same both the liquid and vapour velocities.

$$u_m = u_l = u_v$$

Equation 16

The shear stress for two-phase flow is defined as (Shaughnessy et al., 2004):

$$\tau_{m,W} = \frac{f_{TP}\rho_m u_m^2}{8}$$

Equation 17

Where,

$$f_{TP} = f(\mathrm{Re}_m) = f(\rho_m, u_m, \mu_m)$$

Equation 18

There are many correlations that can be used for the mixture viscosity. Nonetheless, the form of the relationship between the mixture viscosity and the quality must be chosen in order to satisfy the following limiting conditions:

$$x = 0,\ \mu_m = \mu_l;$$
$$x = 1,\ \mu_m = \mu_v$$

Three acceptable formulations are listed below (Collier and Thome, 2001,).

The McAdams Correlation,

$$\frac{1}{\mu_m} = \frac{x}{\mu_v} + \frac{(1-x)}{\mu_l}$$

Equation 19

The Cicchitti Correlation,

$$\mu_m = x\mu_v + (1-x)\mu_l$$

Equation 20

The Dukler Correlation,

$$\mu_m = \rho_m\left[xv_v\mu_v + (1-x)v_l\mu_l\right]$$

Equation 21

3.1.3.4 Two-Phase Frictional Multiplier Approach

In the two-phase frictional multiplier approach, single-phase properties are used to determine the single-phase friction factor. However, to determine the increased pressure drop due to friction of the vapour phase, the single-phase friction factor is multiplied by a two-phase frictional multiplier, $\square_{fo}^2$.

$$\tau_{m,W} = \frac{\phi_{f_o}^2 f_o \rho_l u_l^2}{8}$$

Equation 22

There are many different correlations for the two-phase frictional multiplier, $\square_{fo}^2$, but one of most accurate and widely applicable two-phase multipliers is the one provided by the Friedel correlation. This is due to the large database (25000 points) that was used to develop the two-phase multiplier for vertical upwards and horizontal flow in round tubes (Collier and Thome, 2001).

$$\phi_{lo}^2 = C_{F1} + \frac{3.24 C_{F2}}{Fr^{0.045} We^{0.035}}$$

Equation 23

Where,

$$C_{F1} = (1-x)^2 + x^2 \left(\frac{\rho_L}{\rho_V}\right)\left(\frac{f_{vo}}{f_{lo}}\right)$$

Equation 24

$$C_{F2} = x^{0.78}(1-x)^{0.24}\left(\frac{\rho_L}{\rho_V}\right)^{0.91}\left(\frac{\mu_V}{\mu_L}\right)^{0.19}\left(1-\frac{\mu_V}{\mu_L}\right)^{0.7}$$

Equation 25

$$Fr = \frac{G^2}{g D_H \rho_m^2}$$

Equation 26

$$We = \frac{G^2 D_H}{\rho_m \sigma}$$

Equation 27

Friedel found that the standard deviation of the data relative to the correlation was approximately 30%. The correlation has been recommended for use when (μ_L/μ_V) < 1000 (Collier and Thome, 2001, p. 67), which is the case for this code.

3.1.3.5 Onset of Significant Void (OSV)

The Saha-Zuber correlation (1974) for the point of net vapour generation is used to determine the OSV within the pipe.

$$x_{OSV} = -154\frac{q''_W}{\rho u h_{fg}}$$

Equation 28

This correlation was developed out of attempts to predict net vapour generation using bubble detachment models. It is good at predicting the point of OSV for Peclet number, Pe, values which are greater than 70000 (Zuber & Saha, 1974). The Peclet number is a ratio of the convective forces to diffusive forces. Given that in this problem diffusion is assumed not to occur, the Peclet number is effectively infinite and thus justifies the use of this correlation for the prediction of OSV.

3.1.3.6 Void Fractions for HEM Model

For two-phase flow, predicting the void fraction is required in order to determine the acceleration and gravitational head components of the pressure drop. It has been shown that several of void fraction correlations can be approximated by the flowing form (Carey, 2007):

$$\alpha = \left[1 + B_B\left(\frac{1-x}{x}\right)^{n1}\left(\frac{\rho_V}{\rho_L}\right)^{n2}\left(\frac{\mu_L}{\mu_V}\right)^{n3}\right]^{-1}$$

Equation 29

The constants B_B, n_1, n_2 and n_3 are listed in Table 6 below.

Table 6: Void fraction constants for general Butterworth formation (Carey, 2007)

Correlation or Model	B_B	n_1	n_2	n_3
Homogeneous Equilibrium Model	1	1	1	0
Lockhart and Martinelli	0.28	0.64	0.36	0.07
Thom	1	1	0.89	0.18
Baroczy	1	0.74	0.65	0.13

The HEM values only yield realistic results for limited conditions. The most realistic results would be expected for bubbly or dispersed droplet flows, because the slip velocity between the phases for these flow regimes is small. The Lockhart-Martinelli correlation has been shown to yield accurate results for a wide variety of two-phase flow conditions in round tubes and simple channel geometries. It is expected to yield the most realistic predictions at low pressures for adiabatic or boiling flows at low heat flux levels, given the database from which this correlation was derived. The Baroczy correlation is said to give good agreement with experimental data for a wide variety of conditions. Moreover, Baroczy found that this correlation was within ±20% agreement with a large set of experimental data (Carey, 2007).

3.1.3.7 Mass Quality

The thermodynamic equilibrium quality was obtained from the flowing expression:

$$x_{th} = \frac{h - h_l}{h_v - h_l}$$

Equation 30

The true mass quality is defined as:

$$x_m = \frac{M_v}{M_{total}}$$

Equation 31

Given that the true mass quality expression cannot be solved directly without knowing the void fraction, a correlation converting the thermodynamic

equilibrium quality to true mass quality can be employed. An empirical expression of the mass quality as a function of the thermodynamic quality is given below (Ahmad, 1970).

$$x_m = \frac{x_{th} - x_d e^{(x_{th}/x_d - 1)}}{1 - x_d e^{(x_{th}/x_d - 1)}}$$

Equation 32

Where,

$$x_d = -(C_p \Delta T_d / h_{fg})$$

Equation 33

$$\Delta T_d = \frac{\phi D_e}{2.44 k_l \left(\frac{GD_e}{\mu}\right)^{1/2} \left(\frac{C_p \mu}{k_l}\right)^{1/3} \left(\frac{h_{in}}{h_l}\right)^{1/3} \left(\frac{h_{fg}}{h_l}\right)^{1/3}}$$

Equation 34

This formulation is based on the assumptions that bubble condensation can be neglected and that subcooled boiling begins at the point of bubble detachment (Ahmad, 1970).

3.1.3.8 CHF Heat Transfer

In order to predict the time at which CHF occurs three different correlations were employed: Biasi, Katto and Bowering (Collier and Thome, 2001).

The Biasi correlation,

$$\max = \left[\phi_{CRIT} = \frac{1.883 \times 10^3}{D^n G^{1/6}} \left[\frac{f(p)}{G^{1/6}} - x(z) \right] \quad , \quad \phi_{CRIT} = \frac{3.78 \times 10^3 h(p)}{D^n G^{0.6}} \left[1 - x(z) \right] \right]$$

Equation 35

The Biasi correlation has the advantage of being continuous with respect to the variable pressure in the system with little loss of accuracy. CHF is determined by the higher of the two values presented in Equation 35 above. The error was 7.26% for the 4500 data points examined and 85.5% of all points were correlated within ±10%.

The Katto correlation,

$$\phi_{CRIT} = XG(h_{LV} + K(\Delta i_{SUB})_i)$$

Equation 36

The Katto correlation presents CHF as a function of X and K. X and K are in turn functions of three dimensionless groupings.

$$Z' = z / D$$

Equation 37

$$R' = \rho_V / \rho_L$$

Equation 38

$$W' = \left[\frac{\sigma \rho_L}{G^2 z} \right]$$

Equation 39

The Bowring correlation,

$$\phi_{CRIT} = \frac{A'+DG(\Delta i_{SUB})_i/4}{C'+z}$$

Equation 40

The Bowring correlation is based on the 'local conditions hypothesis', which suggests that the CHF is solely a function of the mass quality at the point of overheating. CHF is a function of A' and C', which are in turn functions of F_1, F_2, F_3, and F_4. Values of F_1, F_2, F_3, and F_4 are generated by linearly interpolating with respect to the pressure.

Collier and Thome (2001) compare the Katto and Bowring CHF correlations to different data sets. The performance of each CHF correlation is listed below in Table 7 for two of the different data sets.

Table 7: Comparison of Bowring and Katto correlations with experimental data sets (Collier and Thome, 2001)

Fluid	Data Range	No. of data	Correlation	Deviation (%)		No. of data with deviation >30%
				Mean	Average	
Water	All data	427	Katto	16.1	+3.1	51
Water	All data	427	Bowring	18.6	-9.6	86
Water	Verified range of Bowring correlation	251	Katto	14.1	-3.2	17
Water	Verified range of Bowring correlation	251	Bowring	11.7	-3.9	19

It can be seen in Table 7 that the Katto correlation can outperform the Bowring correlation in predicting CHF data for water. Nonetheless, both are available for use in the computer code.

3.1.3.9 PDO Heat Transfer

In order to predict the wall temperature for post dryout three different correlations were employed: Groeneveld, Dougall and Rohsenow, and Groeneveld and Delorme (Carey, 2007). The Groeneveld correlation,

$$h = \frac{a\,k_V}{D}\left[\left(\frac{GD}{\mu_V}\right)\left(x + \frac{\rho_V}{\rho_L}(1-x)\right)\right]^b \mathrm{Pr}_{V,W}^{c}\, Y^d$$

Equation 41

Where,

$$Y = 1 - 0.1\left(\frac{\rho_V}{\rho_L} - 1\right)^{0.4}(1-x)^{0.4}$$

Equation 42

The values of the constants a, b, c and d for tubes are 0.00109, 0.989, 1.41 and -1.51 respectively. This correlation is reported to match experimental data to an RMS (Root Mean Squared) error of 11.5%.

The Dougall and Rohsenow correlation,

$$h = \frac{0.023\,k_V}{D}\left[\left(\frac{GD}{\mu_V}\right)\left(x + \frac{\rho_V}{\rho_L}(1-x)\right)\right]^{0.8} \mathrm{Pr}_{V,sat}^{0.8}$$

Equation 43

Like the Groeneveld correlation, the Dougall and Rohsenow correlation is similar to the relation that came from the homogeneous flow model. A major deficiency of these over simplified correlation is that they do not account for non-equilibrium conditions (Carey, 2007).

The Groeneveld and Delorme Correlation,

$$h = \frac{0.008348\,k_{v,f}}{D}\left[\left(\frac{GD}{\mu_V}\right)\left(x + \frac{\rho_V}{\rho_L}(1-x)\right)\right]^{0.8774} \mathrm{Pr}_{V,sat}^{0.6112}$$

Equation 44

Groeneveld and Delorme proposed a modified correlation to account for the non-equilibrium effects. The modified equilibrium correlation employs a single-phase heat transfer correlation, modified for two-phase flow. Once the heat transfer coefficient is obtained from one of the three aforementioned correlations the wall temperature itself can be directly computed using Newton's law of cooling.

$$T_W = T_{SAT} + \frac{q''}{h}$$

Equation 45

3.1.4 Discretization of Equations and Numerical Method

Since the semi-implicit method for pressure linked equations (SIMPLE) algorithm was first proposed by Patankar and Spalding (1972), it has been widely applied to the field of computational fluid dynamics (CFD) and numerical heat transfer (NHT). Over the last three decades at least ten variants have been proposed to improve the convergence performance, and these algorithms consist of the 'SIMPLE-type' (also called 'SIMPLE-series' or 'SIMPLE-family') solution algorithm. Today the SIMPLE-type algorithm is the most popular algorithm for solving incompressible Navier-Stokes equations with primitive variables. Among the different variants, the most often used algorithms are

SIMPLE, SIMPLE revised (SIMPLER), SIMPLE consistent (SIMPLEC) and SIMPLE extrapolation (SIMPLEX). It has been shown that SIMPLE and SIMPLEC have the least computational time whereas SIMPLEX and SIMPLEC have superior robustness (Zeng and Tao, 2003). For these reasons the specific algorithm used for the solution of the conservation equations for the MATLAB single fuel channel model is SIMPLEC.

One method to solve the coupled, non-linear, partial differential conservation equations is to linearize and discretize them in space and time. However, if we were to discretize the conservation equations such that every variable were calculated at each grid point, unrealistic solutions could be obtained. For example, the momentum equation could generate a pressure difference between two alternate grid points and not between two adjacent ones, which overall is not a physically realistic solution to the problem (Patankar, 1980). Similarly, unrealistic solutions could also be obtained for the velocities in the continuity equation and the enthalpies in the energy equation. These difficulties are usually associated with the first derivatives of the Taylor series expansion (Patankar, 1980). The staggered grid method can be used to eliminate these problems, which was first used by Harrow and Welch (1965). This method calculates the velocities at the faces of the pressure, enthalpy and fluid property control volumes and vice versa. The staggered grid representation for one dimensional flow can be seen in Figure 14 below.

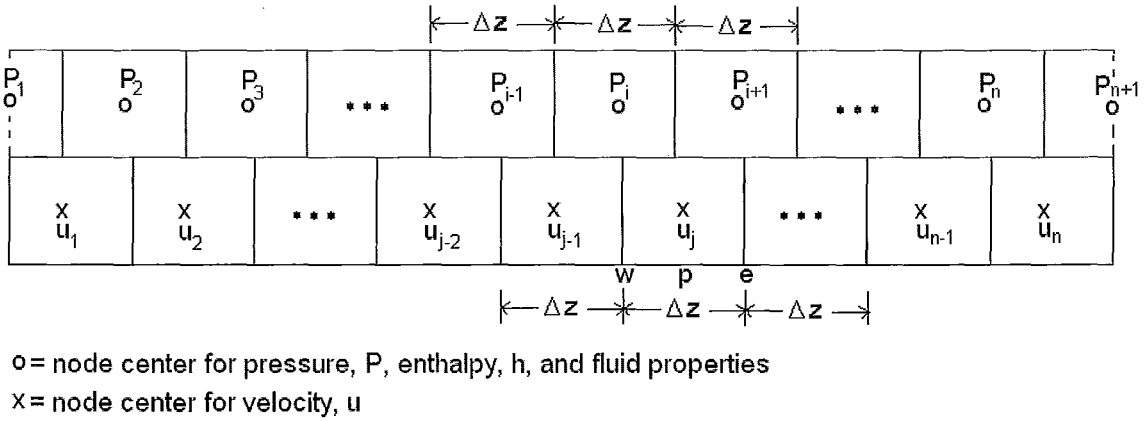

Figure 14: Staggered grid discretization for the MATLAB single fuel channel model

An alternative to the staggered grid discretization is the co-located grid discretization. Three test cases using orthogonal rectilinear grids were studied by Peric, Kessler and Scheuerer (1988) comparing the staggered and collocated grids. The results of the computations demonstrate that the convergence rate, dependency on under-relation parameters, computational effort and accuracy are almost identical for both solution methods. Hence, for the purposes of the MATLAB single fuel channel model either method could have been used. The original staggered grid method employed by Patankar was used. However, it is worth mentioning that if multigrid techniques and non-orthogonal grids are considered the co-located grid converges faster in some cases and has logistical advantages. In these cases the co-located grid should be used.

3.1.4.1 Steady State Case

To solve the transient conservation equations, first initial conditions are needed. These are generated from the steady state case. The set of steady state equations are not listed in this section because they are just a simplified set of the

transient equations. Specifically, the steady state equations can be obtained directly from the transient equations, by setting the derivative time terms (i.e. terms including Δt) equal to zero, such that the parameters do not change with time. The discretization of the transient equations and the numerical methods used to solve these equations are presented below.

3.1.4.2 Transient Case

There are three ways to develop the transient set of conservations equations: fully-explicit, fully-implicit or semi-implicit. First, the fully-explicit method evaluates the system variables at the current time step (i.e. at time t). This method is good in that these variables are known however; it has an associated limitation in the Courant limit, which is defined as:

$$\Delta t < \frac{\Delta z}{u}$$

Equation 46

The Courant limit tells us that the distance the fluid travels in one time step should not be greater than the discretization. Hence, one is restricted by a very small time step, which detracts from the functionality of the code. For the fully implicit method, the system variables are calculated at the next time step (i.e. at time $t+\Delta t$). However, the drawback here is that the method is more time consuming in some cases than the fully-explicit method. A semi-implicit method is in between a fully-explicit and a fully-implicit method; evaluating some variables at the current time step and some variables at the next time step. Nonetheless, the inherent robustness of the implicit method makes it the method

of choice for this program. Thus, as will be seen in the following sections, the development of the code is maintained as fully-implicit as possible.

3.1.4.3 Momentum Conservation & Generation of Velocity Vector

Referring to the Equation 9 and Figure 14, the general discretized momentum conservation equation is:

$$\left(\frac{\left(\rho_j^{t+\Delta t}u_j^{t+\Delta t}\right)-\left(\rho_j^{t}u_j^{t}\right)}{\Delta t}\right)=-\left(\frac{\left(\rho_e^{t+\Delta t}u_e^{t+\Delta t}\right)u_e^{t+\Delta t}-\left(\rho_w^{t+\Delta t}u_w^{t+\Delta t}\right)u_w^{t+\Delta t}}{\Delta z}\right)-\left(\frac{\Delta P_j^{\,t+\Delta t}}{\Delta z}\right)$$
$$-\left(\rho_j^{t+\Delta t}g\sin\theta\right)-\left(\frac{1}{A}\left(\tau_{W,j}^{t+\Delta t}S_W\right)\right)$$

Equation 47

This equation is linearized by assuming that ρu is a constant. Multiplying through by A and Δz the equation becomes:

$$\frac{A\Delta z}{\Delta t}\left(\rho_j^{t+\Delta t}u_j^{t+\Delta t}\right)-\frac{A\Delta z}{\Delta t}\left(\rho_j^{t}u_j^{t}\right)=-A\left(\rho_e^{t+\Delta t}u_e^{t+\Delta t}\right)u_e^{t+\Delta t}+A\left(\rho_w^{t+\Delta t}u_w^{t+\Delta t}\right)u_w^{t+\Delta t}-A\Delta P_j^{\,t+\Delta t}$$
$$-A\rho_j^{t+\Delta t}g\sin\theta\Delta z-\tau_{W,j}^{t+\Delta t}S_W\Delta z$$

Equation 48

As seen in Equation 22 above, the shear stress at the wall is a function of the velocity of the current node,

$$\tau_{W,j}^{t+\Delta t}=\frac{f\left(\rho_j^{t+\Delta t}\left|u_j^{t+\Delta t}\right|\right)u_j^{t+\Delta t}}{8}$$

Equation 49

Substitution of Equation 49 into the 48 yields:

$$\frac{A\Delta z}{\Delta t}\left(\rho_j^{t+\Delta t}u_j^{t+\Delta t}\right)-\frac{A\Delta z}{\Delta t}\left(\rho_j^{t}u_j^{t}\right)=-A\left(\rho_e^{t+\Delta t}u_e^{t+\Delta t}\right)u_e^{t+\Delta t}+A\left(\rho_w^{t+\Delta t}u_w^{t+\Delta t}\right)u_w^{t+\Delta t}-A\Delta P_j^{t+\Delta t}$$
$$-A\rho_j^{t+\Delta t}g\sin\theta\Delta z-\frac{f\left(\rho_j^{t+\Delta t}\left|u_j^{t+\Delta t}\right|\right)u_j^{t+\Delta t}}{8}S_W\Delta z$$

Equation 50

Now the question is what are the values for u_e and u_w? This is dependent on the differencing scheme used. Noting that for large Peclet numbers the central differencing scheme is unstable, the upwind differencing scheme is used since it is inherently stable (Patankar, 1980). The values of u_e and u_w are equal to the values of u at the grid points on the upwind (or upstream) sides of the respective faces, see Figure 14. Thus,

$$u_e^{t+\Delta t}=u_j^{t+\Delta t},\quad if\ A\rho_{j+1}^{t+\Delta t}u_{j+1}^{t+\Delta t}>0$$
$$u_e^{t+\Delta t}=u_{j+1}^{t+\Delta t},\quad if\ A\rho_{j+1}^{t+\Delta t}u_{j+1}^{t+\Delta t}<0$$
$$and$$
$$u_w^{t+\Delta t}=u_{j-1}^{t+\Delta t},\quad if\ A\rho_j^{t+\Delta t}u_{j-1}^{t+\Delta t}>0$$
$$u_w^{t+\Delta t}=u_j^{t+\Delta t},\quad if\ A\rho_j^{t+\Delta t}u_{j-1}^{t+\Delta t}<0$$

Hence,

$$A\left(\rho_e^{t+\Delta t}u_e^{t+\Delta t}\right)u_e^{t+\Delta t}=u_j^{t+\Delta t}\max\left[A\rho_{j+1}^{t+\Delta t}u_{j+1}^{t+\Delta t},0\right]-u_{j+1}^{t+\Delta t}\max\left[-A\rho_{j+1}^{t+\Delta t}u_{j+1}^{t+\Delta t},0\right]$$

Equation 51

$$A\left(\rho_w^{t+\Delta t}u_w^{t+\Delta t}\right)u_w^{t+\Delta t}=u_{j-1}^{t+\Delta t}\max\left[A\rho_j^{t+\Delta t}u_{j-1}^{t+\Delta t},0\right]-u_j^{t+\Delta t}\max\left[-A\rho_j^{t+\Delta t}u_{j-1}^{t+\Delta t},0\right]$$

Equation 52

Once Equation 52 and 51 are substituted into Equation 50, the following general expression is obtained:

$$-a_{j+1}^{t+\Delta t}u_{j+1}^{t+\Delta t}+a_{j}^{t+\Delta t}u_{j}^{t+\Delta t}-a_{j-1}^{t+\Delta t}u_{j-1}^{t+\Delta t}=b$$

Equation 53

Where,

$$a_{j+1}^{t+\Delta t}=\max\left[-A\rho_{j+1}^{t+\Delta t}u_{j+1}^{t+\Delta t},0\right]$$

$$a_{j-1}^{t+\Delta t}=\max\left[A\rho_{j}^{t+\Delta t}u_{j-1}^{t+\Delta t},0\right]$$

$$a_{j}^{t+\Delta t}=\max\left[A\rho_{j+1}^{t+\Delta t}u_{j+1}^{t+\Delta t},0\right]+\max\left[-A\rho_{j}^{t+\Delta t}u_{j-1}^{t+\Delta t},0\right]-\frac{f\left(\rho_{j}^{t+\Delta t}\left|u_{j}^{t+\Delta t}\right|\right)u_{j}^{t+\Delta t}}{8}S_{W}\Delta z+\frac{A\Delta z\rho_{j}^{t+\Delta t}}{\Delta t}$$

$$b=-A\Delta P_{j}^{t+\Delta t}-A\rho_{av,j}^{t+\Delta t}g\sin\theta\Delta z+\frac{A\Delta z\rho_{j}^{t}u_{j}^{t}}{\Delta t}$$

In order to solve this system of equations, one has to make an initial guess at the axial pressure profile and axial velocity profile. Once this is done the set of equations can be solved for the velocity, u, which can be represented using the following matrix notation:

$$Au=b$$

Equation 54

$$u=A^{-1}b$$

Equation 55

However, given that we have linearized a non-linear equation our solution will have to be iterative. A good convergence criterion would be to compare the velocity vector from the previous iteration to the updated velocity and once the 'norm' of the difference between the two is less than a certain value, ε_u, the solution has converged. Let the norm be defined as the maximum value of the

standard deviation of a vector. Specifically, the flowing convergence criterion was used in the computer code:

$$norm[u_{old} - u_{new}] < \varepsilon_u = 10^{-3}$$

Equation 56

In other words, this means to iterate until the norm of the difference between the old and new velocity vectors is less than ε_u, which is equal to 10^{-3}.

The new velocity is made to be a function of both the old and new velocity in order to relax the solution. The weighted equation for the velocity used in the next iteration is:

$$u = ru_{new} + (1 - r)u_{old}$$

Equation 57

Where, r is the relaxation factor or the proportion of the new velocity guess that will be used for the next iteration. This is done so that the velocity will eventually converge. If the relaxation is not done, the new velocity could 'jump' around the solution preventing the program from converging.

The above discretization allows one to obtain a converged solution of the velocity vector. Nonetheless, we have assumed a pressure profile, thus this is just an educated guess at the velocity vector. To determine the velocity for given fluid conditions, we have to correct the pressure by some value. To determine the pressure correction required we turn to the mass conservation equation in order to determine the mass defect which will indicate how well we have guessed.

3.1.4.4 Mass Conservation and Pressure Correction

As we have seen above, the momentum conservation equation to determine the real velocities is:

$$-a_{j+1}^{t+\Delta t}u_{j+1}^{t+\Delta t}+a_j^{t+\Delta t}u_j^{t+\Delta t}-a_{j-1}^{t+\Delta t}u_{j-1}^{t+\Delta t}=-A\Delta P_j^{t+\Delta t}-A\rho_{av,j}^{t+\Delta t}g\sin\theta\Delta z+\frac{A\Delta z\rho_j^t u_j^t}{\Delta t}$$

Equation 58

However, as already mentioned we only have guesses at the velocities from the momentum balance given the guessed pressure profile. In order to distinguish that these are guesses we will implement the notation, u*, which needs to be corrected by a velocity, u'. The same notation will be used for the pressure. Thus,

$$u=u^*+u'$$

Equation 59

$$P=P^*+P'$$

Equation 60

In order to obtain an expression for the correction required we subtract the real equation from the guessed equation to obtain the correction equation:

$$\begin{aligned}
&-a_{j+1}^{t+\Delta t}u_{j+1}^{t+\Delta t}+a_j^{t+\Delta t}u_j^{t+\Delta t}-a_{j-1}^{t+\Delta t}u_{j-1}^{t+\Delta t}=-A\Delta P_j^{t+\Delta t}-A\rho_{av,j}^{t+\Delta t}g\Delta z+\frac{A\Delta z\rho_j^t u_j^t}{\Delta t}\\
&(-)\quad -a_{j+1}^{t+\Delta t}u_{j+1}^{*,t+\Delta t}+a_j^{t+\Delta t}u_j^{*,t+\Delta t}-a_{j-1}^{t+\Delta t}u_{j-1}^{*,t+\Delta t}=-A\Delta P_j^{*,t+\Delta t}-A\rho_{av,j}^{t+\Delta t}g\Delta z+\frac{A\Delta z\rho_j^t u_j^t}{\Delta t}\\
&\text{---}\\
&-a_{j+1}^{t+\Delta t}u_{j+1}^{',t+\Delta t}+a_j^{t+\Delta t}u_j^{',t+\Delta t}-a_{j-1}^{t+\Delta t}u_{j-1}^{',t+\Delta t}=-A\Delta P_j^{',t+\Delta t}
\end{aligned}$$

Equation 61

Given that the effect of the a_{j+1} and a_{j-1} terms are neglected in the SIMPLE algorithm (Patankar, 1980), this equation reduces to:

$$a_j^{t+\Delta t} u_j'^{,t+\Delta t} = -A\Delta P_j'^{,t+\Delta t}$$

Equation 62

Referring to the mass conservation equation, Equation 8 and Figure 14 above, the discretized mass conservation can be written as:

$$\frac{\rho^{t+\Delta t} - \rho^t}{\Delta t} = \frac{\rho_e^{t+\Delta t} u_e^{t+\Delta t} - \rho_w^{t+\Delta t} u_w^{t+\Delta t}}{\Delta z}$$

Equation 63

Multiplying through by Δz we get:

$$\frac{\Delta z}{\Delta t}\left(\rho^{t+\Delta t} - \rho^t\right) = \rho_e^{t+\Delta t} u_e^{t+\Delta t} - \rho_w^{t+\Delta t} u_w^{t+\Delta t}$$

Equation 64

Knowing that:

$$u_e = u_e{}^* + u_e{}'$$

Equation 65

$$u_w = u_w{}^* + u_w{}'$$

Equation 66

We can substitute Equation 66 and 65 into Equation 64 to obtain:

$$\rho_w^{t+\Delta t} u_w'^{,t+\Delta t} - \rho_e^{t+\Delta t} u_e'^{,t+\Delta t} = \rho_e^{t+\Delta t} u_e^{*,t+\Delta t} - \rho_w^{t+\Delta t} u_w^{*,t+\Delta t} + \frac{\Delta z}{\Delta t}\left(\rho^t - \rho^{t+\Delta t}\right)$$

Equation 67

Re-writing the momentum conservation correction equation:

$$u_j^{',t+\Delta t} = \frac{-A\Delta P_j^{',t+\Delta t}}{a_j^{t+\Delta t}}$$

Equation 68

This result is derived from Figure 15 below.

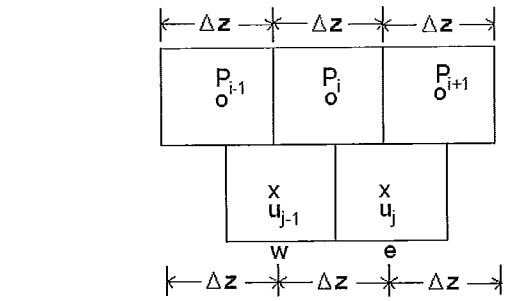

o = node center for pressure, P, enthalpy, h, and fluid properties
x = node center for velocity, u

Figure 15: Staggered grid discretization for pressure correction

Thus using Equation 68 and Figure 15 we can obtain expressions for u_w and u_e:

$$u_w^{',t+\Delta t} = u_{j-1}^{',t+\Delta t} = \frac{-A(P_j^{',t+\Delta t} - P_{j-1}^{',t+\Delta t})}{a_{j-1}^{t+\Delta t}}$$

Equation 69

$$u_e^{',t+\Delta t} = u_j^{',t+\Delta t} = \frac{-A(P_{j+1}^{',t+\Delta t} - P_j^{',t+\Delta t})}{a_j^{t+\Delta t}}$$

Equation 70

Substitution of Equation 69 and 70 into 68 yields,

$$\rho_{j-1}^{t+\Delta t}\left(\frac{-A(P_j^{',t+\Delta t}-P_{j-1}^{',t+\Delta t})}{a_{j-1}^{t+\Delta t}}\right)-\rho_j^{t+\Delta t}\left(\frac{-A(P_{j+1}^{',t+\Delta t}-P_j^{',t+\Delta t})}{a_j^{t+\Delta t}}\right)$$
$$=\rho_j^{t+\Delta t}u_j^{*,t+\Delta t}-\rho_{j-1}^{t+\Delta t}u_{j-1}^{*,t+\Delta t}+\frac{\Delta z}{\Delta t}\left(\rho^{t}-\rho^{t+\Delta t}\right)$$

Equation 71

Letting,

$$d_j^{t+\Delta t}=\frac{A}{a_j^{t+\Delta t}}$$

Equation 72

Substitution of Equation 72 into 71 yields,

$$-\rho_{j-1}^{t+\Delta t}d_{j-1}^{t+\Delta t}(P_j^{',t+\Delta t}-P_{j-1}^{',t+\Delta t})+\rho_j^{t+\Delta t}d_j^{t+\Delta t}(P_{j+1}^{',t+\Delta t}-P_j^{',t+\Delta t})=\rho_j^{t+\Delta t}u_j^{*,t+\Delta t}-\rho_{j-1}^{t+\Delta t}u_{j-1}^{*,t+\Delta t}+\frac{\Delta z}{\Delta t}\left(\rho_j^{t}-\rho_j^{t+\Delta t}\right)$$

Equation 73

Expanding, collecting like terms and rearranging,

$$\rho_j^{t+\Delta t}d_j^{t+\Delta t}P_{j+1}^{',t+\Delta t}-(\rho_{j-1}^{t+\Delta t}d_{j-1}^{t+\Delta t}+\rho_j^{t+\Delta t}d_j^{t+\Delta t})P_j^{',t+\Delta t}+\rho_{j-1}^{t+\Delta t}d_{j-1}^{t+\Delta t}P_{j-1}^{',t+\Delta t}=\rho_j^{t+\Delta t}u_j^{*,t+\Delta t}-\rho_{j-1}^{t+\Delta t}u_{j-1}^{*,t+\Delta t}+\frac{\Delta z}{\Delta t}\left(\rho_j^{t}-\rho_j^{t+\Delta t}\right)$$

Equation 74

Where,

$$d_j=\frac{A}{a_p(j,j)}\ and\ d_{j-1}=\frac{A}{a_p(j-1,j-1)}$$

This is now in the tri-diagonal form we have seen before:

$$b_{j+1}^{t+\Delta t}P_{j+1}^{',t+\Delta t}+b_j^{t+\Delta t}P_j^{',t+\Delta t}+b_{j-1}^{t+\Delta t}P_{j-1}^{',t+\Delta t}=c$$

Equation 75

The set of equations can now be solved for P', which can be represented in matrix notation:

$$BP' = c$$

Equation 76

$$P' = B^{-1}c$$

Equation 77

Where,

$$b_{j+1} = \rho_j^{t+\Delta t} d_j^{t+\Delta t}$$
$$b_{j-1} = \rho_{j-1}^{t+\Delta t} d_{j-1}^{t+\Delta t}$$
$$b_j = -(\rho_j^{t+\Delta t} d_j^{t+\Delta t} + \rho_{j-1}^{t+\Delta t} d_{j-1}^{t+\Delta t})$$
$$c = \rho_j^{t+\Delta t} u_j^{*,t+\Delta t} - \rho_{j-1}^{t+\Delta t} u_{j-1}^{*,t+\Delta t} + \frac{\Delta z}{\Delta t}\left(\rho_j^t - \rho_j^{t+\Delta t}\right)$$

Given that these are corrected pressures, and that the pressures are actually known at the boundaries, no boundary conditions are needed for the c-vector. This will yield the pressure correction vector which can be used to update the pressure profile.

In order to assure convergence, the relaxation factor is used again. The pressures are made to be a function of both the old and the corrected values in order to relax the solution. The weighted equations for the velocity and the pressures are:

$$P_{new} = P_{old} + rP'$$

Equation 78

Where, r is the relaxation factor or amount of the pressure correction that will be used for the next iteration.

The mass defect is summed for every c-vector until the defect is less than a given value, $\varepsilon_{p'}$. At this point the solution is considered to have converged. Specifically, the flowing convergence criterion was used:

$$norm[defect] < \varepsilon_{p'} = 10^{-3}$$

Equation 79

In other words, this means to iterate until the norm of the defect is less ε_p.

3.1.4.5 SIMPLE-C Algorithm

In section 3.1.4.4 above, the a_{j+1} and a_{j-1} in Equation 61 were neglected as per Patankar's SIMPLE algorithm (1980). However, the algorithm can be improved by making an adjustment for this approximation. The SIMPLE-C algorithm is one way to improve the algorithm (Zeng and Tao, 2003).

The equations and sequence of steps in the SIMPLEC algorithm are identical to those in SIMPLE with the following exceptions (Doorball and Raithby, 1984):

1. The d's are computed from Equation 80 below.
2. These d's replace the previous d's in the P' coefficients and in the velocity correction equation.
3. P' should not be under-relaxed.

$$d_j^{t+\Delta t} = \frac{A}{a_j^{t+\Delta t} - \sum a_{nb}^{t+\Delta t}}$$

Equation 80

Where,

$$\sum a_{nb}^{t+\Delta t} = \left(a_{j-1}^{t+\Delta t} + a_{j+1}^{t+\Delta t}\right)$$

Equation 81

3.1.4.6 Energy Conservation and Fluid Properties

Referring to Equation 10 for energy conservation equation and Figure 14, the general discretized energy conservation equation is:

$$\left(\frac{A\left(\rho_j^{t+\Delta t} e_j^{t+\Delta t} - P_j^{t+\Delta t}\right) - A\left(\rho_j^t e_j^t - P_j^t\right)}{\Delta t}\right) = -\left(\frac{A\left(\rho_e^{t+\Delta t} u_e^{t+\Delta t}\right) e_e^{t+\Delta t} - A\left(\rho_w^{t+\Delta t} u_w^{t+\Delta t}\right) e_w^{t+\Delta t}}{\Delta z}\right) - 2P^{t+\Delta t} A \frac{\alpha^{t+\Delta t} - \alpha^t}{\Delta t} + q''_H S_H$$

Equation 82

Multiplying through by Δz and rearranging the equation becomes:

$$\frac{A\Delta z}{\Delta t}\left(\rho_j^{t+\Delta t} e_j^{t+\Delta t}\right) = -\left(\left(\rho_e^{t+\Delta t} u_e^{t+\Delta t}\right) e_e^{t+\Delta t} - \left(\rho_w^{t+\Delta t} u_w^{t+\Delta t}\right) e_w^{t+\Delta t}\right) + q''_H S_H \Delta z + \frac{A\Delta z}{\Delta t} \rho_j^t e_j^t - \frac{A\Delta z}{\Delta t}\left(P_j^t - P_j^{t+\Delta t}\right) + \frac{2P^{t+\Delta t} A\Delta z}{\Delta t}\left(\alpha^t - \alpha^{t+\Delta t}\right)$$

Equation 83

We now have to determine the values of e_e and e_w as was done in the case of velocity in the momentum equation. The values of e_e and e_w are equal to the values of e at the grid points on the upwind (or upstream) sides of the respective faces. (Figure 14) Thus,

$$e_e^{t+\Delta t} = e_j^{t+\Delta t}, \quad if\ A\rho_{av,j}^{t+\Delta t} u_j^{t+\Delta t} > 0$$
$$e_e^{t+\Delta t} = e_{j+1}^{t+\Delta t}, \quad if\ A\rho_{av,j}^{t+\Delta t} u_j^{t+\Delta t} < 0$$
$$and$$
$$e_w^{t+\Delta t} = e_{j-1}^{t+\Delta t}, \quad if\ A\rho_{av,j-1}^{t+\Delta t} u_{j-1}^{t+\Delta t} > 0$$
$$e_w^{t+\Delta t} = e_j^{t+\Delta t}, \quad if\ A\rho_{av,j-1}^{t+\Delta t} u_{j-1}^{t+\Delta t} < 0$$

Hence,

$$A\left(\rho_e^{t+\Delta t} u_e^{t+\Delta t}\right) e_e^{t+\Delta t} = e_j^{t+\Delta t} \max\left[A\rho_{av,j}^{t+\Delta t} u_j^{t+\Delta t}, 0\right] - e_{j+1}^{t+\Delta t} \max\left[-A\rho_{av,j}^{t+\Delta t} u_j^{t+\Delta t}, 0\right]$$

Equation 84

$$A\left(\rho_w^{t+\Delta t} u_w^{t+\Delta t}\right) e_w^{t+\Delta t} = e_{j-1}^{t+\Delta t} \max\left[A\rho_{av,j}^{t+\Delta t} u_{j-1}^{t+\Delta t}, 0\right] - e_j^{t+\Delta t} \max\left[-A\rho_{av,j}^{t+\Delta t} u_{j-1}^{t+\Delta t}, 0\right]$$

Equation 85

Once Equation 84 and 85 are substituted into Equation 83 the following general expression is obtained:

$$-c_{j+1}^{t+\Delta t} e_{j+1}^{t+\Delta t} + c_j^{t+\Delta t} e_j^{t+\Delta t} - c_{j-1}^{t+\Delta t} e_{j-1}^{t+\Delta t} = d$$

Equation 86

The set of equations can now be solved for e, which can be represented in matrix notation:

$$Ce = d$$

Equation 87

$$e = C^{-1} d$$

Equation 88

Where,

$$c_{j+1}^{t+\Delta t} = \max\left[-A\rho_{m,j}^{t+\Delta t}u_{m,j}^{t+\Delta t},0\right]$$
$$c_{j-1}^{t+\Delta t} = \max\left[A\rho_{m,j+1}^{t+\Delta t}u_{m,j-1}^{t+\Delta t},0\right]$$
$$c_{j}^{t+\Delta t} = \max\left[A\rho_{m,j}^{t+\Delta t}u_{m,j}^{t+\Delta t},0\right]+\max\left[-A\rho_{m,j-1}^{t+\Delta t}u_{m,j-1}^{t+\Delta t},0\right]+\frac{A\Delta z\rho_{m,j}^{t+\Delta t}}{\Delta t}$$
$$d = q''_{H}S_{H}+\frac{A\Delta z}{\Delta t}\rho_{m,j}^{t}e_{m,j}^{t}+\frac{A\Delta z}{\Delta t}\left(P_{j}^{t}-P_{j}^{t+\Delta t}\right)+\frac{2P^{t+\Delta t}A\Delta z}{\Delta t}\left(\alpha^{t}-\alpha^{t+\Delta t}\right)$$

In order to assure convergence, the concept of the relaxation factor is used again. Where, r is the relaxation factor or amount of the new enthalpy value that will be used for the next iteration.

$$e_{new} = re+(1-r)e_{old}$$

Equation 89

A good convergence criterion is to compare the enthalpy vector from the previous iteration to the updated enthalpy and once the norm of the difference between the two is less than a certain value, ε_e, the solution has converged. Specifically, the flowing convergence criterion was used in the code:

$$norm\left[e_{old}-e_{new}\right]<\varepsilon_{e}=10^{-3}$$

Equation 90

In other words, this means to iterate until the norm of the difference between the old and new enthalpy vectors is less than ε_e. Once the enthalpies have converged, they are used to update the fluid properties for the next iteration in time.

3.1.5 Temperature within Fuel, Sheath and Pressure Tube

To determine the temperature distribution in the fuel that is generating heat we can use general form of the heat equation in cylindrical coordinates:

$$\frac{1}{r}\frac{\partial}{\partial r}\left(kr\frac{\partial T}{\partial r}\right)+\frac{1}{r^2}\frac{\partial}{\partial \phi}\left(k\frac{\partial T}{\partial \phi}\right)+\frac{\partial}{\partial z}\left(k\frac{\partial T}{\partial z}\right)+\dot{q}=\rho c_p\frac{\partial T}{\partial t}$$

Equation 91

At steady-state, for a constant thermal conductivity and when there is only heat transfer in the radial direction. The heat equation reduces to:

$$\frac{1}{r}\frac{\partial}{\partial r}\left(r\frac{\partial T}{\partial r}\right)+\frac{\dot{q}}{k}=0$$

Equation 92

Two boundary conditions can be applied to this system. The first condition results from the symmetry of the situation. That is, for the solid cylinder the centerline is a line of symmetry for the temperature distribution and the temperature gradient must be zero. The second condition is that at the outer radius of the fuel pin the temperature is that of the surface of the fuel. Mathematically, these two boundary conditions are represented as follows:

$$\left.\frac{dT}{dt}\right|_{r=0}=0$$

Equation 93

$$T(r_o)=T_{fo}$$

Equation 94

Hence after integrating twice and applying the above boundary conditions we obtain the following temperature distribution:

$$T(r) = \frac{\dot{q} r_O^2}{4k}\left(1 - \frac{r^2}{r_O^2}\right) + T_{fo}$$

Equation 95

Respectively, the outer fuel temperature, the sheath temperature and the pressure tube temperature can be estimated using a series of thermal resistances posed by the cladding and the coolant:

$$T_{fo} = T_b + q'\left(\frac{\ln\left(\frac{R_{co}}{R_{ci}}\right)}{2\pi k_c} + \frac{1}{2\pi R_{co} h}\right)$$

Equation 96

$$T_w = T_b + q'\left(\frac{1}{2\pi R_{co} h}\right)$$

Equation 97

$$T_w = T_b - q'\left(\frac{1}{2\pi R_{pt} h}\right)$$

Equation 98

3.1.6 MATLAB Model Structure and Logic

As stated above, the MATLAB single fuel channel model has been developed using a numerical method that is a variant of Patankar's SIMPLE (Semi-Implicit Method for Pressure-Linked Equations) algorithm (1980) called the SIMPLEC algorithm. The model presented in this thesis couples the energy equation and updates the fluid properties only after the velocity and the pressure correction values have converged for a given set of fluid properties and enthalpies. Furthermore, once the onset of significant void (OSV) is determined, the true

mass quality, the void fraction and the mixture properties of the fluid are calculated. It is assumed that the saturation properties can be employed for this purpose. However, the OSV is a function of density and therefore it is necessary to converge on the density to ensure that the correct OSV criterion is being used. In addition, if it is determined that the heat flux is larger than the critical heat flux the fuel, sheath and pressure tube temperatures are then calculated. Once the sheath temperature is calculated to be larger than 1200°C (1473 K) the program terminates and the output is used as boundary conditions for the high power fuel channel experiencing flow stagnation in the MELCOR primary heat transport system model. A verbal description the algorithm used in this code is as follows:

1. Set the pressure profile, -dP/dt. (-dP/dt=0 for stagnate flow)
2. Solve the momentum equation to obtain the velocity, u.
3. Solve the for the pressure correction, P', using the mass defect as the stop criterion.
4. Once the values of P and u are obtained, solve the energy equation for the enthalpies, h.
5. Using the values of h, update the fluid properties and return to Step 2.
6. Once the converged values of u, P, and h are obtained, the steady state (t=0) solution has been obtained. Use the steady state values of u, P, and h as the initial conditions for the transient case.

7. Once the thermodynamic quality of the fluid has reached the Saha-Zuber criterion for onset of significant void (OSV) boiling has occurred in the horizontal fuel channel.
8. Calculate the new mixture properties including void.
9. Calculate the critical heat flux, q''_{CHF}.
10. Once the heat flux, q", is higher than the critical heat flux, q''_{CHF}, calculate the temperature of the fuel, sheath and pressure tube temperatures.
11. Stop the program once the sheath temperature, Tw, is larger than 1473 K.

The MATLAB single fuel channel code structure is shown as a flow chart in Figure 16. Within the MATLAB model light water properties were used and obtained from the program X Steam Tables for MATLAB®.

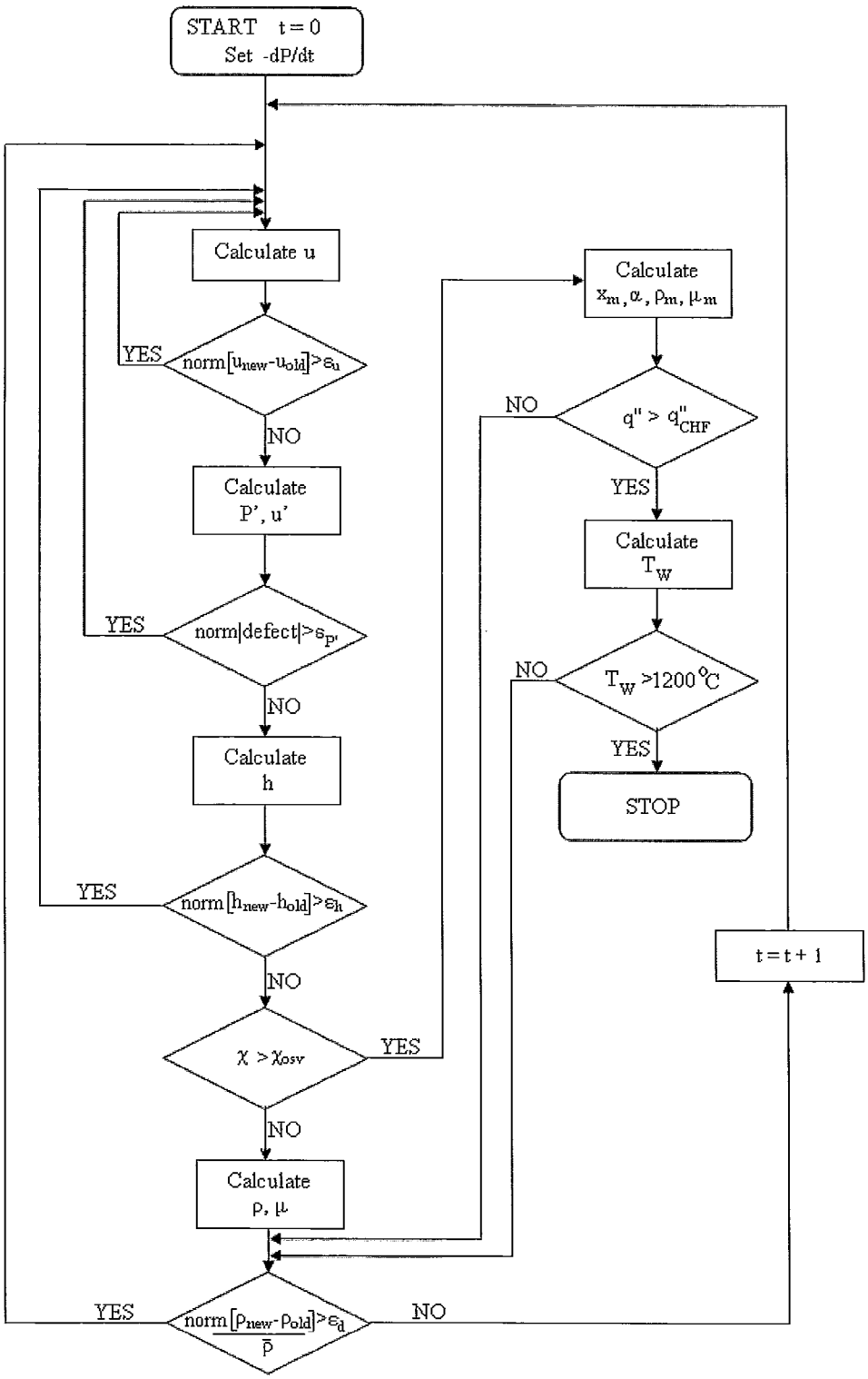

Figure 16: Flow chart of code structure and logic

3.2. SCDAP/RELAP5 Single Fuel Channel Model

Similar to the approach use by Mladin et al. (2008, 2009), a hydrodynamic representation of single, horizontal fuel channel modelled in SCDAP/RELAP5 is shown in Figure 17 below.

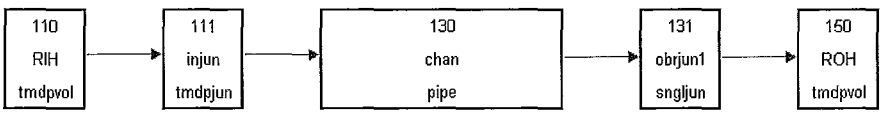

Figure 17: RELAP/SCDAPSIM CANDU fuel channel

The single fuel channel model uses 2 time-dependent volumes (tmdpvol), 1 time-dependent junction (tmdpjun), 1 pipe component (pipe) and 1 single junction (sngljun). The 2 time-dependent volumes represent the reactor inlet header and the reactor outlet headers and simulate pressure and temperature for steady state runs and pressure and static quality for transient runs. The inlet time dependent junction facilitates flow from the reactor inlet header and controls the mass flow rate boundary condition for steady state runs and controls the mixture of water and steam for transient runs. The pipe component simulates the fuel channel and the single junction facilitates the flow from the channel to the reactor outlet header. Each internal junction of the fuel channels (5 in total) have local pressure loss coefficients summing up the contributions of the end plates and of the mid-plane spacers were assumed to be 0.82 for the channel.

The fuel was modelled continuously over length of the fuel channel where 2 fuel bundles are represented by 1 axial node (i.e. 6 axial nodes in total). The

individual fuel rods have the same geometry, power history, axial power profile, radial power profile, void volume and internal pressure as individual elements in a 37-element fuel bundle. The pressure tube (PT), carbon dioxide filled gap and calandria tube (CT) are modelled using the SCDAP shroud component. The face of the inner shroud component (i.e. inner face of the PT) is thermally connected with the hydrodynamic channel and exchanges energy by radiation with the outside of the fuel bundle. The face of the outer shroud component (i.e. outer face of the CT) is thermally connected with the moderator which is modelled as a large stagnant heavy water volume at 122 kPa and 71°C.

There are 3 modes of fuel channel deformation to consider for CANDU:

1. PT ballooning – Occurs at high pressure PT balloons into uniform contact with CT
2. PT sagging – Occurs at low pressure PT sags into local contact with contact angle, ψ_o
3. Fuel bundle slumping – Occurs for both ballooning and sagging

Given that sagging is the limiting case, because it causes higher temperatures in the fuel (a lower limit of 850 °C) this is the phenomenon that was modelled (Mladin et al., 2009). Once the channel sags and the PT comes into contact with the CT heat transfer is enhanced. The enhanced heat transfer due to PT sagging into contact with the CT was calculated as follows (Mladin et al., 2009):

$$k'_{co2} = C \cdot k_{co2}$$

Equation 99

Where;

$$C = a + b \cdot \psi_o + c \cdot \psi_o \cdot T_p + d \cdot T_p$$
$$a = 0.03, b = -0.964, c = 0.000355, d = 0.00437$$

For a contact angle of 5°, a typical value of C is 6. This is used above the sagging threshold. This model of enhanced heat transfer was used in order to compare against the approached used by Mladin et al. (2008, 2009). For comparison purposes, the temperature dependence of k'_{co2} was linearly introduced starting at 873 K and in full effect by 1083 K. At sheath temperatures of 1473 K to 1673 K the fuel bundle slumping occurs for both ballooning and sagging which leads to 'close-packed configuration' as seen in Figure 18.

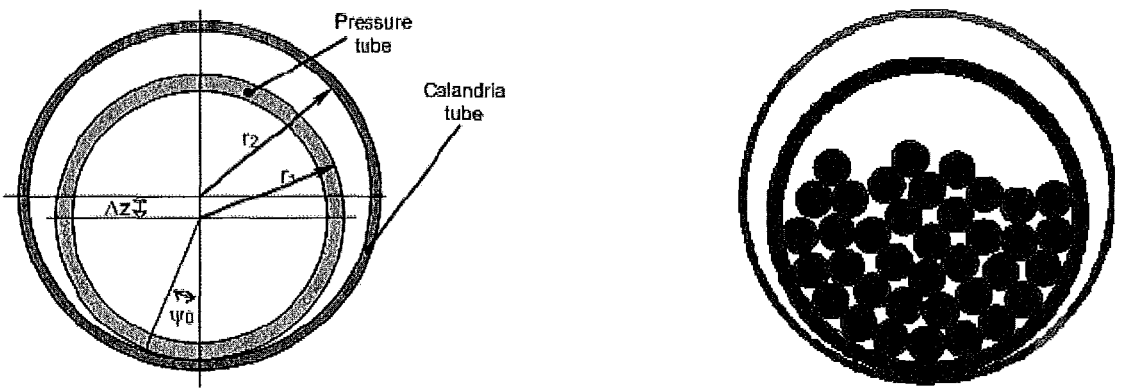

Figure 18: a) Sagged pressure tube in contact with the calandria tube

b) Close-packed configuration as a result of bundle slumping (Mladin et al., 2009)

It should be noted that this method of modifying the heat transfer is not representative of post-contact sagged PT heat transfer behaviour. Experimental studies have shown that high temperature sagged pressure tubes contacting calandria tubes shows that they contact over a 120 degree angle due to plastic creep deformation associated with bundle loading. (Luxat, 2009)

It is also noteworthy that the SCDAP/RELAP5 has no adequate models for relocation of the metallic/ceramic melt in horizontal fuel channels. Therefore a null melt velocity was imposed in the input file to prevent any melt relocation.

3.3. MELCOR CANDU 6 Model

3.3.1 Fuel Model

In order to aid the nodalization of a typical 37-element CANDU 6 fuel bundle in MELCOR, the fuel bundle's geometry was changed to a single fuel pin using a heat structure (Figure 19). As described in Section 2.5.2 this was the same approach used in the ISAAC code.

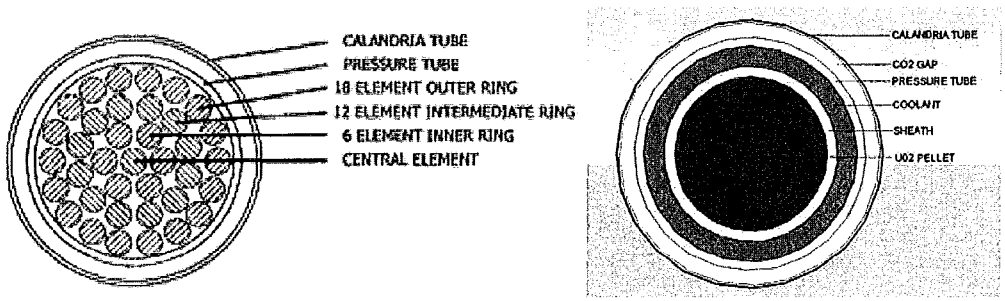

Figure 19: Transformation of 37-element fuel bundle into single fuel pin

The concentric ring approach to modelling the fuel bundle employed in MELCOR (Section 3.1) was also considered (Figure 20).

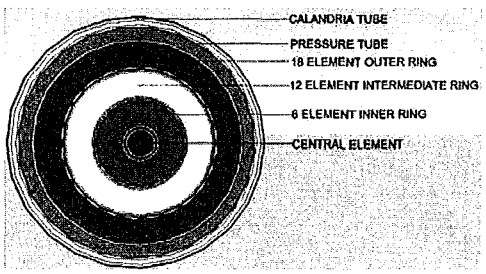

Figure 20: Transformation of 37-element fuel bundle into concentric rings

Through initial attempts at simulating the fuel channel in MELCOR it was found that the single fuel pin model yielded a more realistic temperature profile and had greater computational efficiency than the concentric ring model. The CPU time taken to simulate the concentric ring fuel bundle model took 20 times longer for a single fuel channel. Therefore the single fuel pin model of the fuel bundle was deemed a more appropriate heat structure for simulating the fuel bundle within MELCOR.

3.3.2 Reactor Core and Moderator System Model

For the reactor core, a simplified fuel channel model was used. The model used was similar to the approaches taken in the MAAP4-CANDU and ISAAC models as discussed in Sections 2.5.1 and 2.5.2 respectively. The 380 fuel channels were reduced to 36 representative fuel channels or 18 representative channel groups per each loop as seen in Figure 21. Each representative fuel channel represents 10.56 actual channels. This takes the form of 6 rows by 6 columns in the calandria vessel. Each of the primary heat transport system loops is composed of 6 rows and 3 columns and they are separated from each other by the central vertical plane of the reactor. The flow through the core is in a typical 'checker board' pattern and flows through the primary heat transport systems in a figure-of-eight. The 12 fuel bundles per channel were only coarsely nodalized into 1 representative axial node within the MELCOR model.

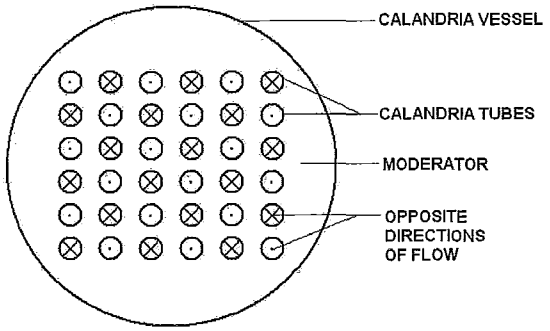

Figure 21: Moderator system model

The moderator system was modelled as a large stagnant volume of water at 122 kPa and 71°C. The calandria tubes are in contact with the moderator and are a source of heat input into this system. The heat injected into the moderator system was removed at a constant heat flux of 120 MW, which is the maximum rating for the moderator cooling system.

3.3.3 Primary Heat Transport System Model

The primary heat transport system model nodalization (Figure 22) is similar to the approaches taken in the MAAP4-CANDU and ISAAC model discussed in sections 2.5.1 and 2.5.2 respectively. Each loop was modelled to contain 2 steam generators, 2 pumps, 2 inlet headers, and 2 outlet headers. The feeders connect the inlet and outlet end of fuel channels to reactor inlet and reactor outlet headers respectively. The flow through one primary heat transport system loop follows the shape of figure-of-eight with some channels carrying the flow inward and others outward from the reactor face. Each pass through figure-of-eight loop consists of 14 hydrodynamic control volumes and 14 flow paths.

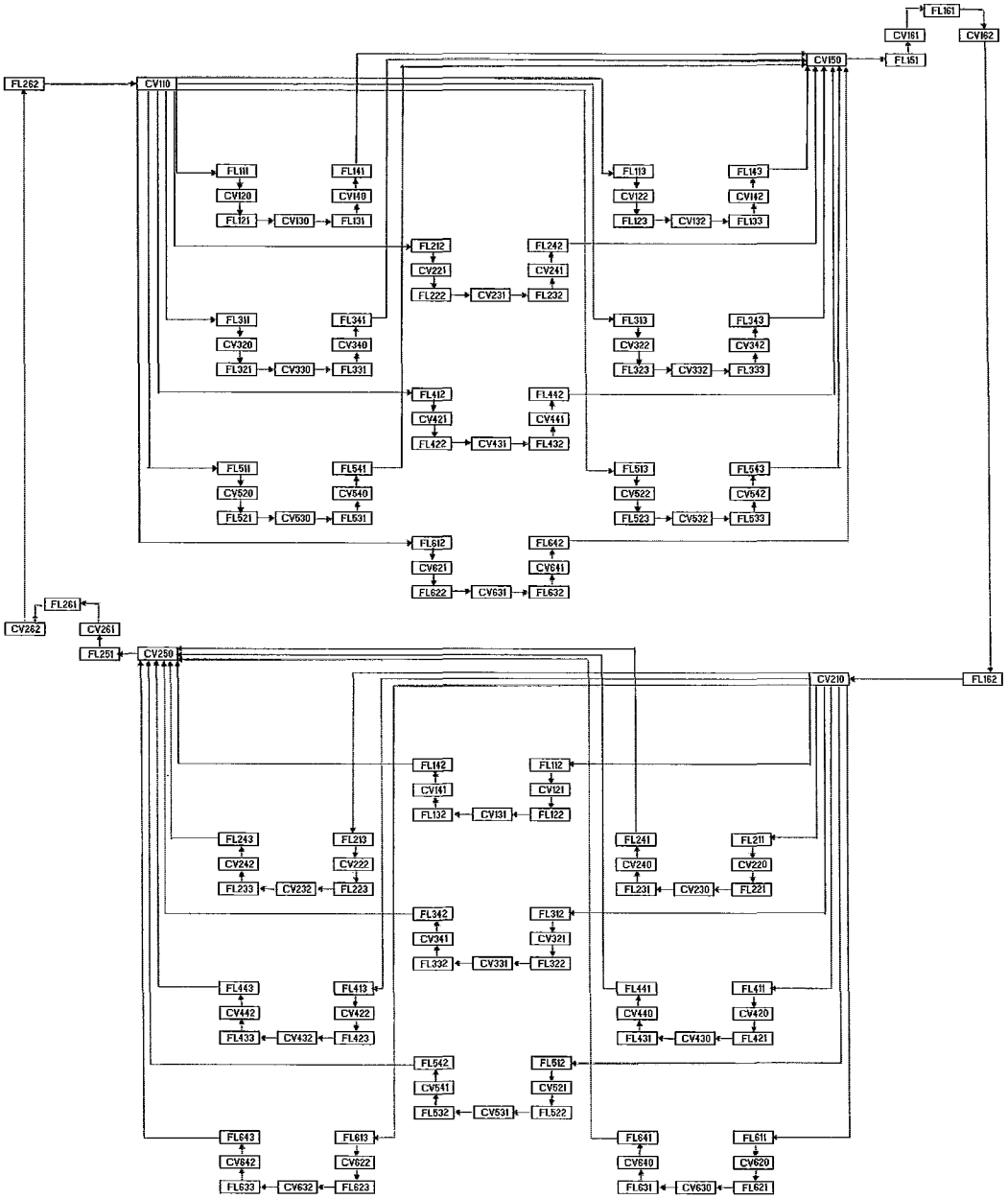

Figure 22: Figure-of-eight nodalization of loop in CANDU 6 primary heat transport system

In total, the MELCOR primary heat transport system is modelled with 140 control volumes, 156 flow paths and 22 heat structures. The steam generator secondary sides, the calandria vessel and the containment make up another 4 control volumes.

4. Results and Analysis of Stagnation Feeder Break

A small break loss of coolant accident (SBLOCA) in an individual reactor inlet feeder pipe of exactly the right size can cause flow stagnation in the fuel channel to which it is attached. The location of this break was chosen to be near the top of a reactor inlet feeder close to the reactor inlet header. For conservatism, the inlet feeder is chosen as one that is attached to a high power channel at high elevation. The coolant inventory leaving the reactor enters the containment building, which is seen in Figure 23.

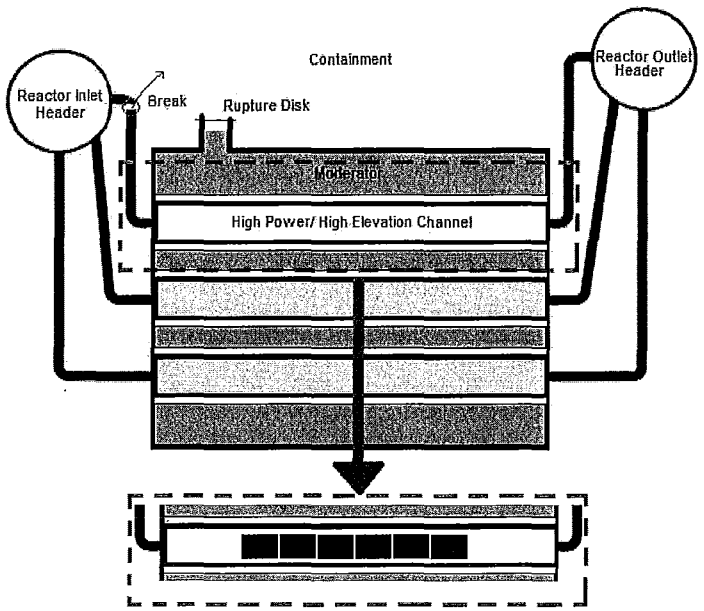

Figure 23: Stagnation inlet feeder break in high power channel.

It is assumed that the reactor is initially at full power. It is also postulated that the emergency core cooling system (ECCS) fails and thus there is a loss of emergency cooling injection (LOECI).

By definition, during the flow stagnation there is no net flow leaving or entering the fuel channel. It was during this period of stagnant flow that the high powered fuel channel was modelled independently from the rest of the reactor. Modelling of the fuel channel was done using the MATLAB single fuel channel model and the SCDAP/REALP5 single fuel channel model discussed in Sections 3.1 and 3.2 respectively. The MELCOR model, as discussed in Section 3.3, was also used to determine the behaviour of the rest of the reactor during this stagnation period. This first simulation with the MELCOR model determined the mass flows, void distribution and the system pressure where as the MATLAB and SCDAP/RELAP5 models separately determined the fuel temperature. In addition, the SCDAP/RELAP5 model also determined the fission product generation and hydrogen production in the high power fuel channel experiencing flow stagnation. The first MELCOR simulation implied that the flow would become stagnant and the channel would become devoid of coolant after 1.0 second, which was used as the basis for the flow rundown in the high powered fuel channel in the MATLAB and SCDAP/RELAP5 simulations. Moreover, through trials with the MELCOR model, the stagnation break size was determined to be 8.03 cm^2 (i.e. 14% of twice the cross sectional area of a feeder).

Both the MATLAB and SCDAP/RELAP5 models were run until the sheath temperature of the fuel in the high power channel experiencing flow stagnation was equal to 1473K, which is used as a simplified threshold temperature. It is assumed that both the pressure tube and the calandria tubes ruptured at that

temperature which is similar to the approach used in the MAAP4-CANDU model. The mass flows, pressures, void distribution and temperatures from these two simulations were then used as boundary conditions for a continuing transient in another MELCOR simulation. The MELCOR model was renodalized (Figure 24) with the following features:

- Fuel is located at the bottom of the high power fuel channel, resting upon the pressure tube
- A break establishing a flow path between the fuel channel and the calandria, which is assumed to be equal in size to the reactor inlet feeder break and is not large enough to release any fuel from the fuel channel
- A single rupture disk break establishing a flow path between the calandria and the containment, which is sized to accommodate all flow from the single channel event

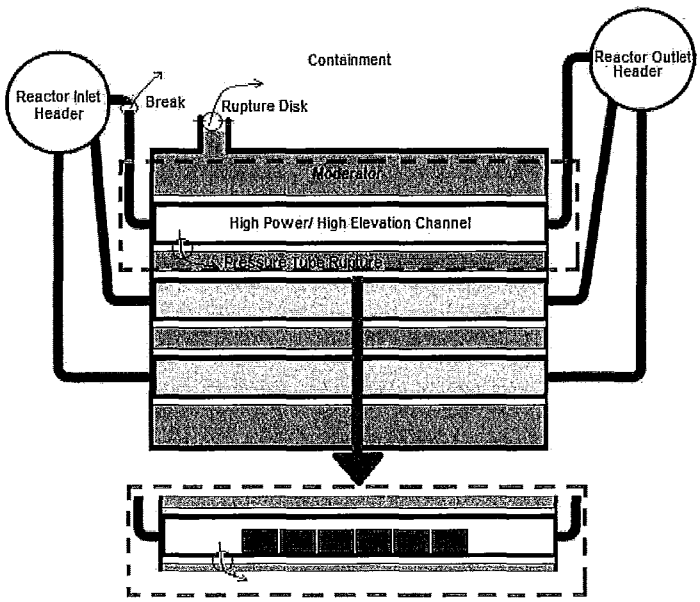

Figure 24: Fuel sags to bottom of fuel channel rupturing pressure tube.

The reactor was assumed to have tripped at the start of this second MELCOR simulation. The simulation was terminated once the moderator cooling system was able to accommodate the generated decay heat. Given the time scale of the current analysis, the effects of losing ECCS were minimized.

4.1 MATLAB-MELCOR Simulation

4.1.1 Feeder Break, Calandria Rupture Disk and PT-CT Rupture

As mentioned above through trial and error tests with the MELCOR primary heat transport system model, the stagnation break was determined to be 14% of the largest permissible SBLOCA (i.e. the break was 14% of twice the cross sectional flow area of a feeder or 8.03 cm^2). The mass discharge and enthalpy for this break can be seen respectively in Figures 25 and 26.

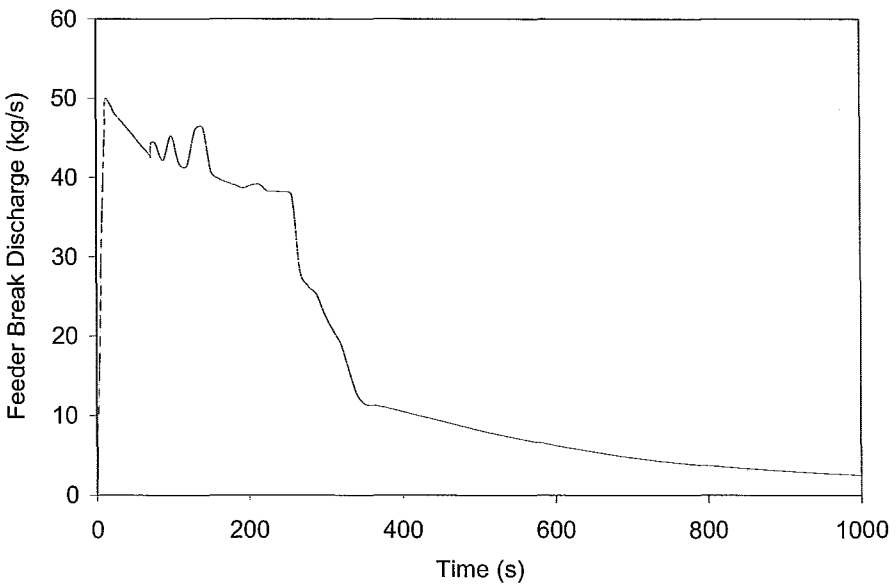

Figure 25: Inlet feeder break mass discharge into containment building

The mass discharge through the break exited the feeder and entered the containment building at 50 kg/s, which is approximately twice the nominal flow rate through the channel. The increased flow rate out of the feeder was attributed to the large pressure difference between the primary heat transport system and the containment building. At steady state, the primary heat transport system is pressurized to approximately 11.5 MPa in the reactor inlet header, which was similar to the initial value of the pressure at the break. The pressure in the containment building however was near atmospheric pressure. Initially this mass discharge decreased as the pressure of the primary heat transport system decreased.

As seen in Figure 26 below, the enthalpy of the coolant exiting through the break increased and rapidly reached a plateau twice during the course of the transient. The initial increase was obviously due to the start of the transient. The coolant enthalpy reached a plateau of approximately 1450 kJ/kg due to the steady flow of coolant out of the break. The next rapid rise in coolant enthalpy exiting through the break is due to declining coolant inventory. The coolant inventory decreased much more rapidly than the decay heat in the fuel from fission products. Roughly the same heat input into a smaller amount of coolant caused the coolant to heat up and turn into vapour. This resulted in a rapid rise in break enthalpy, which steadied once new quasi-static flow rates were established.

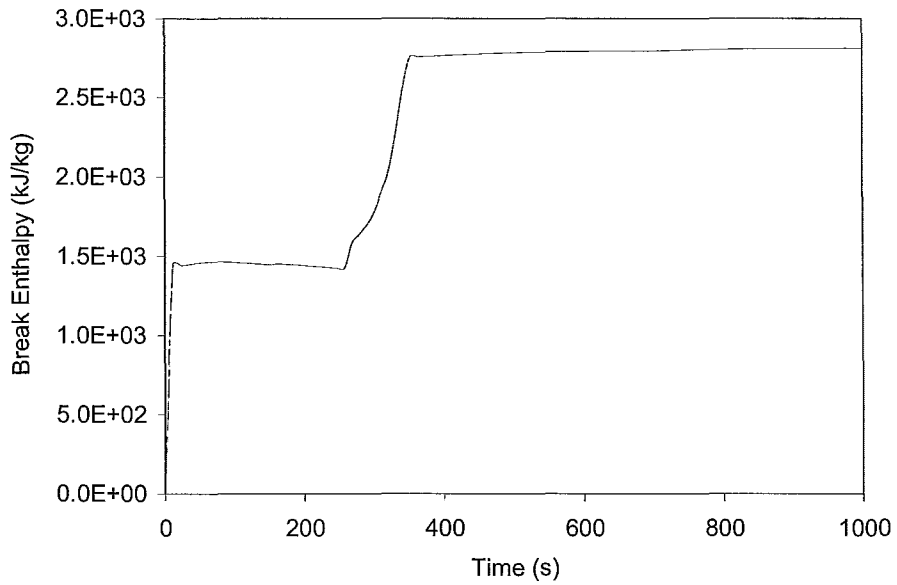

Figure 26: Inlet feeder break enthalpy discharge into containment

At 13 seconds after the initial inlet feeder break, the fuel had heated up to the point where it had slumped into closed packed configuration (Figure 18) and ended up resting on top of the pressure tube. At this time the pressure tube has also sagged into contact with the calandria tube and both are assumed to rupture instantaneously, which established a flow path between the high powered fuel channel and the calandria vessel. The transient flow from the high powered fuel channel to the calandria vessel can be seen in Figure 27.

At the onset of the pressure tube rupture, the pressure difference between the primary heat transport system and the moderator was very high and thus provided a large driving force for the high flow rate from the fuel channel to the calandria vessel. This maximum flow rate is 41 kg/s and is established at 45

seconds. This flow rate is maintained until the 288 second mark of the transient at which point the flow starts to gradually decrease. As the flow into the high power channel decreases so does the flow of coolant from the channel to the moderator. At 372 seconds, the flow in the high power fuel channel underwent a rapid decrease in flow rate.

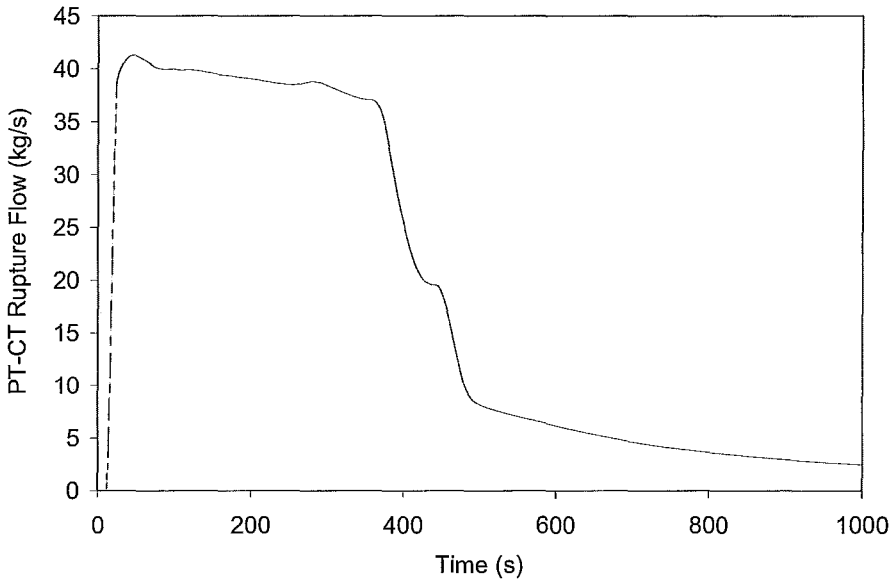

Figure 27: Flow rate through break in PT-CT into calandria vessel after rupture

A single rupture disk break was assumed to occur at the same time as the pressure tube rupture given the rapid pressurization of the calandria vessel. The mass discharge through the rupture disk is presented in Figure 28.

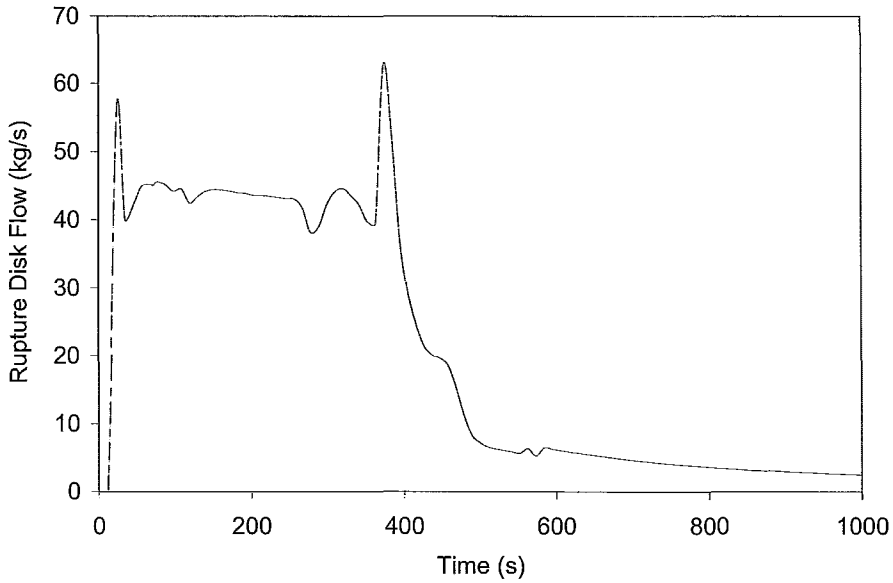

Figure 28: Flow rate through rupture disk from calandria vessel to containment building

As the high temperature, high pressure coolant was injected into the moderator it started to boil off. Once it started to boil off, the heavy water exited the calandria vessel at rate of approximately 60 kg/s. Over time, as the heat load to the moderator decreased, less moderator boiled off and thus decreased mass discharged through the rupture disk.

4.1.2 Loop Inventory and Void Distribution

As expected for a SBLOCA-LOECI, the broken loop inventory decreased over time, as seen in Figure 29.

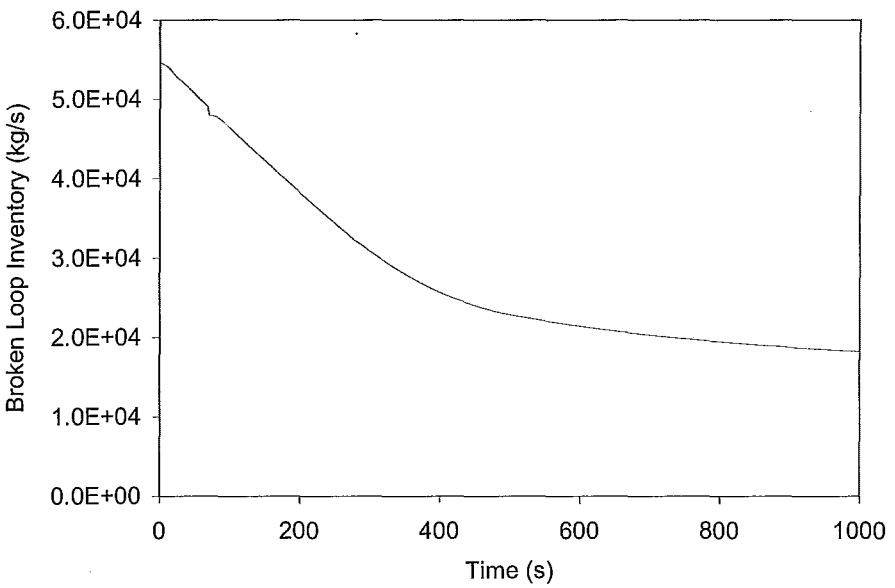

Figure 29: Broken loop inventory

The coolant inventory initially started to decrease at a rate proportional to the loss of coolant through the single inlet feeder break. Toward the end of the transient the rate of coolant loss slowed due to the decreased rate of depressurization of the primary heat transport system, which limited the driving force for the flow exiting the reactor through the feeder break, pressure tube rupture and calandria rupture disk.

The average amount of void in the primary heat transport system increased steadily over time as seen in Figure 30. Void generation occurs when the heat input into a given amount of coolant is high enough to cause a phase change. The decay heat from the fission products in the fuel continually decreased with time however this is a slow process as seen in Figure 31; after the reactor trip occurs.

The coolant inventory is continually lost from the primary heat transport system at a relatively fast rate. These two factors combined with the LOECI, contributed to the fact that the void continued to rise in the primary heat transport system. The rate of average void generation did decrease towards the 1000 second mark of the transient due to the reduced coolant flow rate out of the break. The moderator acts as an ultimate heat sink for the decay heat. It is expected that the void fraction will eventually reach a maximum and start to decrease due to the diminishing amount of decay heat produced from the fission products.

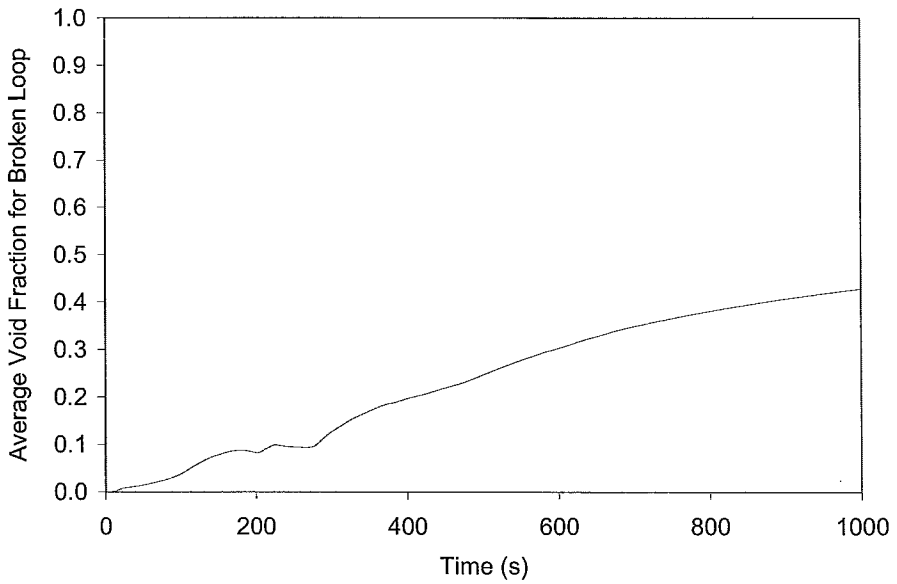

Figure 30: Average void fraction for broken loop

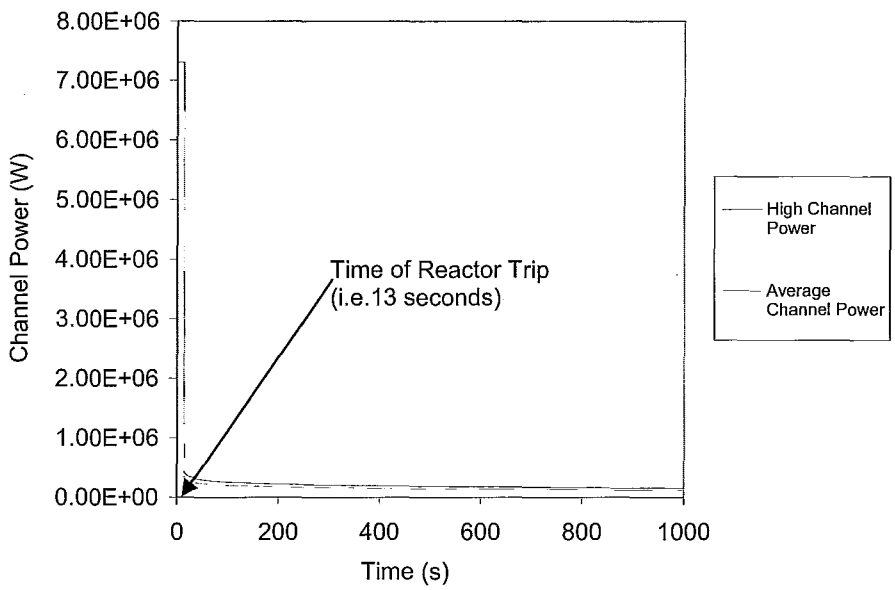

Figure 31: Power history for high power and average power fuel channels

Although Figure 30 indicates how the average void in the broken loop is increasing with time it does not indicate the distribution of the void within the system. As seen in Figure 32, most of the void accumulated in the reactor headers. The vapour is less dense than the liquid coolant and tends to move to high elevation and remain there. Given that the headers are higher than the fuel channels they were found to have collected more void. Given that the flow is driven through the core partially by the hydrostatic pressure difference between the headers once the reactor inlet header reached a void fraction of close to 1.0 the density gradient became drastically smaller. Here we anticipate that the flow through the core will be reduced.

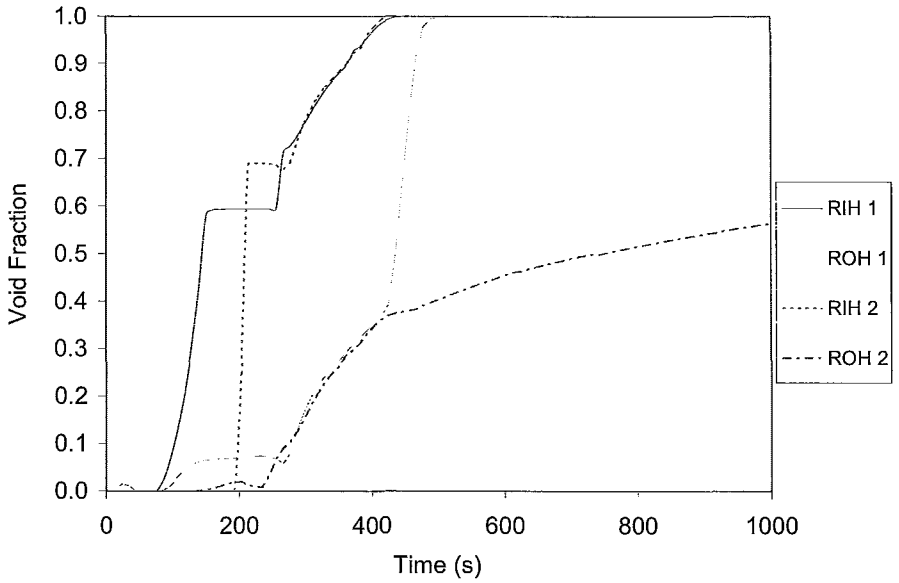

Figure 32: Void fraction in reactor inlet and reactor outlet headers of broken loop

4.1.3 Primary Coolant Flow in the Core

Flow in the core was reduced upon introducing a single inlet feeder break. As shown in Figure 33 the flow through the core was reduced from a steady state flow rate of 10640 kg/s to 8300 kg/s. After reaching this local minimum the flow increased as flow was re-established in the high power channel that experienced flow stagnation. The values for the flow through the core ranged from 7500kg/s to 9000 kg/s up until the point where the void fraction in the reactor inlet head becomes close to 1.0. This occurred at approximately 340 seconds and flow dropped rapidly to approximately 2700 kg/s at 414 seconds.

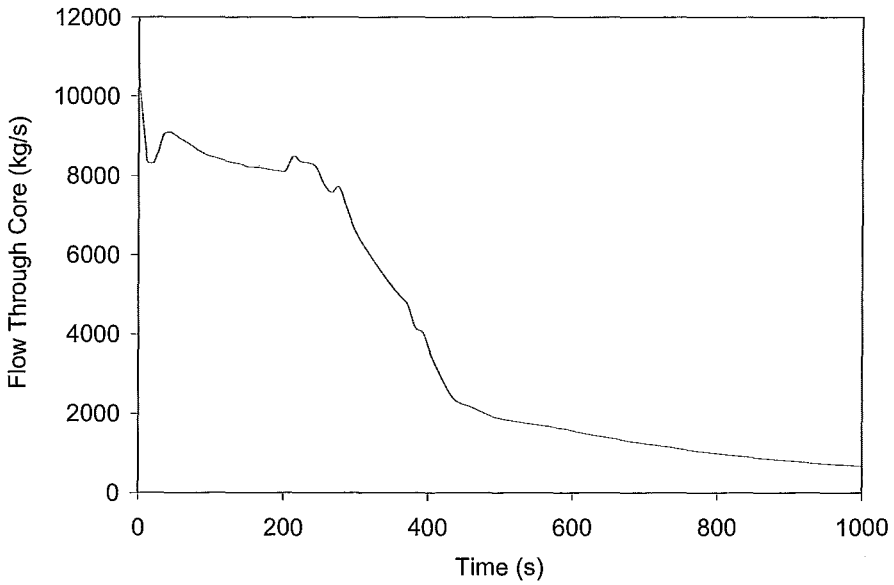

Figure 33: Total primary coolant f low through core

Observing the flow through the core does not highlight the specific flow rate occurring in individual fuel channels. On closer inspection, once the reactor inlet feeder broke, the flow was reduced in an average power fuel channel from the steady state mass flow rate of 28 kg/s to approximately 23 kg/s, as seen in Figure 34. Given that all feeders were modelled with the same diameter and connected to the headers at the same elevation, flow was similarly reduced in all of the other average power channels. However, the flow of coolant in the high powered channel was reduced to 0 kg/s for the stagnation break (i.e. by definition) until the pressure tube ruptured at 13 seconds.

Once the pressure tube ruptured, the average flow into the high power channel was quickly re-established and well surpassed the steady state flow rate,

reaching a value of 43 kg/s at 24 seconds. The flow maintained a quasi-static flow rate until 404 seconds into the transient at which point void in the reactor inlet header become appreciable and decreased flow through all fuel channels.

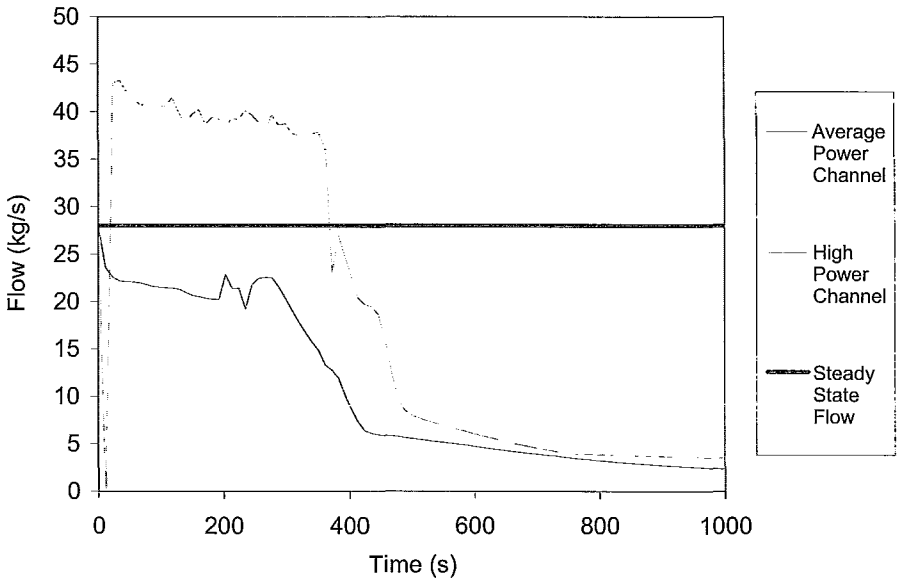

Figure 34: Primary coolant flow through core in high and average powered channels

4.1.4 PHTS Pressure

As seen in Figure 35, the primary heat transport system pressure decreased over time. This was due to a continual loss of coolant through the inlet feeder break and subsequently through the pressure tube rupture. As less coolant is present in the primary heat transport system to transfer the decay heat from the fuel, the coolant undergoes a phase change from liquid to vapour. Vapour contributes to a larger pressure drop due to friction as the transient progresses.

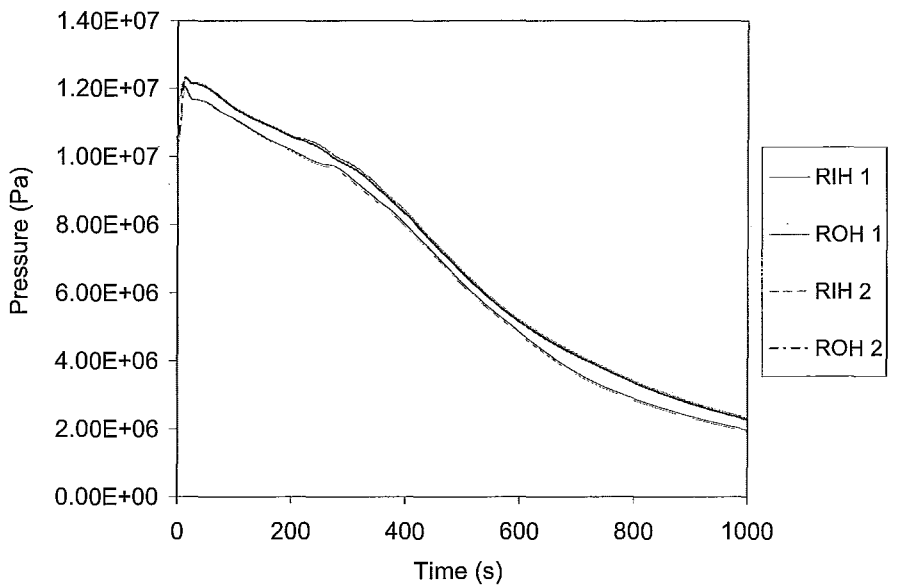

Figure 35: Reactor inlet and outlet header pressure transients

4.1.5 Fuel Channel, Fuel and Sheath Temperatures

From the simulation of the high powered fuel channel undergoing flow stagnation in the MATLAB single fuel channel model, it was determined that the temperatures from axial node number 18 would be used for the temperature boundary conditions in the renodalized MELCOR transient simulation. As seen in Figure 36, the temperature of the sheath, and subsequently the pressure tube, first reached the threshold temperature of 1473 K at axial node 18. The temperatures from axial node number 18 were used as boundary conditions for the second MELCOR transient, at 13 seconds.

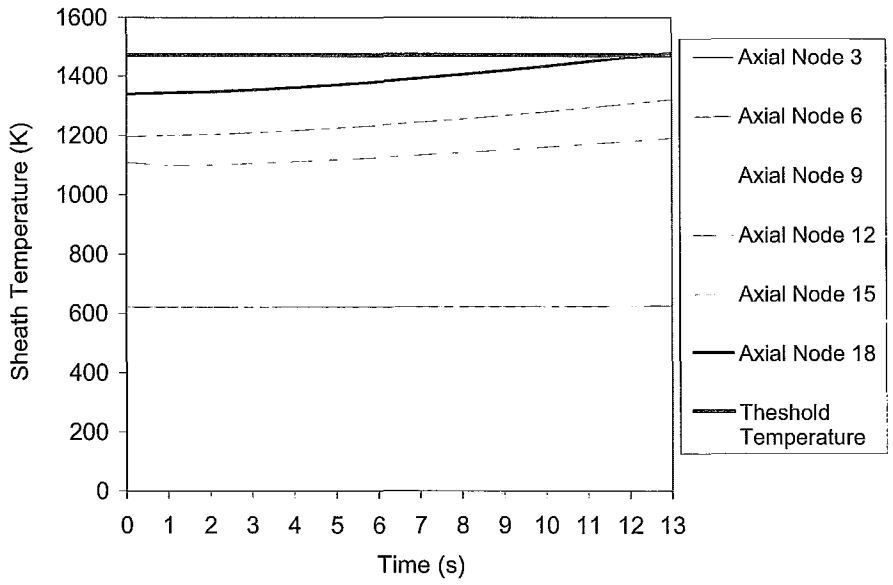

Figure 36: MATLAB simulation showing sheath temperature at 6 different axial nodes

Once the pressure tube ruptures at 13 seconds, there was a sharp decline in the fuel temperature and even sharper in the sheath temperature, as seen in Figure 37. This rapid reduction in fuel and sheath temperatures was due to the restoration of coolant flow through the high power fuel channel.

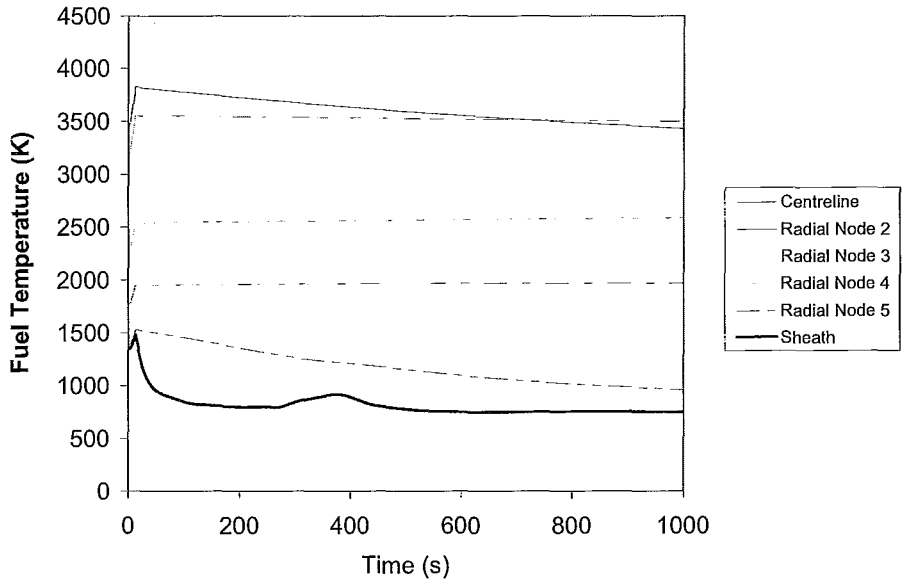

Figure 37: Fuel and sheath temperatures for hottest bundle in high power fuel channel

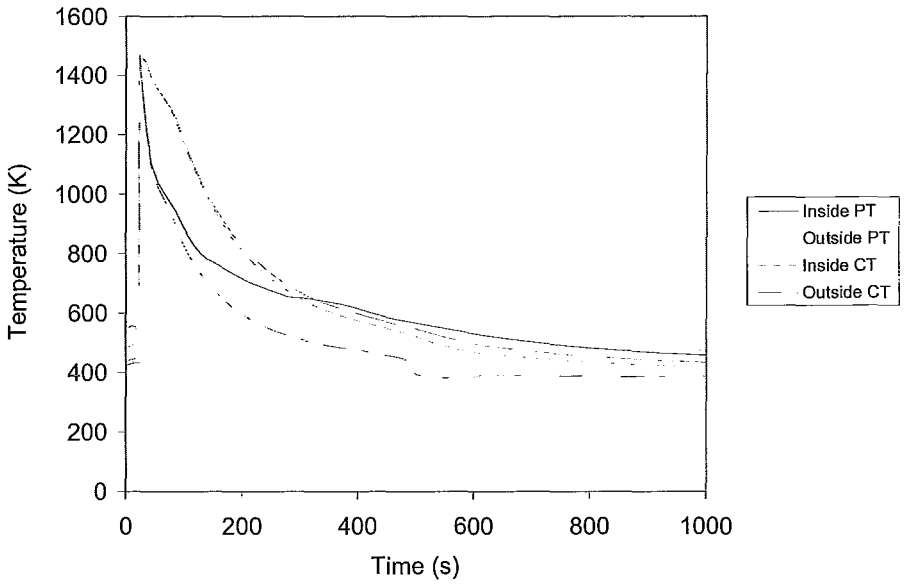

Figure 38: Pressure tube temperatures for location next to hottest bundle in high powered channel

The pressure tube temperatures can be seen in Figure 38. The fuel sag and eventual contact between the fuel and the pressure tube caused a rise in the pressure tube temperature up to the threshold temperature of 1473 K. This caused

the pressure tube to rupture. To reiterate, it is assumed that once the pressure tube ruptured that calandria tube would also rupture. Upon rupture, a flow path was established between the high power fuel channel and the calandria vessel. Coolant quickly began to flow through the fuel channel arresting any further deformation of the channel and preserving the integrity of the core geometry. With flow occurring on the inside of pressure tube as well as the outside of the calandria tube the inside temperature of the pressure tube initially fell below that of the interior portion of the tubes. Once the heat is removed from the tubes the inside of the pressure tube returns to being the highest in temperature given that it is next to the coolant which is higher in temperature than the moderator.

4.1.6 Hydrogen Production

Hydrogen production was not modelled within the MATLAB single fuel channel model. It is therefore suspected that if the exothermic reaction between hydrogen and Zircaloy were modelled that the sheath and pressure tube temperatures would increase at faster rate.

4.1.7 Moderator Transients

As the high pressure, high temperature coolant is injected into the calandria vessel it initially undergoes a very rapid pressure transient. This rapidly exceeded the rating of the rupture disks in the calandria vessel (i.e. 238 kPa) at 24 seconds. In this accident only one rupture disk was modelled to break, although there are 4 attached to the calandria vessel. It is seen that these other rupture disks

were not necessary to depressurize the calandria because the calandria vessel never again went above the rupture disk rating.

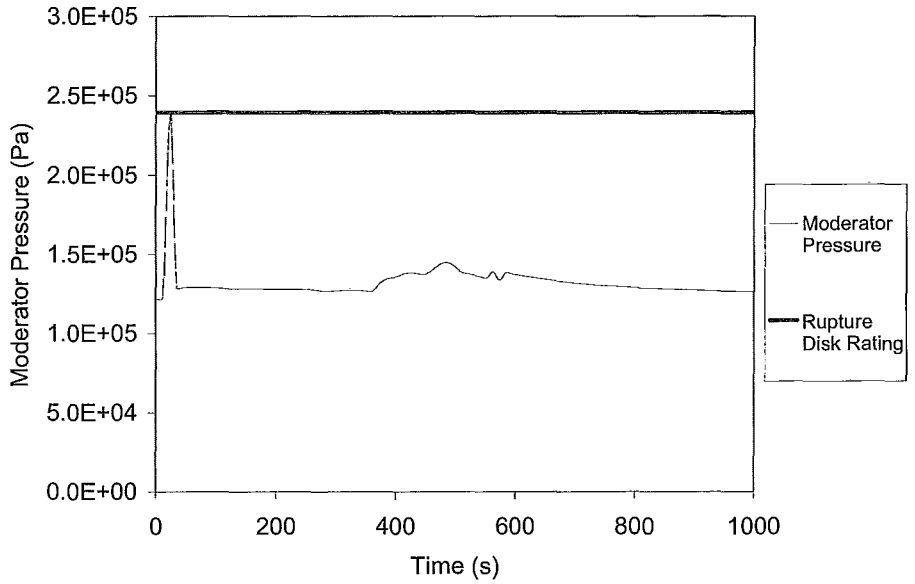

Figure 39: Moderator pressure transient and rupture disk rating

The moderator temperature initially increased as the fuel channel heated up as seen in Figure 40. The largest temperature of 378K was reached at 446 seconds but decreased as the heat load to the moderator decreased.

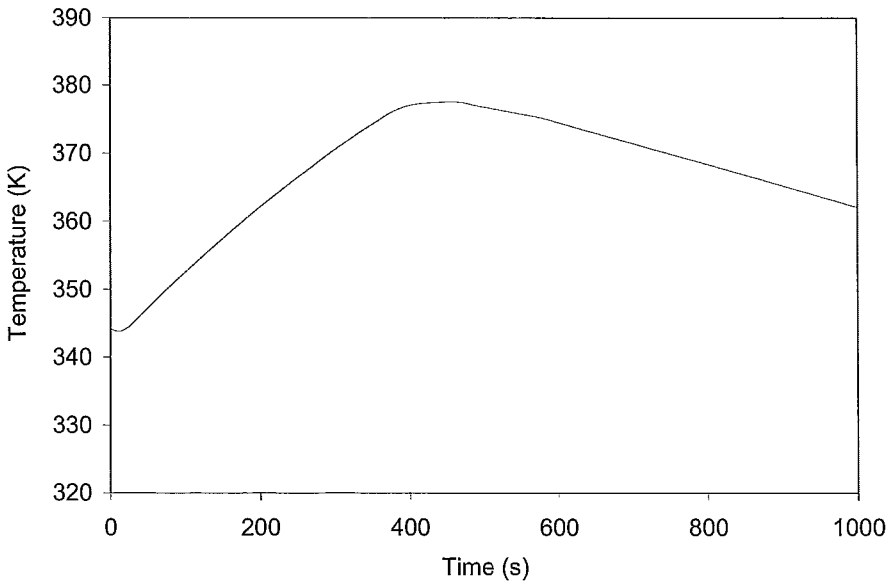

Figure 40: Moderator temperature transient

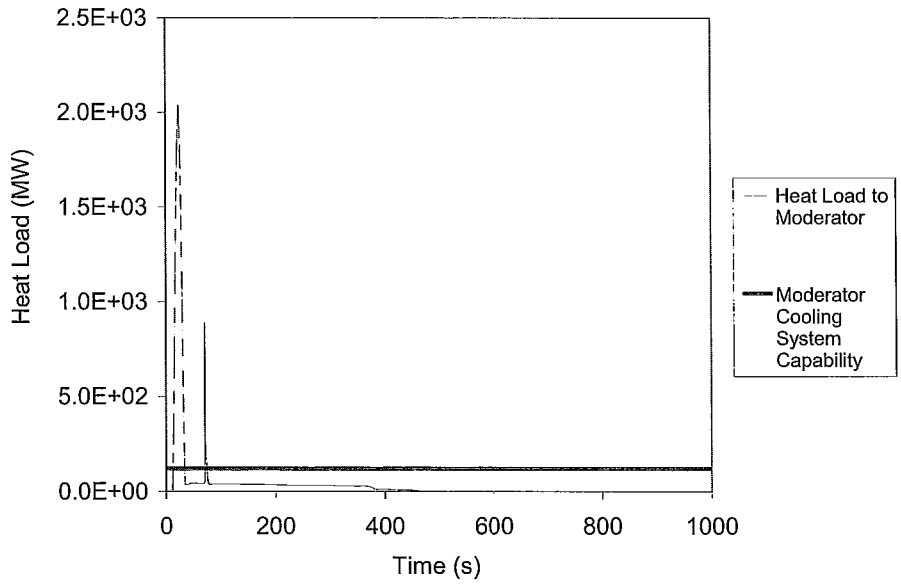

Figure 41: Heat load to moderator and moderator cooling system capability

The heat load to the moderator is shown in Figure 41. The limited flow of heat to the moderator was initially due to convection heat transfer of the coolant from the fuel to the pressure tube which then conducted the heat to the carbon dioxide gap and then the calandria tube. The highest spike in heat transfer to the moderator occurred when the pressure tube ruptured. At 24 seconds, the flow of hot coolant back into the channel and then into the moderator increased the heat input into the moderator, to a maximum of 2000 MW. The moderator cooling system has the capability of removing heat up to 120 MW. This cooling system regains the ability remove all the heat at the rate it's being produced at 71 seconds.

The integral amount of heat deposited in the moderator is seen in Figure 42 below. The excess heat going into the moderator can be seen as causing the moderator to boil off.

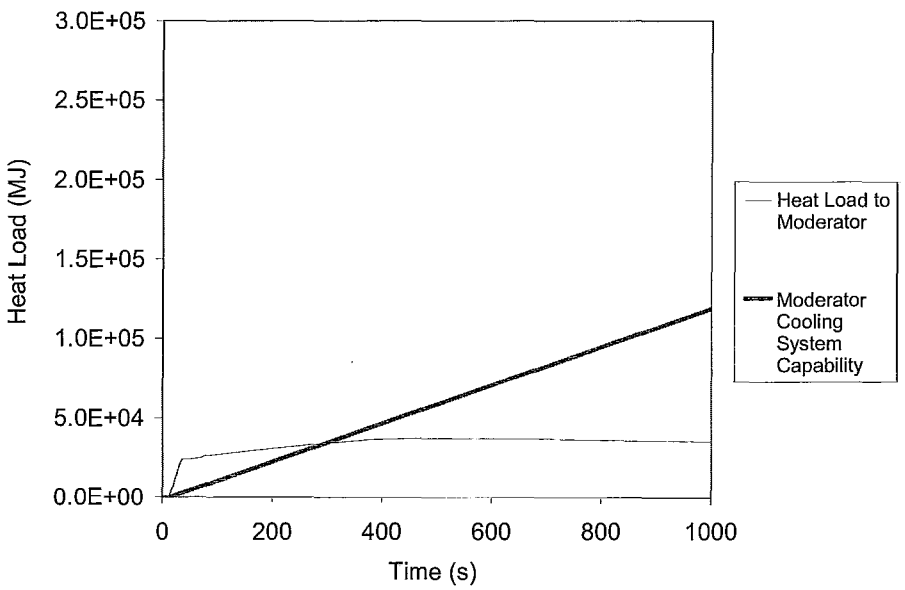

Figure 42: Integral heat load to moderator and integral moderator cooling system capability

If the moderator cooling system was fully operational at the start of the event then it would regain the ability to remove all heat at 298 seconds.

4.1.8 Containment and Fission Product Release

Given that the containment was modelled as a single large control volume with no compartments or control systems the containment pressure and temperature remained constant over time. That is to say the temperature and pressure of the containment were constant at 298.15 K and 124 kPa respectively. Nevertheless, the containment has a leakage rate of 0.5% at these nominal values of temperature and pressure (Doria, 2001).

No fission product release was modelled in this simulation. However, in the worst case scenario for a single channel event the entire fission product inventory for the channel could be postulated to be released into the containment. See Table 8 below for the maximum power channel inventories in a CANDU reactor.

Table 8: Maximum power channel inventories in CANDU reactor (Hussein, 1989)

Element	Channel free activity (Ci)	Maximum bundle free activity (Ci)	Maximum channel total inventory (Ci)	Maximum bundle total inventory (Ci)
^{131}I	12140	3380	164873	20947
Xe + Kr	36724	12960	1526154	193900

Using this leakage rate and the free inventory of the maximum power channel in a CANDU reactor as seen Table 8 above, at 298 s the total activity released outside containment would be estimated to be:

$$^{121}I: \quad 12140Ci \times \frac{0.005}{day} \times \frac{day}{24 \times 3600\,\text{sec}} \times 298\,\text{sec} = 0.21Ci$$

$$Xe + Kr: \quad 36724Ci \times \frac{0.005}{day} \times \frac{day}{24 \times 3600\,\text{sec}} \times 298\,\text{sec} = 0.63Ci$$

Fortunately, the rupture of the pressure tube in a timely manner enabled the moderator to act as an ultimate heat sink and prevented the fuel from heating up to the point of this release.

4.1.9 Major Event Sequence Summary

Table 9: Major event sequence for MATLAB & MELCOR code-coupling simulation

Time		Event	Codes Used
Hours	**Seconds**		
0.0	0.0	• SBLOCA - single inlet feeder break • LOECI • Broken loop isolated • Reactor at full power	MATLAB & MELCOR
0.0	1.0	• Reduced flow in all fuel channels • Flow stagnation in high power fuel channel attached to broken reactor inlet feeder	MATLAB & MELCOR
0.00	13.0	• Closed pack configuration • Pressure tube rupture • Reactor trip • Calandria rupture disks breaks due to overpressure • Moderator boil-off begins	MATLAB & MELCOR
0.01	24.0	• Flow re-established in high power fuel channel	MELCOR
0.08	298.0	• Moderator cooling system capable of removing remaining decay heat • Termination of accident	MELCOR

4.2 SCDAP/RELAP5-MELCOR Simulation

4.2.1 Feeder Break, Calandria Rupture Disk and PT-CT Rupture

The mass discharge and enthalpy for this break can be seen respectively in Figures 43 and 44.

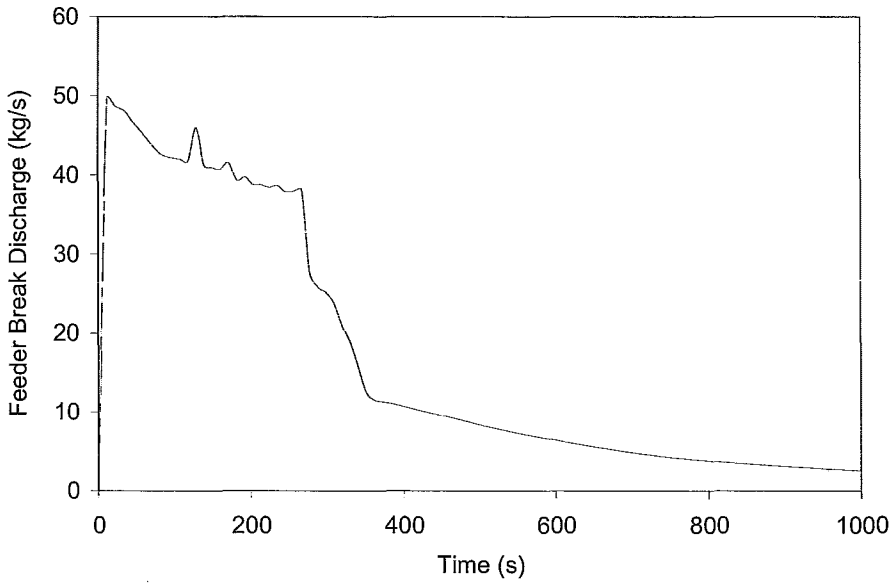

Figure 43: Inlet feeder break mass discharge into containment building

The mass discharge through the break exited the feeder and entered the containment building at 50 kg/s. This is approximately double the nominal flow rate through the channel. The increased flow rate out of the feeder was attributed to the large pressure difference between the primary heat transport system and the containment building. At steady state, the primary heat transport system is pressurized to approximately 11.5 MPa in the reactor inlet header, which was similar to the initial value of the pressure at the break. The pressure in the

containment building however was near atmospheric pressure. Initially this mass discharge decreased as the pressure of the primary heat transport system decreased.

As seen in Figure 44 below, the enthalpy of the coolant exiting through the break increased and rapidly reached a plateau twice during the course of the transient. The initial increase was obviously due to the start of the transient. The coolant enthalpy reached plateau of approximately 1450 kJ/kg due to the steady flow of coolant out of the break. The next rapid rise in coolant enthalpy exiting through the break is due to declining coolant inventory. The coolant inventory decreased much more rapidly than the decay heat in the fuel from fission products. Roughly the same heat input into a smaller amount of coolant cause the coolant to heat up and turn into vapour. This break enthalpy steadied once new quasi-static flow rates were established.

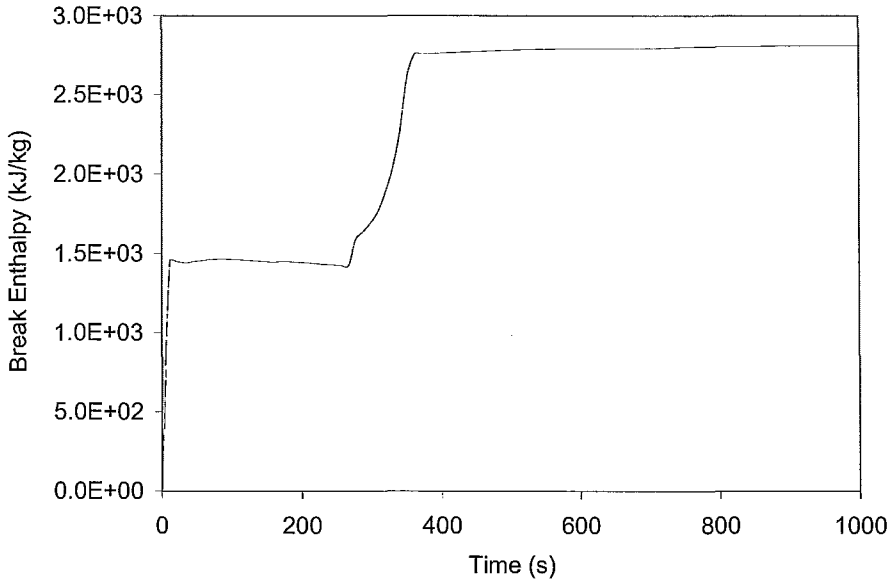

Figure 44: Inlet feeder break enthalpy discharge into containment

At 23 seconds after the initial inlet feeder break, the fuel had heated up to the point where it had slumped into closed packed configuration (Figure 18) and ended up resting on top of the pressure tube. At this time the pressure tube has also sagged into contact with the calandria tube and both are assumed to rupture instantaneously, which established a flow path between the high powered fuel channel and the calandria vessel. The transient flow from the high powered fuel channel to the calandria vessel can be seen in Figure 45.

At the onset of the pressure tube rupture, the pressure difference between the primary heat transport system and the moderator was very high and thus provided a large driving force for the high flow rate from the fuel channel to the calandria vessel. This maximum flow rate is 41 kg/s and is established at 55 seconds. This flow rate is maintained until the 393 second mark of the transient at

which point the flow starts to gradually decrease. As the flow into the high power channel decreases so does the flow of coolant from the channel to the moderator.

A single rupture disk break was assumed to occur at the same time as the pressure tube rupture given the rapid pressurization of the calandria vessel. The mass discharge through the rupture disk is presented in Figure 46.

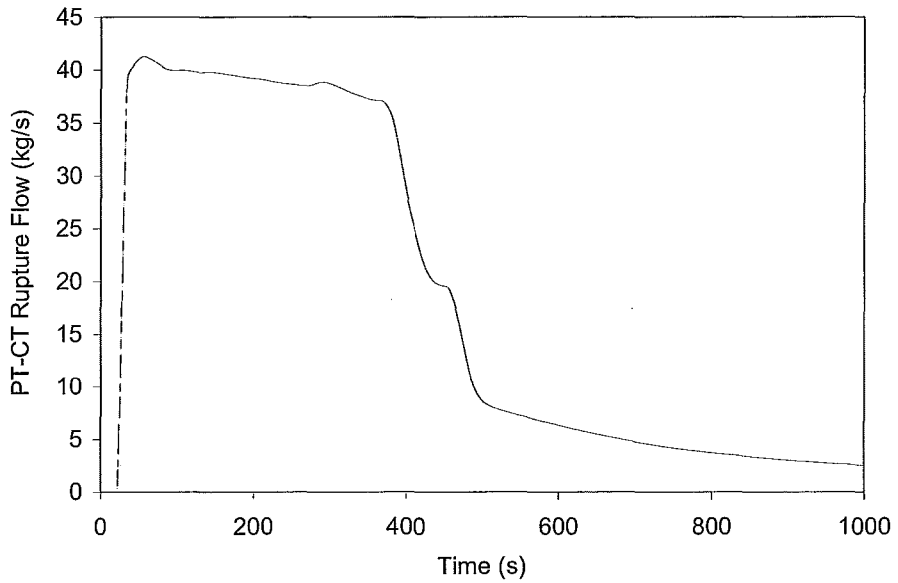

Figure 45: Flow rate through break in PT-CT into calandria vessel after rupture

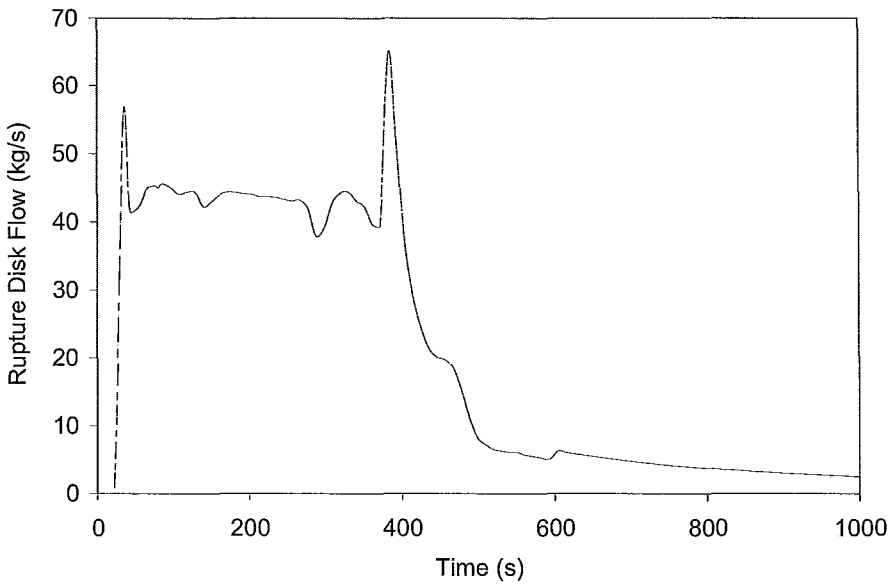

Figure 46: Flow rate through rupture disk from calandria vessel to containment building

As the high temperature, high pressure coolant was injected into the moderator it started to boil off. Once it started to boil off, the heavy water exited the calandria vessel at rate of approximately 55 kg/s. Over time, as the head load to the moderator decreased, less moderator boiled off and thus decreased mass discharged through the rupture disk.

4.2.2 Loop Inventory and Void Distribution

As expected for a SBLOCA-LOECI, the broken loop inventory decreased over time, as seen in Figure 47.

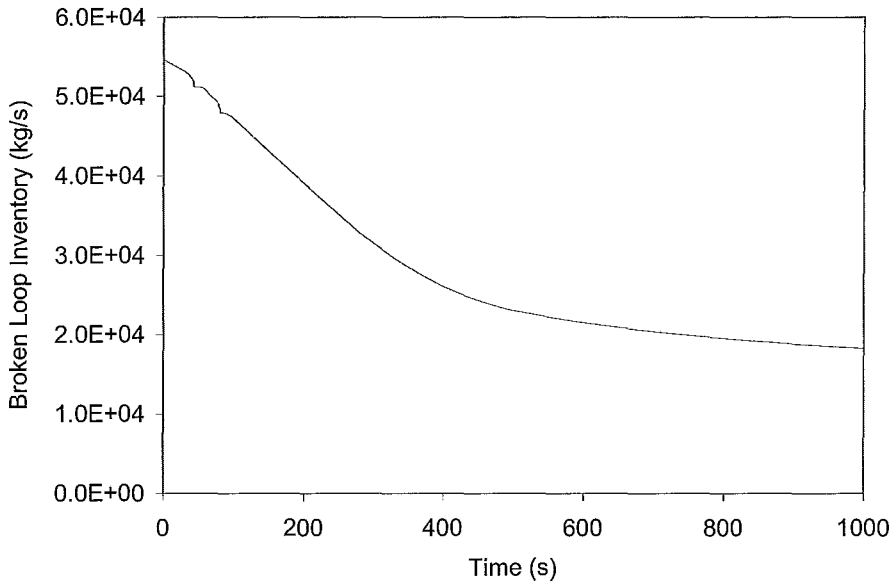

Figure 47: Broken loop inventory

The coolant inventory initially started to decrease at a rate proportional to the loss of coolant through the single inlet feeder break. Toward the end of the transient the rate of coolant loss slowed due to the decreased rate of depressurization of the primary heat transport system, which limited the driving force for the flow exiting the reactor through the feeder break, pressure tube rupture and calandria rupture disk.

The average amount of void in the primary heat transport system increased steadily over time as seen in Figure 48. Void generation occurs when the heat input into a given amount of coolant is high enough to cause a phase change. The decay heat from the fission products in the fuel continually decreased with time however this is a slow process as seen in Figure 49; after the reactor trip occurs.

The coolant inventory is continually lost from the primary heat transport system at a relatively fast rate. These two factors combined with the LOECI, contributed to the fact that the void continued to rise in the primary heat transport system. The rate of average void generation did decrease towards the 1000 second mark of the transient due to the slowed coolant flow rate out of the break. The moderator acts as an ultimate heat sink for the decay heat. It is expected that the void fraction will eventually reach a maximum and start to decrease due to the diminishing amount of decay heat produced from the fission products.

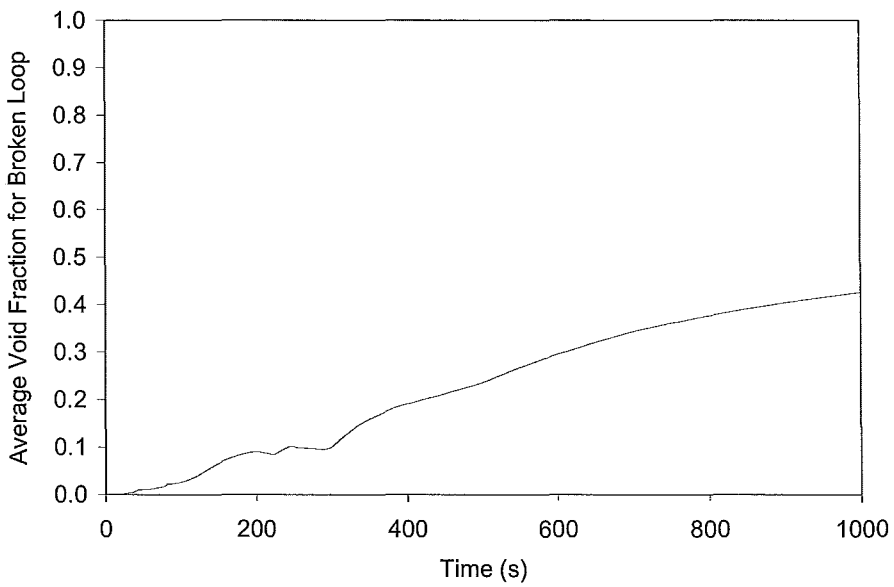

Figure 48: Average void fraction for broken loop

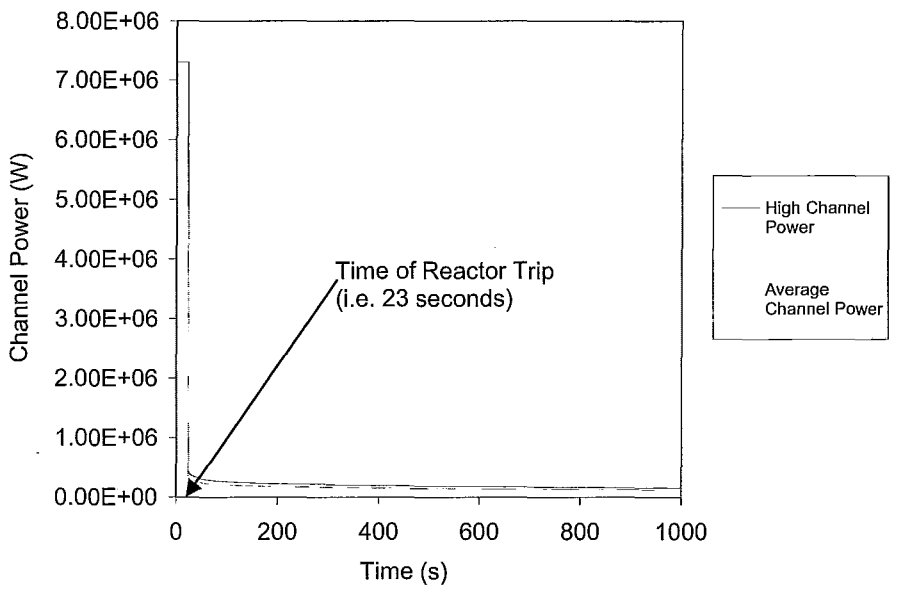

Figure 49: Power history for high power and average power fuel channels

Although Figure 48 indicates how the average void in the broken loop is increasing with time it does not indicate the distribution of the void within the system. As seen in Figure 50, most of the void accumulated in the reactor headers. The vapour is less dense than the liquid coolant and tends to move to high elevation and remain there. Given that the headers are higher than the fuel channels they were found to have collected more void. Given that the flow is driven through the core partially by the hydrostatic pressure difference between the headers once the reactor inlet header reached a void fraction of close to 1.0 the density gradient became drastically smaller. Here we anticipate that the flow through the core will be reduced.

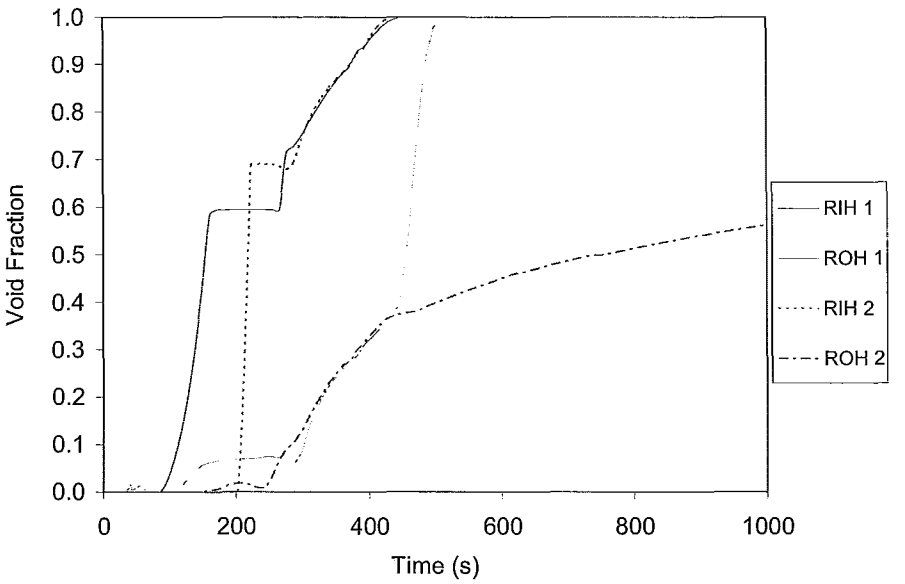

Figure 50: Void fraction in reactor inlet and reactor outlet headers of broken loop

4.2.3 Primary Coolant Flow in the Core

Flow in the core was reduced upon introducing a single inlet feeder break. As seen in Figure 51 the flow through the core was reduced from a steady state flow rate of 10640 kg/s to 8300 kg/s. After reaching this local minimum the flow increased as flow was re-established in the high power channel that experienced flow stagnation. The values for the flow through the core ranged from 7500kg/s to 9000 kg/s up until the point where the void fraction in the reactor inlet head becomes appreciable. This occurred at approximately 287 seconds and flow dropped rapidly to approximately 2700 kg/s at 424 seconds.

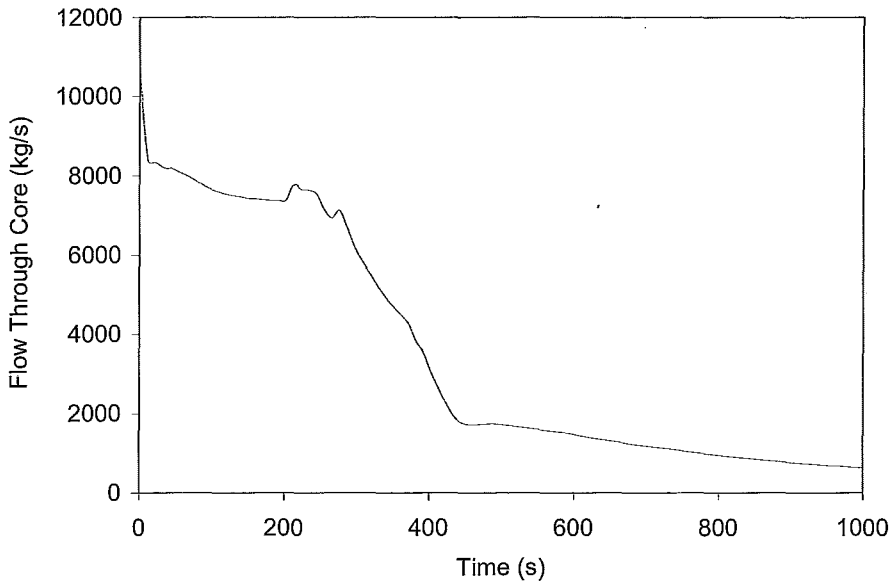

Figure 51: Total primary coolant f low through core

Observing the flow through the core does not highlight the specific flow rate occurring in individual fuel channels. On closer inspection, once the reactor inlet feeder broke, the flow was reduced in an average power fuel channel from the steady state mass flow rate of 28 kg/s to approximately 23 kg/s, as seen in Figure 52. Given that all feeders were modelled with the same diameter and connected to the headers at the same elevation, flow was similarly reduced in all of the other average power channels. However, the flow of coolant in the high powered channel was reduced to 0 kg/s for the stagnation break (i.e. by definition) until the pressure tube ruptured at 23 seconds.

Once the pressure tube ruptured, the average flow into the high power channel was quickly re-established and well surpassed the steady state flow rate,

reaching a value of 41 kg/s at 34 seconds. The flow maintained a quasi-static flow rate until 371 seconds into the transient at which point void in the reactor inlet header becomes close to 1.0 and decreased flow through all fuel channels.

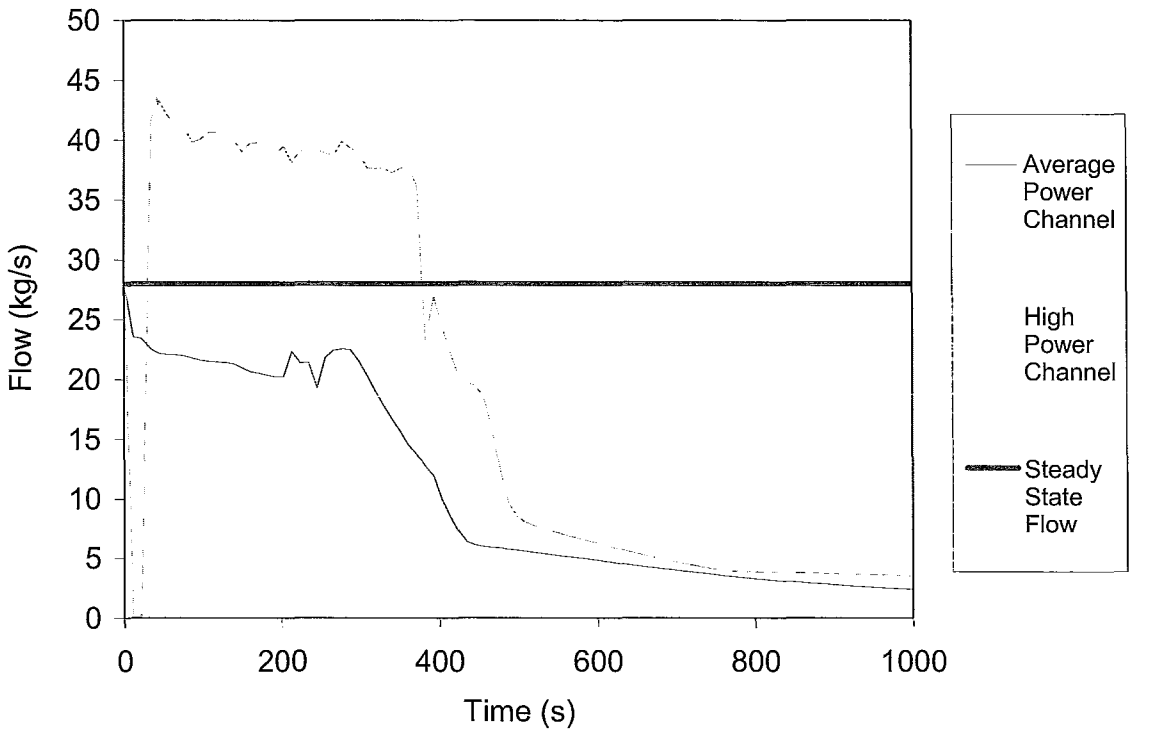

Figure 52: Primary coolant flow through core in high and average powered channels

4.2.4 PHTS Pressure

As seen in Figure 53, the primary heat transport system pressure decreased over time. This was due to a continual loss of coolant through the inlet feeder break and subsequently through the pressure tube rupture. As less coolant is present in the primary heat transport system to transfer the decay heat from the fuel, the coolant undergoes a phase change from liquid to vapour. Vapour contributes to a larger pressure drop due to friction as the transient progresses.

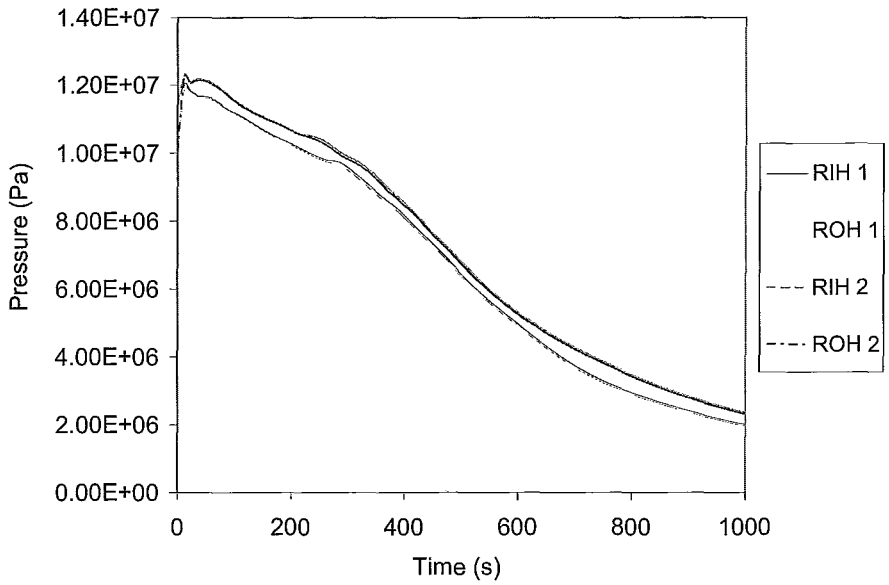

Figure 53: Reactor inlet and outlet header pressure transients

4.2.5 Fuel Channel, Fuel and Sheath Temperatures

From the simulation of the high powered fuel channel undergoing flow stagnation in the SCDAP/RELAP5 single fuel channel model, it was determined that the temperatures from axial node number 6 would be used for the temperature boundary conditions in the renodalized MELCOR transient simulation. As seen in Figure 54, the temperature of the sheath, and subsequently the pressure tube, first reached the threshold temperature of 1473 K at axial node number 3.

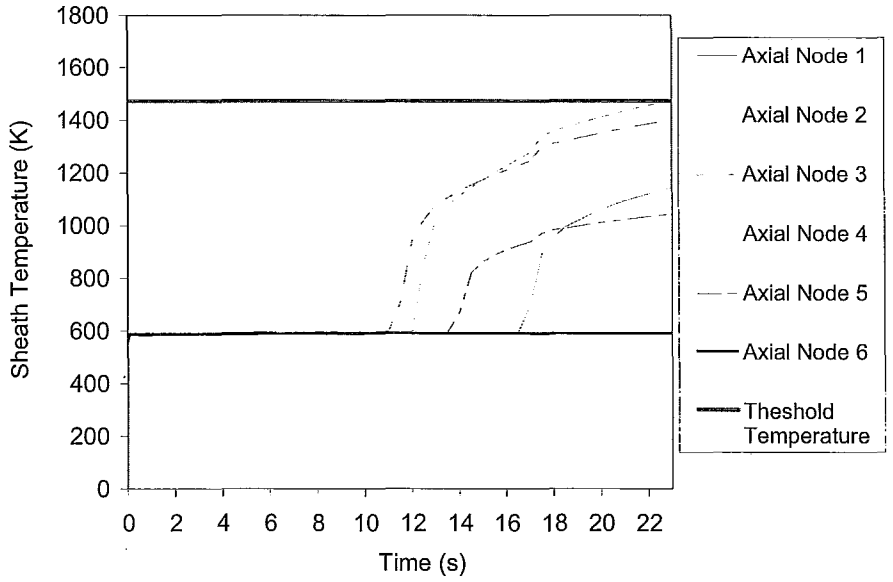

Figure 54: SCDAP/RELAP5 simulation showing sheath temperature at 6 axial nodes

The sheath temperature remained below the melting point of Zircaloy (i.e. 2098 K) and prevented the release of fission products from the fuel. The temperatures from axial node number 3 were used as boundary conditions for the second MELCOR transient, at 23 seconds.

Once the pressure tube ruptures at 23 seconds, there was a sharp decline in the fuel temperature and even sharper in the sheath temperature, as seen in Figure 55. This rapid reduction in fuel and sheath temperatures was due to the restoration of coolant flow through the high power fuel channel.

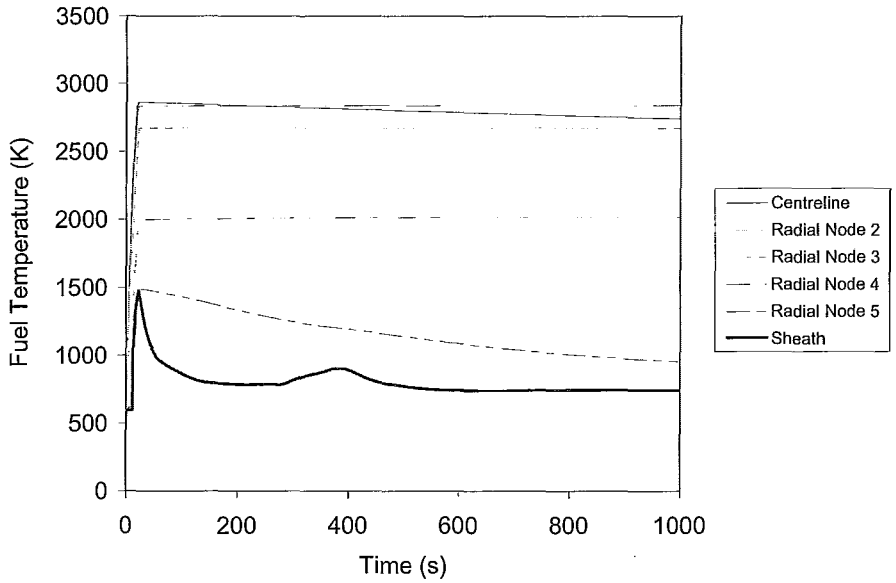

Figure 55: Fuel and sheath temperatures for hottest bundle in high power fuel channel

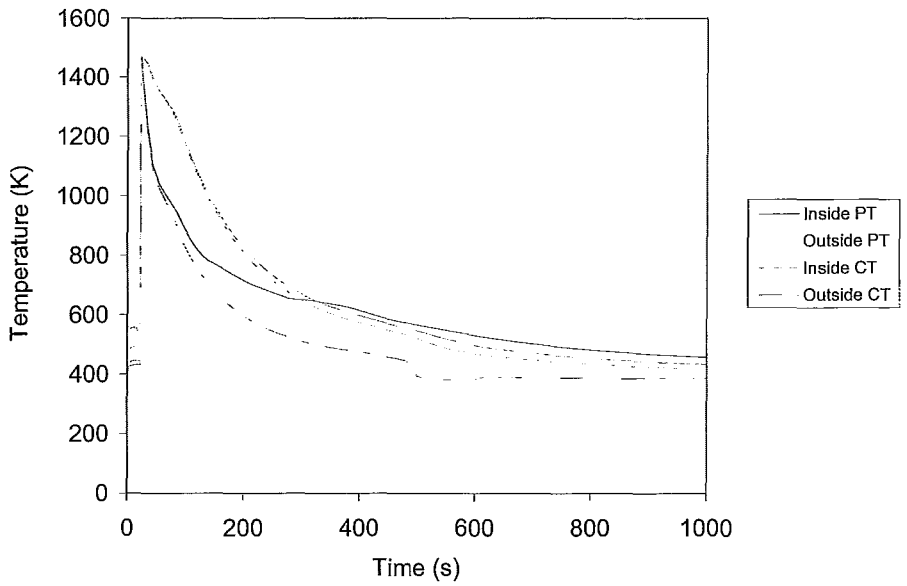

Figure 56: Pressure tube temperatures for location next to hottest bundle in high powered channel

The pressure tube temperatures can be seen in Figure 56. The fuel sag and eventual contact between the fuel and the pressure tube caused a rise in the pressure tube temperature up to the threshold temperature of 1473 K. This caused

the pressure tube to rupture. To reiterate, it is assumed that once the pressure tube ruptured that calandria tube would also rupture. Upon rupture, a flow path was established between the high power fuel channel and the calandria vessel. Coolant quickly began to flow through the fuel channel arresting any further deformation of the channel and preserving the integrity of the core geometry. With flow occurring on the inside of pressure tube as well as the outside of the calandria tube the inside temperature of the pressure tube initially fell below that of the interior portion of the tubes. Once the heat is removed from the tubes the inside of the pressure tube returns to being the highest in temperature given that it is next to the coolant which is higher in temperature than the moderator.

4.2.6 Hydrogen Production

Although no fission products were released, hydrogen production did occur, as seen in Figure 57. After the pressure tube ruptured, hydrogen generation drops quickly because the sheath temperature dropped to nominal values. The total hydrogen produced in this accident is seen to be approximately 6.4^{-4} kg. This amount of hydrogen is too small to lead combustible concentrations in the containment building.

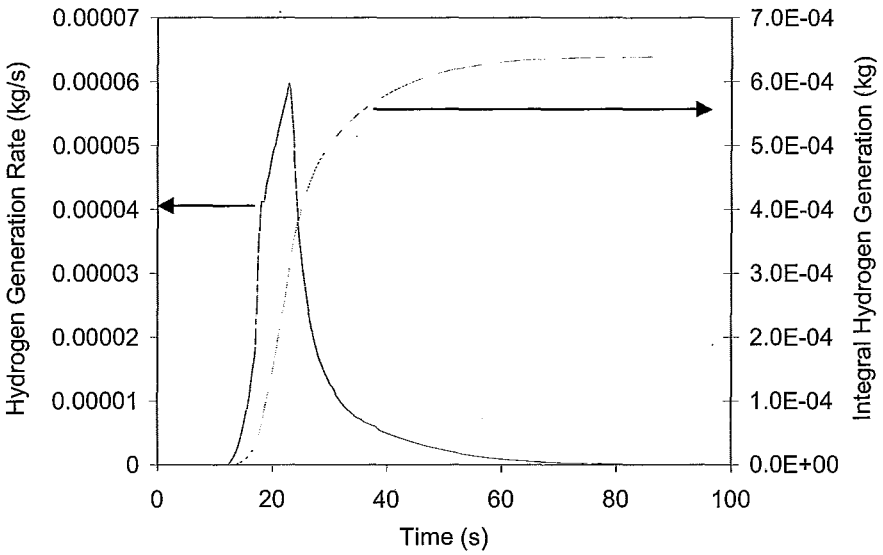

Figure 57: Actual hydrogen generation in high powered fuel channel

Hydrogen production occurs due to the oxidation reaction occurring between zircaloy and the steam generated the high power fuel channel. This oxidation reaction is exothermic and does contribute to fuel heat up. (Figure 58) The production of hydrogen starts at 13 seconds when the fuel sheath has reached a temperature of approximately 1000 K. The hydrogen generation rate reaches a maximum at 23 seconds when the temperature of the sheath is the highest and then drops. The hydrogen production stops altogether at 72 seconds.

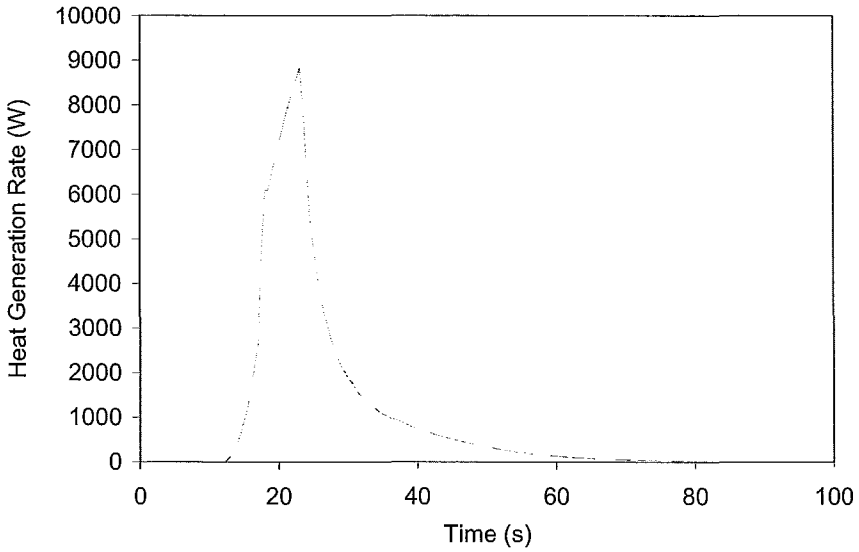

Figure 58: Heat generation from decay heat and oxidation

4.2.7 Moderator Transients

As the high pressure, high temperature coolant is injected into the calandria vessel it initially undergoes a very rapid pressure transient. This rapidly exceeded the rating of the rupture disks in the calandria vessel (i.e. 238 kPa) at 34 seconds. In this accident only one rupture disk was modelled to break, although there are 4 attached to the calandria vessel. It is seen that these other rupture disks were not necessary to depressurize the calandria because the calandria vessel never again went above the rupture disk rating.

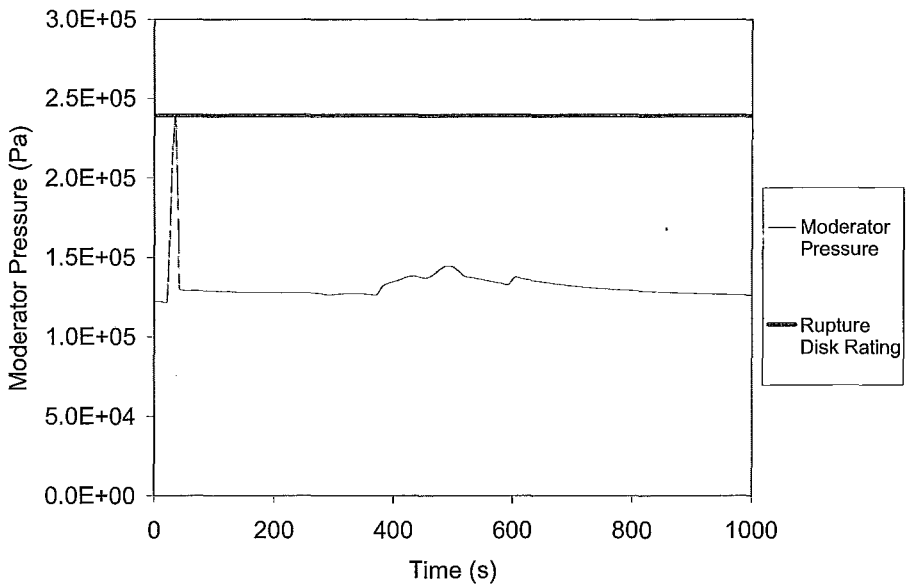

Figure 59: Moderator pressure transient and rupture disk rating

The moderator temperature initially increased as the fuel channel heated up as seen in Figure 60. The largest temperature of 378K was reached at 456 seconds but decreased as the heat load to the moderator decreased.

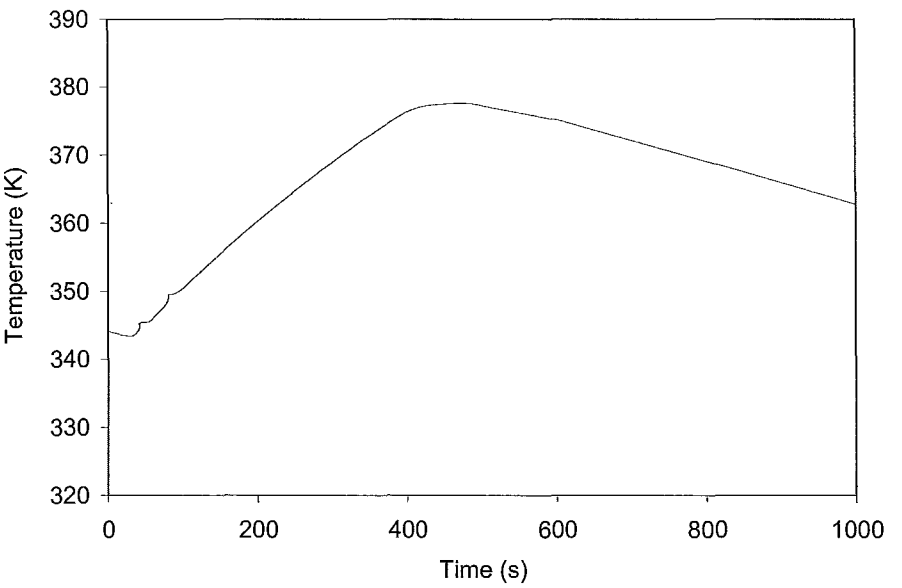

Figure 60: Moderator temperature transient

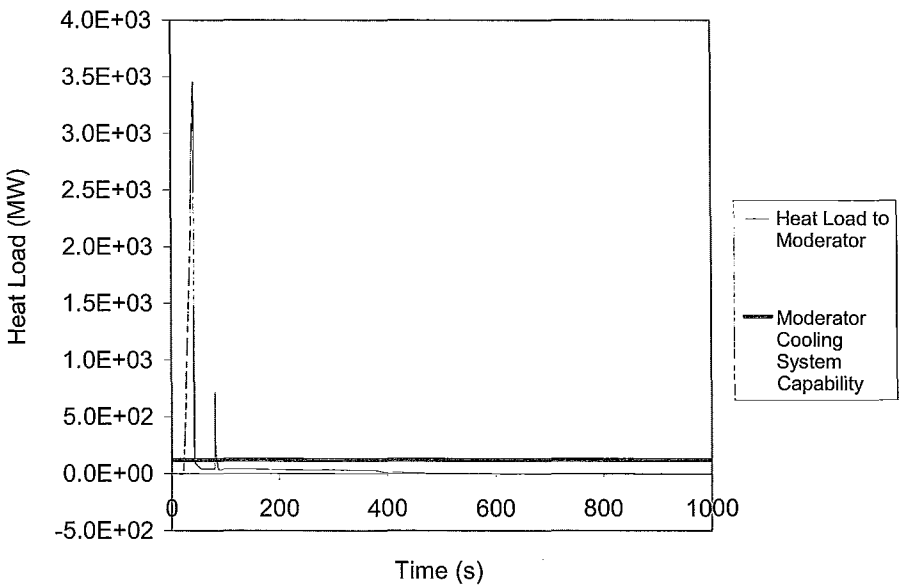

Figure 61: Heat load to moderator and moderator cooling system capability

The heat load to the moderator is shown in Figure 61. The limited flow of heat to the moderator was initially due to convection heat transfer of the coolant from the fuel to the pressure tube which then conducted the heat to the carbon dioxide gap and then the calandria tube. The highest spike in heat transfer to the moderator occurred when the pressure tube ruptured. At 42 seconds, the flow of hot coolant back into the channel and then into the moderator increased the heat input into the moderator, to a maximum of 3400 MW. The moderator cooling system has the capability of removing heat up to 120 MW. This cooling system regains the ability remove all the heat at the rate it's being produced at 86 seconds.

The integral amount of heat deposited in the moderator is seen in Figure 62 below. The excess heat going into the moderator can be seen as causing the moderator to boil off.

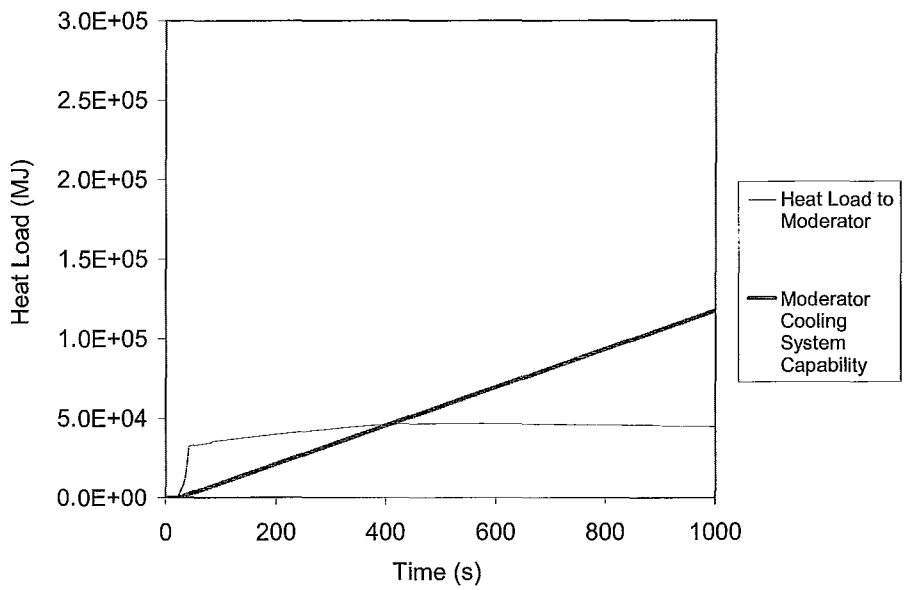

Figure 62: Integral heat load to moderator and integral moderator cooling system capability

If the moderator cooling system was fully operational at the start of the event then it would regain the ability to remove all heat at 403 seconds.

4.2.8 Containment and Fission Product Release

In the simulation of the inlet feeder stagnation break, no fission products were generated. Given that the containment was modelled as a single large control volume with no compartments or control systems the containment pressure and temperature remained constant over time. That is to say the temperature and pressure of the containment were constant at 298.15 K and 124 kPa respectively. Nevertheless, the containment has a leakage rate of 0.5% at these nominal values of temperature and pressure (Doria, 2001).

Given that in the actual simulation no fission product release was observed a release from containment was also prevented. However, in the worst case scenario for a single channel event the entire fission product inventory for the channel could be postulated to be released into the containment. See Table 8 above for the maximum power channel inventories in a CANDU reactor.

Using this leakage rate and the free inventory of the maximum power channel in a CANDU reactor from Table 8, at 403s the total activity released outside containment would be estimated to be:

$$^{121}I: \quad 12140Ci \times \frac{0.005}{day} \times \frac{day}{24 \times 3600\,\text{sec}} \times 403\,\text{sec} = 0.28Ci$$

$$Xe + Kr: \quad 36724Ci \times \frac{0.005}{day} \times \frac{day}{24 \times 3600\,\text{sec}} \times 403\,\text{sec} = 0.86Ci$$

Fortunately, the rupture of the pressure tube in a timely manner enabled the moderator to act as an ultimate heat sink and prevented the fuel from heating up to the point of this release.

4.2.9 Major Event Sequence Summary

Table 10: Major event sequence for SCDAP/RELAP5 & MELCOR simulation

Time		Event	Codes Used
Hours	Seconds		
0.0	0.0	• SBLOCA - single inlet feeder break • LOECI • Broken loop isolated • Reactor at full power	SCDAP/RELAP5 & MELCOR
0.0	1.0	• Reduced flow in all fuel channels • Flow stagnation in high power fuel channel attached to broken reactor inlet feeder	SCDAP/RELAP5 & MELCOR
0.0	13.0	• Hydrogen production starts	SCDAP/RELAP5
0.01	24.0	• Closed pack configuration • Pressure tube rupture • Reactor trip • Calandria rupture disks breaks due to overpressure • Moderator boil-off begins	SCDAP/RELAP5 & MELCOR
0.01	34.0	• Flow re-established in high power fuel channel	MELCOR
0.02	72.0	• Hydrogen production ends	SCDAP/RELAP5
0.08	403.0	• Moderator cooling system capable of removing remaining decay heat • Termination of accident	MELCOR

4.3. Intercomparison and Validation of Models

In this section the intercomparison and validation is considered for the individual models in MATLAB, SCDAP/RELAP5 and MELCOR as well as the code-coupled MATLAB-MELCOR and SCDAP/RELAP5-MECLOR simulations.

4.3.1 Validation of MATLAB Model

Multiple combinations of the correlations used in the MATLAB single fuel channel model are shown in Table 11 below. The different combinations of the correlations were employed in order to isolate the effects of the individual correlations relative to the others.

Table 11: Correlation validation matrix with results for time to a sheath temperature of temperature of 1200 °C (1473 K)

Mixture Properties/ Two-Phase Multiplier	Viscosity Correlation	CHF Correlation	PDO Correlation	Time to 1200 °C (s)
Dukler	Baroczy	Biasi	Groeneveld and Delorme	13
McAdams	Baroczy	Biasi	Groeneveld and Delorme	14
Cicchitti	Baroczy	Biasi	Groeneveld and Delorme	10
Friedel	Baroczy	Biasi	Groeneveld and Delorme	18
Dukler	HEM	Biasi	Groeneveld and Delorme	7
Dukler	LM	Biasi	Groeneveld and Delorme	10
Dukler	Thom	Biasi	Groeneveld and Delorme	9
Dukler	Baroczy	Biasi	Groeneveld and Delorme	13
Dukler	Baroczy	Biasi	Groeneveld and Delorme	13
Dukler	Baroczy	Katto	Groeneveld and Delorme	10
Dukler	Baroczy	Bowring	Groeneveld and Delorme	4
Dukler	Baroczy	Biasi	Groeneveld	15
Dukler	Baroczy	Biasi	Dougall and Rohsenow	8
Dukler	Baroczy	Biasi	Groeneveld and Delorme	13

In order to compare the results of the validation matrix the arithmetic mean and standard deviation are computed for the time it takes for the sheath to reach 1200°C (1473). These values are listed in Table 12 below.

Table 12: Comparison of results generated from validation matrix

Time for sheath temperature to reach 1200°C (s)	
Mean (s)	**Standard Deviation (s)**
11.2	+/- 3.6

Using one standard deviation as the criterion to determine an outlier we see that the Friedel correlation and the Bowring correlation generate results that that are considered outliers relative to the other correlations. Given the vast data set from which the Friedel correlation was derived indicates that it should differ somewhat in the predicted time at which CHF occurs. On the other hand, the Bowring correlation under predicts the time it will take the temperature to reach 1200°C (1473 K). As discussed in Section 3.1.3.8, Katto correlation can outperform the Bowring correlation in predicting CHF data for water. For these reasons the Bowring correlation is suspected to be outside of its range of applicability.

It is important to ensure that there is no spatial dependence on the times to the sheath temperature of 1200 °C (1473 K). To test this, multiple simulations were conducted by varying only the number of nodes. The results are graphed in Figure 63 below.

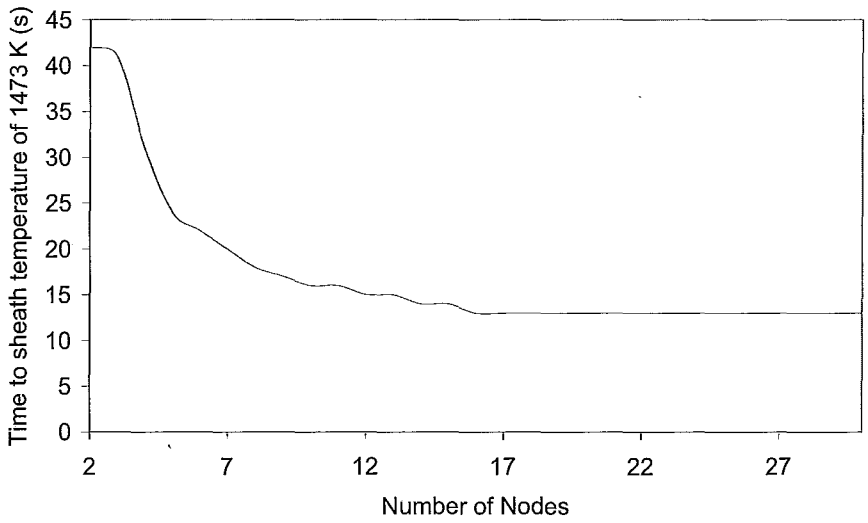

Figure 63: Spatial dependence on time to sheath temperature of 1200°C (1473 K)

As illustrated in Figure 63, as the number of nodes is increased the time to a sheath temperature of 1200°C (1473 K) levels off at values of 13 seconds. Hence, to ensure that there is no spatial dependence present for a simulation a value of 16 nodes or greater should be used. The total operable number of nodes tested ranged between 2 and 30.

Given that the numerical methods employed in the computer code are slightly semi-implicit there will still be some effect of the time step size on the results, given the Courant limit. The Courant limit is defined as:

$$\Delta t < \frac{\Delta z}{u}$$

Equation 100

The Courant limit tells us that the distance the fluid travels in one time step should not be greater than the discretization. It is therefore important to ensure that there is no temporal dependence on the time to a sheath temperature of 1200°C (1473 K) during a simulation. To test this, multiple simulations were conducted by only varying the size of the time step.

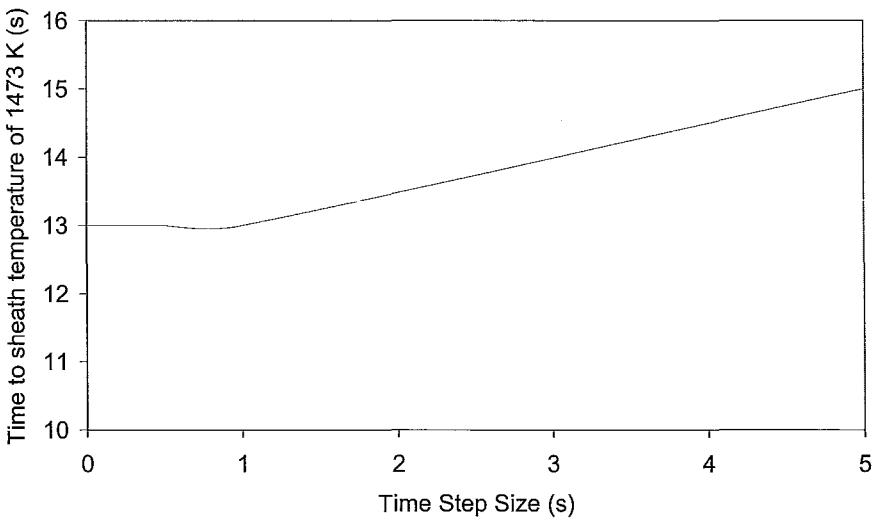

Figure 64: Temporal variance on time to sheath temperature of 1200°C (1473 K)

Figure 64 illustrates that as the time step decreases in size the times to a sheath temperature of 1200°C (1473 K) approach values of 13 seconds. This time of 13 seconds first occurs for a time step of 1 second. Hence, it is suggested that a time step of 1 second or less be used while running simulations with the code. The total operable time step sizes tested ranged between 0.01 seconds and 5 seconds.

4.3.2 Intercomparison and Validation of SCDAP/RELAP5

In order to validate the SCDAP/RELAP5 model it was compared with the results from Mladin et al. (2009). Using RELAP/SCDAPSIM Mod 3.4 (bi7), Mladin et al. (2009) developed a model with postulated boundary conditions to simulate the evolution of the fuel channel in a CANDU6 during a large break loss of coolant accident (LBLOCA) in conjunction with a loss of emergency cooling injection (LOECI). Given that the original SCDAP/RELAP5 model that had been created for SBLOCA-LOCEI event the power, pressure and flow rate transients were altered to coincide with the values used by Mladin et al. Also available in the paper by Mladin et al. (2009) were the results for a CHAN II model for the same accident boundary conditions, concerning the fuel and pressure tube temperatures, power components (generated and exchanged to the moderator) and hydrogen production. The LBLOCA-LOECI conditions for Mladin et al., CHAN II (also available in Mladin et al., 2009) and SCDAP/RELAP5 models are listed in the Table 13 below.

Table 13: Conditions for Mladin et al., CHAN II and SCDAP/RELAP5

Model Conditions	SCDAP/RELAP5 (Mladin et al., 2009)	CHAN II (Mladin et al., 2009)	SCDAP/RELAP5
Radial power peaking factors	0.778, 0.817, 0.915, 1.130	Unknown	0.778, 0.817, 0.915, 1.130
Steam mass flow rate	5 g/s	5 g/s	5 g/s
Time to liquid phase = 0 g/s	5 seconds	5 seconds	5 seconds
Pressure loss coefficients	0.82	Unknown	0.82
Max axial power factor	1.415	1.415	1.415
Radiation heat transfer	Yes	Yes	Yes
PT and CT emissivities	ε_{PT}=0.85, ε_{CT}=0.95	ε_{PT}=0.7, ε_{CT}=0.2	ε_{PT}=0.7, ε_{CT}=0.2
Moderator	Large stagnant volume at 1.25 bar and 74 °C	Large stagnant volume at 1.25 bar and 74 °C	Large stagnant volume at 1.25 bar and 74 °C
Water properties	Light water	Light water	Light water
Fission products data	ANS79-1	ANS79-1	ANS79-1
Channel power (max rating)	7.3 MW	7.3 MW	7.3 MW
Positive void reactivity effect	Yes	Unknown	No
Sagging	Yes	No	Yes
Contact angle	5°	5°	5°
CO_2 thermal conductivity	Function of Temperature	0.043 W/mK	Function of Temperature

Comparison with the Mladin et al. model and CHAN II code was done for both the fuel temperatures and the hydrogen production. The lowest amount of steam flow tested by Mladin et al. was 5 g/s. This steam flow rate was chosen for a basis of comparison given that is relatively close to stagnant flow conditions. The fuel temperature for each of the codes is shown in Figure 65.

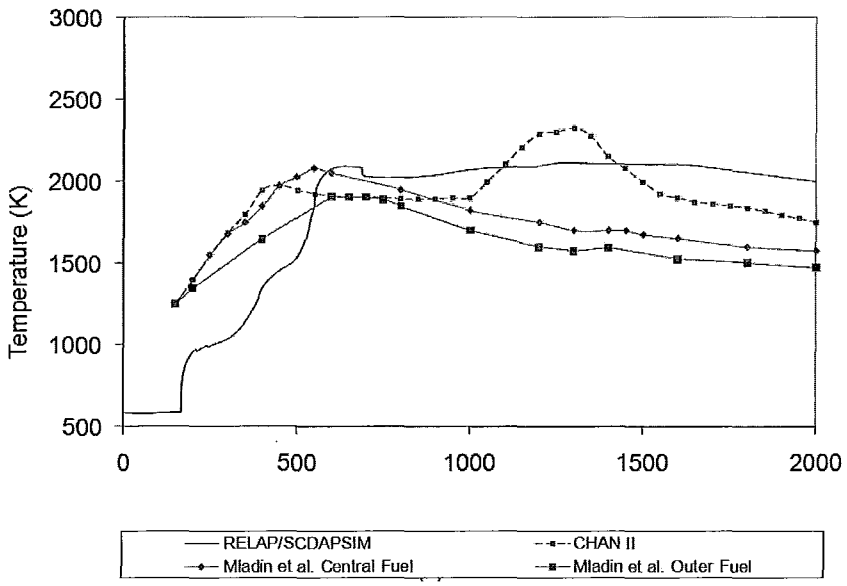

Figure 65: Fuel surface temperatures comparison between SCDAP/RELAP5, CHAN II, Mladin et al. central and outer fuel and fuel temperature; steam flow: 5 g/s

The temperature transient in the SCDAP/RELAP5 model is comparable to the results presented by Mladin et al. (2009). This was anticipated given the similarities between the two models. The only difference between the two models is the timing of the transient. Mladin et al. had modelled the fuel channel with 4 pipe components including cross-flow junctions as seen in Figure 9 above. This

would have increased the convective heat transfer from the fuel and thus caused the fuel to cool faster.

The temperature in the SCDAP/RELAP5 model is higher than fuel temperature in CHAN II for most of the time for the same mass flow rate. However, the peak temperature is up to 200 degrees lower than in CHAN II. The moments for attaining the temperature peaks are more or less the same in the two codes. A reason for lower temperatures in CHAN II could be the existence of the model for direct metal–metal contact, which is not modelled in SCDAP/RELAP5. In addition, CHAN II required an input criterion to trigger the simulation of the slumping bundle deformation model that would cause direct contact and flow bypass which seems not to be activated, otherwise CHAN II temperatures would be as low as SCDAP/RELAP5 results for the close-packed configuration for the given flow rates.

Another source of differences in the results could be the heat transfer towards the moderator. The constant value of gas conductivity in CHAN II versus the temperature dependent conductivity in SCDAP/RELAP5 would have an effect on the temperatures. The temperature dependence of conductivity in SCDAP/RELAP5 should be more limiting with higher temperatures, since the CO_2 conductivity is increasing with temperature.

The comparison of the hydrogen produced during the transient is shown in Figure 66 below. The difference in hydrogen production for the codes can be attributed to the difference in the sheath temperatures within the codes. The level

of the hydrogen production is different by 28% between the three codes, in the range of maximum values.

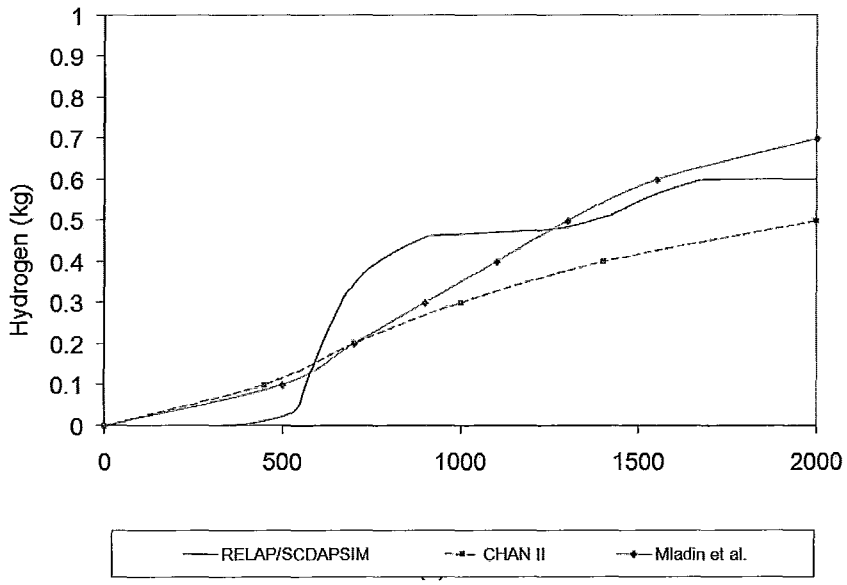

Figure 66: Hydrogen production comparison between SCDAP/RELAP5, CHAN II, Mladin et al. central and outer fuel and fuel temperature; steam flow: 5 g/s

The SCDAP/RELAP5 provides results that are comparable to the Mladin et al. fuel channel model and the CHAN II model.

4.3.3 Intercomparison and Validation of MELCOR Model

Brown, Petoukhov and Mathew (2006) compared simulation results for the initial primary heat transport system blow-down, during a large break loss of coolant accident (LBLOCA) in conjunction with a total loss of emergency cooling injection (LOECI), as postulated for a CANDU 6 nuclear power plant. The comparison was made between results obtained with two independent CANDU 6 models using the computer codes MAAP4-CANDU v4.05A and CATHENA Mod 3.5 Rev0.

The results from MAAP4-CANDU analyses support Level 2 PSA activities performed for CANDU stations. While CATHENA MOD 3.5 Rev 0 was validated against critical and other sizes of reactor inlet header breaks in the RD-14M thermalhydraulic loop, among other phenomena and integral tests. Hence the MELCOR primary heat transport system model was compared to these codes to provide confidence in the use of MELCOR for thermalhydraulic phenomena involved in LOCA blow-down scenarios. The LBLOCA-LOECI conditions for MAAP4-CANDU, CATHENA and MELCOR models are listed in the Table 14 below.

Table 14: Conditions for CATHENA, MAAP4-CANDU and MELCOR

Model Conditions	CATHENA (Brown et al. 2006)	MAAP4-CANDU (Brown et al. 2006)	MELCOR
Break	35% of twice the cross-sectional area of RIH	35% of twice the cross-sectional area of RIH	35% of twice the cross-sectional area of RIH
Reactor trip	0.43 seconds	0.43 seconds	0.00 seconds
Class III and IV power	Available continuously	Available continuously	Available continuously
Start of loop isolation	8.6 seconds	8.6 seconds	0.00 seconds
Start of crash cooling	38.7 seconds	38.7 seconds	Steam generator modelled with constant heat removal
Moderator cooling	Available	Available	Available
Turbine steam valve close	40 seconds	40 seconds	Not applicable (steam generator modelled with constant heat removal)
Containment	Large junction area ($100m^2$) at atmospheric conditions	Large junction area ($100m^2$) at atmospheric conditions	Large coarse volume at atmospheric conditions
Initial system pressure	(RIH ~ 11.38 MPa and ROH ~ 10.02 MPa)	10.69MPa (single system pressure)	(RIH ~ 11.5 MPa and ROH ~ 10.0 MPa)
Water properties	Heavy water	Light water	Light water
Initial void	6.8%	6.8%	0.0%
Discharge model	Henry-Fauske	Henry-Fauske	Henry-Fauske
Discharge coefficient	0.61	0.61	0.61

The comparison of the results for CATHENA, MAAP4-CANDU and MELCOR can be seen in Figures 67 through 71 below. The codes show similar trends for the depressurization in Figure 67. However, it is noted that MAAP4-

CANDU has one primary system pressure because no flow calculations are performed with the primary heat transport system. The exceptions to this are the break flow and the channel steam flow rates during the later core heat up stage.

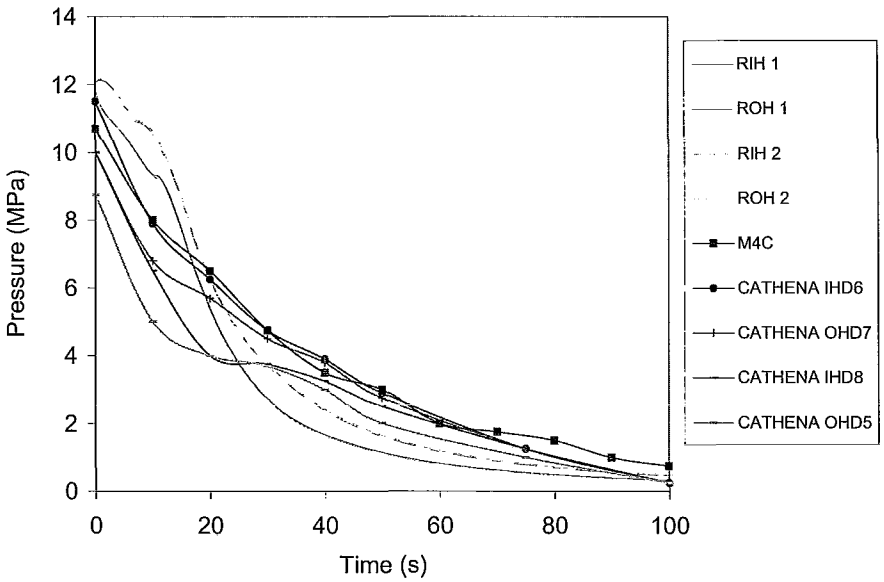

Figure 67: Broken loop pressure

The pressure within the headers is mostly affected by the mass discharge rate from the headers through the break. The mass discharge from the 35% inlet header break can be seen in Figure 68 below.

It is worth noting that the CANTHEA LBLOCA-LOECI simulation was performed with heavy water properties, where as the MAAP4-CANDU and MELCOR simulations were performed with light water properties. To aid the comparison Brown, Petoukhov and Mathew divided the heavy water fluid masses predicted with CATHENA by 1.103 to give the equivalent light water masses. The value of 1.103 is the density ratio of liquid heavy water to liquid light water

at typical CANDU operating conditions. Hence the CATHENA fluid masses presented are in "light-water equivalent masses" of heavy water.

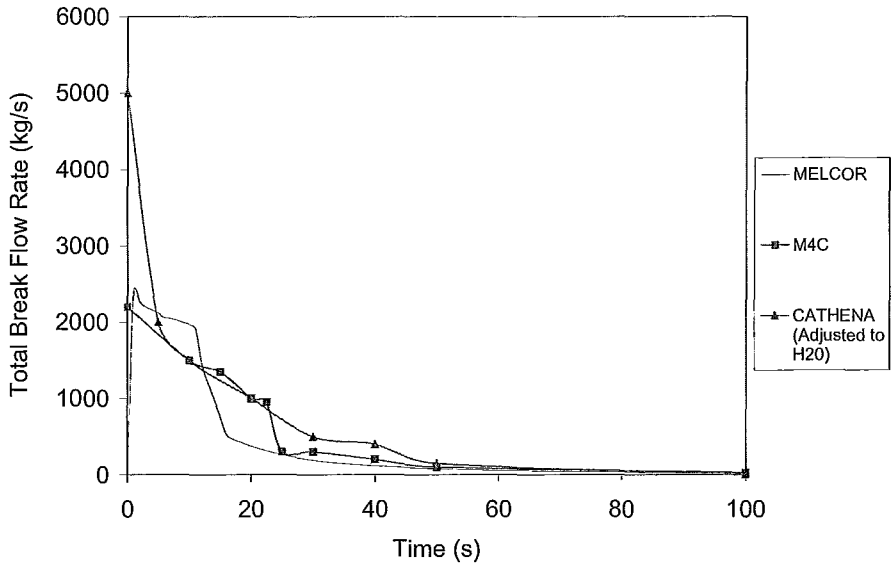

Figure 68: Total break flow rate

The total break flow rate for CATHENA was initially much higher than both the MAAP4-CANDU and MELCOR simulations. This provides the reason as to why the header pressures for the CATHENA simulation depressurized more rapidly. The Henry-Fauske two-phase critical flow break discharge model was used in the CATHENA simulation. In the CATHENA simulation, the primary heat transport coolant was discharged through the break in the reactor inlet header into a containment compartment at atmospheric conditions. Brown, Petoukhov and Mathew highlighted that the area of the junction connection between the primary heat transport system and the containment may cause the differences in

the break flow rate. It is suspected that the junction areas used in MAAP4-CANDU and CATHENA were larger than in the MELCOR simulation. This may be why the integrated break flow mass is also lower for MELCOR as seen in Figure 69.

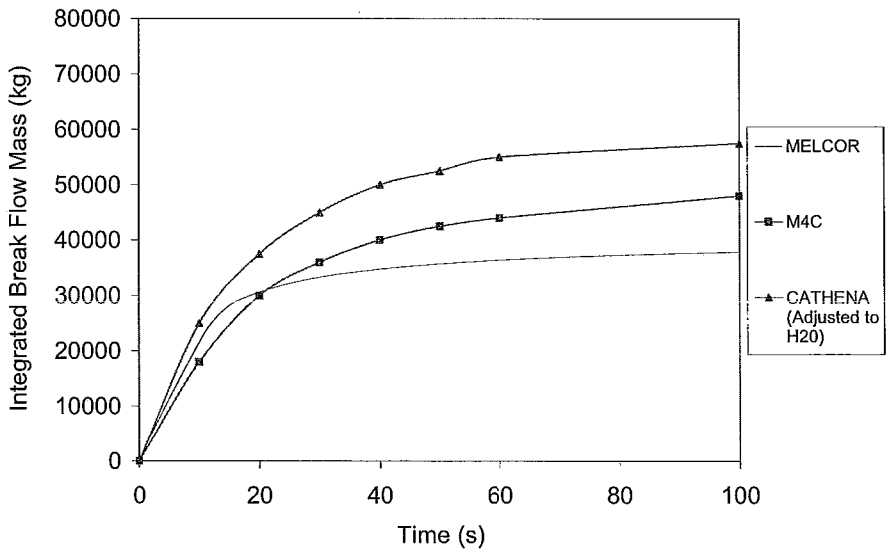

Figure 69: Integrated break flow mass

The total mass within the primary heat transport system is shown in Figure 70. The total mass within the system is approximately 20% higher for MELCOR simulation than the MAAP4-CANDU and CATHENA. This is due to two factors. First, both MAAP4-CANDU and CATHENA initially contained void within the primary heat transport system where as MELCOR did not. In fact, Brown, Petoukhov and Mathew (2006) stated that they initially adjusted the void fraction such that the total primary heat transport system fluid masses were the same. This would mean that there would be less liquid in the system and thus

there would be a lower total mass. Second, both MAAP4-CANDU and CATHENA had the rector trip occur at 0.43 seconds whereas the reactor trip occurred at 0.00 seconds for the MELCOR simulation. This initial extra heat input into the coolant would cause further void generation and further displacement of liquid with void within the primary heat transport system.

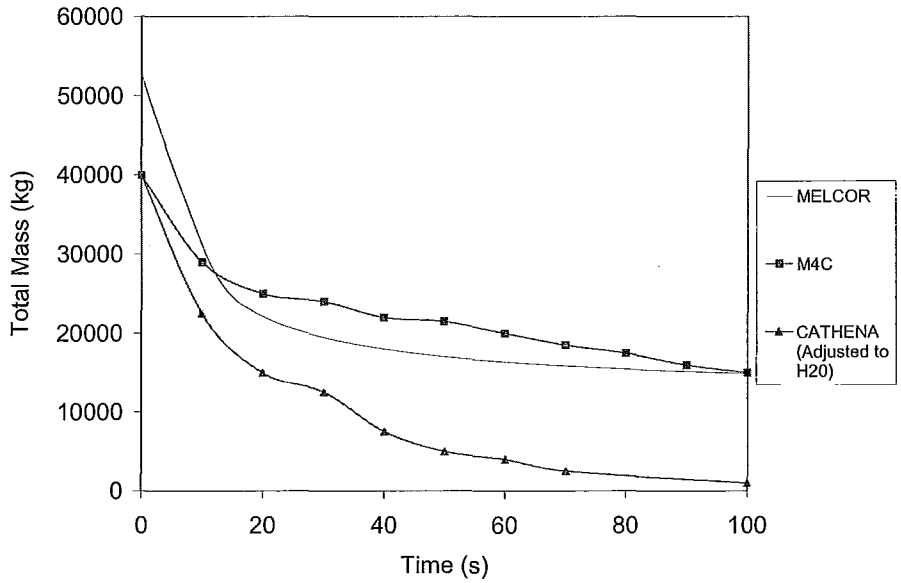

Figure 70: Broken loop total fluid mass

This initial difference in the void of the system is seen in Figure 71. Basically if the void had been adjusted in the MELCOR simulation the integrated void fraction for the MELCOR simulation would match very well. Given that the void fraction was not adjusted for the MELCOR simulation, it was consistently a value of 0.1 to 0.2 smaller than the MAAP4-CANDU value throughout the course of the transient.

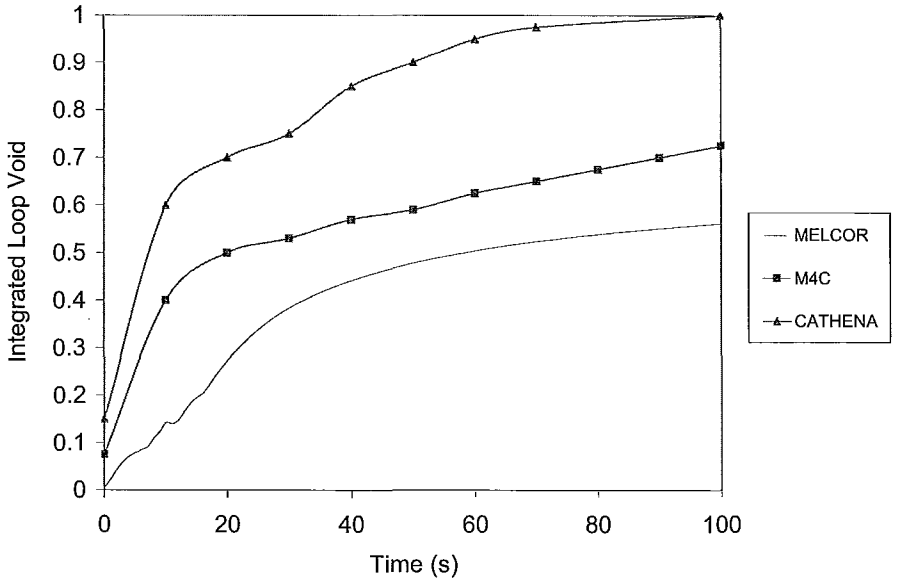

Figure 71: Integrated loop void fraction

Beside the minute differences that can be attributed to difference in the way the three simulations are set up CATHENA, MAAP4-CANDU and MELCOR are in good agreement. The models display the same trends for key system variables.

4.3.4 Code-coupling Intercomparison and Validation

Hussein (1989) modelled an accident scenario in a CANDU nuclear reactor in which the flow in a single fuel channel at high power was reduced due to a reactor inlet feeder break. Hussein studied different break sizes, including a stagnation break (10.69 cm^2) and the release to the atmosphere (^{131}I and Xe+Kr). For the stagnation break the AECL computer code FIREBIRD was used to simulate the thermalhydraulics of the primary heat transport system. The mass discharge rate and enthalpy were thus obtained and then introduced into the

containment response AECL code PRESCON to find the integrated overpressure. Estimates of the fission product inventories in the channel were obtained from the AECL computer code CURIES. Fuel centerline, fuel surface and sheath temperatures were calculated using the AECL computer HOTSPOT.

The comparison of Hussein's results with the results of the code-coupling of MATLAB-MELCOR and SCDAP/RELAP5-MELCOR of mass and enthalpy discharge can be seen in Figures 72 and 73 respectively.

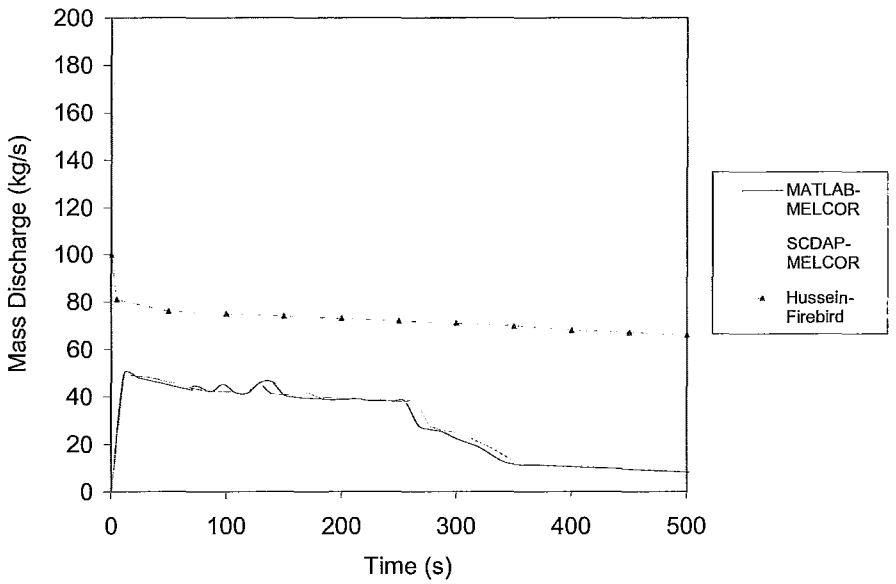

Figure 72: Inlet feeder break mass discharge into containment building

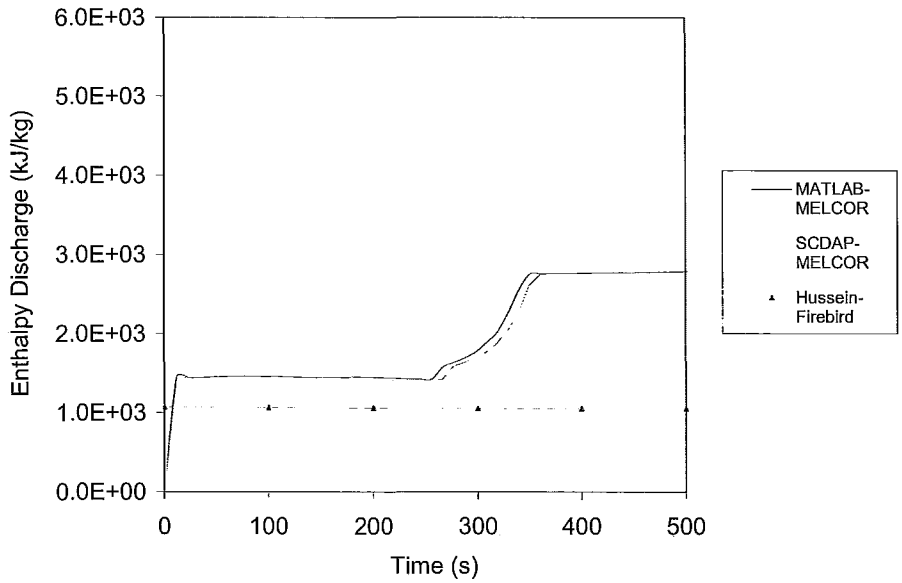

Figure 73: Inlet feeder break enthalpy discharge into containment

It can be seen that the mass discharge for Hussein's simulation is higher than both MATLAB-MELCOR and the SCDAP/RELAP5-MELCOR simulations. This is due to the fact that the stagnation break for the FIREBIRD code was 10.69 cm^2 where as it was 8.03 cm^2 for the MATLAB-MELCOR and the SCDAP/RELAP5-MELCOR simulations. This is a difference in area of 25% where as the differences in mass and enthalpy discharges are 37.5 % and 26% respectively. The difference in the mass discharge is most likely due to the loss coefficient used in modelling the break in MATLAB-MELCOR and the SCDAP/RELAP5-MELCOR simulations. The forward loss and reverse loss coefficient were kept at the default value of 1.0 within MELCOR. It is suspected that the loss coefficients within the FIREBIRD code would be somewhat less. Given that the enthalpy discharge scales appropriately with the difference in area and the mass discharge does not suggests that this is the case.

As seen in Figure 73, the enthalpy of the coolant exiting through the break increased and rapidly reached a plateau twice during the course of the transient MATLAB-MELCOR and the SCDAP/RELAP5-MELCOR simulations. The initial increase was obviously due to the start of the transient. The rapid rise in coolant enthalpy around 250 seconds exiting through the break is due to declining coolant inventory. The coolant inventory decreased much more rapidly than the decay heat in the fuel from fission products. Roughly the same heat input into a smaller amount of coolant caused the coolant to heat up and turn into vapour. Given that Hussein was only modelling a single fuel channel the effect of the void accumulating in the headers was not seen.

The comparison of the fuel centerline temperatures for Hussein's model, MATLAB-MELCOR and SCDAP/RELAP5-MELCOR are seen in Figure 74 below.

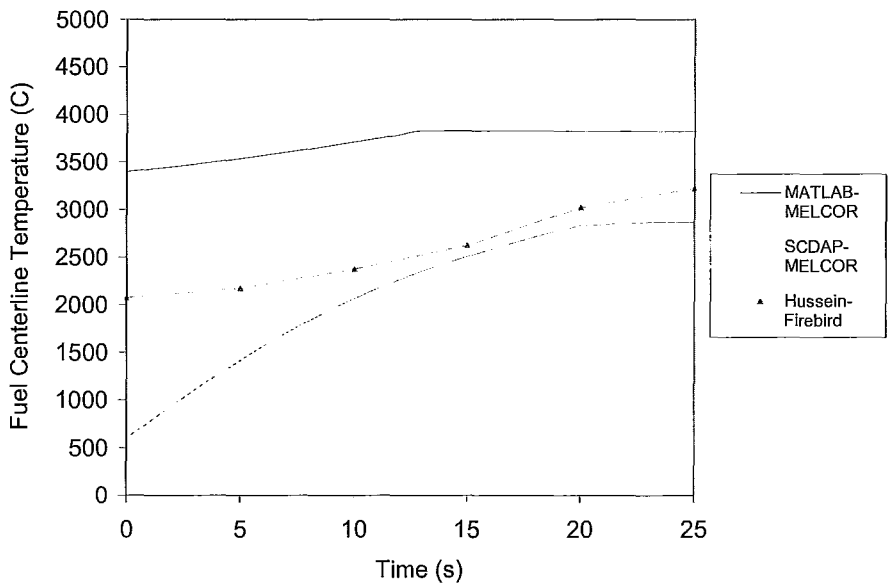

Figure 74: Fuel centerline temperatures

It is seen that the centerline temperatures are in reasonable agreement. The MATLAB-MELCOR model predicts a higher temperature than Hussein's model and the SCDAP/RELAP5-MELCOR model because it does not account for radiation heat transfer which would help cool the fuel at higher temperatures.

The SCDAP/RELAP5 model predicts lower temperatures than Hussein's model. It is suspected that Hussein did not model the enhanced heat transfer due to pressure tube sagging into contact with the calandria tube. Regardless of this fact the trend of temperatures of both models are in good agreement with one another. This is also seen for the sheath and pressure tube temperatures which are seen in Figure 75 and Figure 76 respectively.

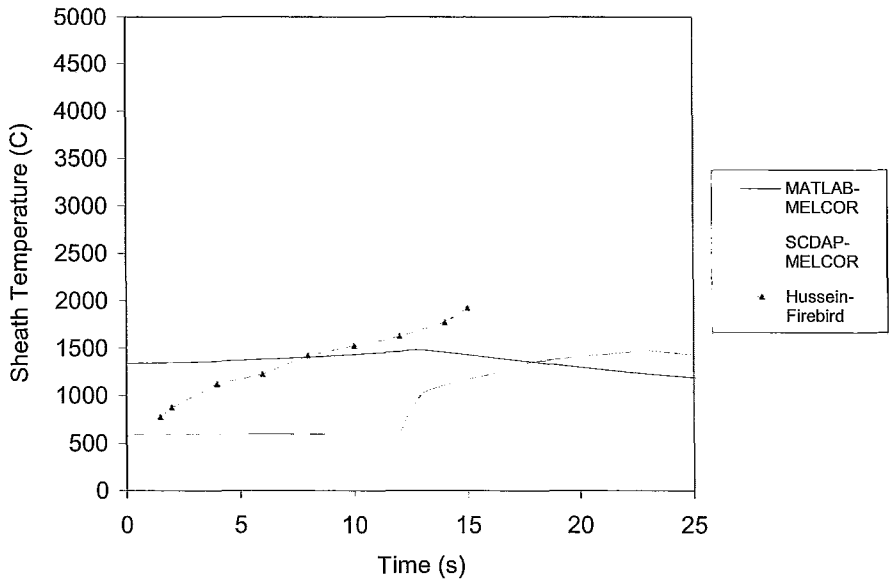

Figure 75: Fuel bundle sheath temperatures

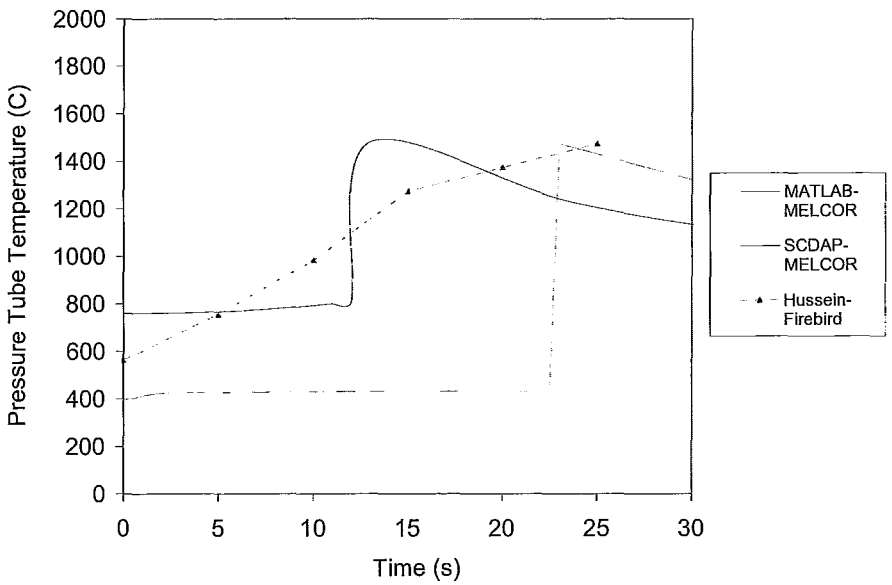

Figure 76: Pressure tube temperatures

Hussein's prediction is that the pressure tube will rupture at 25 seconds. This is in good agreement with SCDAP/RELAP5-MELCOR model which predicts that the pressure tube will rupture at 23 seconds. However, given that the MATLAB-MELCOR simulation does not take into account radiation heat transfer within the fuel channel experiencing flow stagnation accounts for the fact that it will experience the pressure tube rupture sooner (i.e. 13 seconds after the initiation of the feeder break).

5. Limitations and Recommended Future Work

Although it has been shown that the current analysis is in reasonably good agreement with the results generated by the models of other computer codes, the analysis highlights the possible areas for model improvements within the MATLAB, SCDAP/RELAP5 and MELCOR models. In addition, some future work is recommended.

5.1 Limitations of the MATLAB Single Fuel Channel Model

One of the major limitations within the MATLAB single fuel channel model is its ability to model fuel deformation. It was taken that the high power fuel channel experiencing flow stagnation rapidly becomes devoid of coolant. This leads to a uniform temperature that persists around the circumference of the fuel. This eventually leads to fuel end plate failure and the fuel elements resting at the bottom of the fuel channel in the close-packed configuration. The pressure tube will then rupture due to contact with the fuel at a temperature of 1473 K. Under high system pressure (as in the case for a SBLOCA) this would lead to ballooning of the pressure tube. Instead in the current analysis, sagging was modelled to occur instead so that higher temperatures persisted which made the analysis comparable to the work done by Mladin et al. (2009). However, if the fuel channel experienced slow coolant removal it would then be possible to have subsequent phase separation of the coolant in the fuel channel. This could lead to circumferential temperature gradients, clad melting and relocation onto the

pressure tube, which is predicted to cause failure. This would necessitate adequate models for relocation of the metallic/ceramic melt in horizontal fuel channels.

Besides the sagging phenomena, the MATLAB model was limited in its ability to model fuel deformation. The model did not consider the following deformation mechanisms:

- Fuel element bowing
- Zircaloy oxidation
- Be-braze penetration

Another limitation of the MATLAB model was that it did not consider thermal radiation. At higher temperatures this would have increased the heat transfer from the fuel causing a longer time to pressure tube rupture.

Fission product behaviour was another factor not considered within the MATLAB model. This was not modelled due to the model limitations with regards to fuel deformation.

The SCDAP/RELAP5 single fuel channel model was seen as an improvement to the MATLAB single fuel channel in that it included: zircaloy oxidation, radiation heat transfer, enhanced heat transfer in the CO_2 gap between the pressure tube and the calandria tube and fission product behaviour. Although it did resolve most deficiencies experienced with the MATLAB single fuel channel model it had limitations as well.

5.2 Limitations of the SCDAP/RELAP5 Single Fuel Channel Model

Similar to the MATLAB single fuel channel model, the SCDAP/RELAP5 model's major limitation was its ability to model fuel deformation, specifically within a horizontal fuel channel.

In the current model, it was taken that the high power fuel channel experiencing flow stagnation rapidly becomes devoid of coolant. As stated above, this leads to a uniform temperature that persists around the circumference of the pressure tube. However, if the fuel channel experienced slow coolant removal and subsequent circumferential temperature gradients around the fuel it would then be possible to have subsequent phase separation of the coolant in the fuel channel. This could lead to clad melting and relocation onto the pressure tube, which is predicted to cause failure. It was found that RELAP/SCDAPSIM Mod 3.4 (bi7) does not contain any adequate models for relocation of the metallic/ceramic melt in horizontal fuel channels.

Within RELAP/SCDAPSIM Mod 3.4 (bi7) code, when melt is located in a horizontal hydrodynamic node it relocates to other nodes that are associated with the lower fuel. In other words, it relocates to the ends of the fuel channel. To prevent this from happening within the current model a null melt velocity was used.

Further work will be needed in developing relocation of the metallic/ceramic melt in horizontal fuel channels, if SCDAP/RELAP5 is to be used beyond CDS1. This challenge has been recognized by Mladin et al. (2009).

They are currently developing models for early phase degradation in a CANDU fuel for the SCDAP code.

5.3 Limitations of MELCOR CANDU 6 Model

Overall the MELCOR model produced the expected trends for the system variables. Even though the MELCOR model used the approaches taken in the MAAP4-CANDU and ISAAC models (Sections 3.1 and 3.2), further work could be done on investigating the affects of the nodalization scheme used on the fuel channels, moderator, steam generators and containment.

The 12 fuel bundles of each fuel channel were only coarsely nodalized into 1 representative axial node within the MELCOR model. The boundary conditions for this 1 axial node were taken from highest temperature node within the single fuel channel models. It would be worthwhile to investigate the effect of a finer nodalization.

The moderator system was modelled as large stagnant volume of water at 122 kPa and 71°C. The calandria tubes are in contact with the moderator and are a source of heat input into this system. The heat injected into the moderator system was removed at a constant heat flux of 120 MW, which is the maximum rating for the moderator cooling system.

The steam generator secondary side was modelled in similar fashion to the moderator system. It was modelled as a large stagnant volume of water. The heat transferred to the steam was removed at a constant heat flux removal of 516 MW

from both the hot and cold legs of the steam generator, which is the normal operation heat removal rate.

Moreover, the containment building was only modelled as a single large volume at atmospheric conditions. It is for this reason that the containment system does not undergo any noticeable pressure or temperature transient.

5.4 Limitations of Code-coupling

There are many techniques for coupling advanced codes. In essence, the coupling may be either loose (meaning that two or more codes only communicate after a number of time steps) or tight such that the codes update one another time step to time step. Whether a loose coupling or a tight coupling is required depends on the phenomena that are being modelled and analyzed. It has been assumed that the loose coupling between the models for a single channel and the primary heat transport system was sufficient for the case of stagnant flow. The effects of coupling the codes time step to time step should be studied.

5.5 Further Work Recommendations

It is recommended that further work be conducted regarding: the long term effect of LOECI, investigation and implementation of CANDU-specific mechanistic models regarding fuel channel failure, sensitivity analysis with respect to important model parameters and verification of the simulation accuracy with respect to experimental results.

The specific focus of the accident analysis within this thesis was on the early stages of a SBLOCA-LOECI event, with particular attention to how the fuel channel experiencing flow stagnation affects the moderator. Given that this occurred in a relatively short time frame the consequences of the LOECI was minimal. The time frame should be extended such that the coolant inventory continues to decrease to the point where the event consequences propagate to other fuel channels.

A simplistic threshold temperature was used as the criterion for pressure tube rupture. A more mechanistic approach to this process should be employed in future work.

Sensitivity analysis is needed on key model variables to understand the implications of some of the assumptions made during this analysis. One prime example is the time of reactor trip. The reactor was assumed to trip at the moment of pressure tube rupture. This is most likely not the case given that for a SBLOCA the usual trip is low HTS pressure. Determination of the exact trip time would lead to a more physically realistic simulation.

Cross code intercomparison was used as validation technique because no experimental data was available. Determining the code accuracies with respect to experimental data should be conducted in order to give further confidence in the results.

If required please refer to the CD in the possession of my supervisor Professor John C. Luxat for the raw data and input files for the SCDAP/RELAP5 and MELCOR models (Pohl, 2009).

6. Conclusions

It has been shown above that the MACPISA-CANDU methodology has been successfully applied to the analysis of a small break loss of coolant accident (SBLOCA) with a loss of emergency coolant injection (LOECI) in a CANDU 6 nuclear power plant. The type of SBLOCA analyzed was a stagnation break in a reactor inlet feeder attached to a high powered fuel channel.

Coupling the MATLAB single fuel channel model with the MELCOR (MELCOR 1.8.5) primary heat transport system model led the pressure tube to reach a temperature of 1473 K and rupture at 13 seconds. The moderator was subsequently able to act as an ultimate heat sink at 298 seconds. However the MATLAB model was simplistic in nature. The simulation was improved by replacing the MATLAB single fuel channel model with a single fuel channel modelled in SCDAP/RELAP5 (RELAP/SCDAPSIM Mod 3.4 (bi7)) that included: zircaloy oxidation, radiation heat transfer, enhanced heat transfer in the CO_2 gap between the pressure tube and the calandria tube and fission product behaviour. The improved SCDAP/RELAP5-MELCOR simulation predicted the pressure tube to reach a temperature of 1473 K and rupture at 23 seconds and that the moderator system was able terminate the accident at 403 seconds. It is noted that the SCDAP/RELAP5-MELCOR simulation could be further improved by the inclusion of adequate models for relocation of the metallic/ceramic melt in horizontal fuel channels.

The results of the models compared well to results from other validated models both individually as well as after being coupled. Individually, the SCDAP/RELAP5 model compared well with results from the Mladin et al. (2009) RELAP/SCDAP5 model and the CHAN II model. The MELCOR model compared well with the MAAP4-CANDU and CATHENA models. Whereas the coupled results from the MATLAB-MELCOR and SCDAP/RELAP5-MELCOR simulations compared well with the results from coupling the AECL computer codes FIREBIRD, PRESCON, CURIES and HOTSPOT, which predict the pressure tube to reach a temperature of 1473 K at 25 seconds.

In the final analysis, the MACPISA-CANDU methodology, and code-coupling in general, has advantages over using fully-integrated severe accident codes for analyzing severe accidents in CANDU nuclear power plants. Code-coupling provides the diversity needed for intercomparison and validation purposes. It allows for incremental updating of computer codes with the latest research and experimental results such as bundle slumping in order to aid engineering judgment. Code-coupling allows the easier optimization of computational time given that smaller mechanistic models can be individually tuned. For these reasons, the MACPISA-CANDU methodology, and code-coupling in general, should be utilized as an alternative to fully-integrated codes to further the development of the nuclear industry in Canada.

7. References

AECL. *Comparison of DNGS, Bruce 'B' and CANDU 6: PHT System and Components*. Rep. Atomic Energy of Canada Limited, 1991. Print.

AECL Technologies Inc. "A Plan for the Pre-Application Review of the ACR, (Issued for discussion with the NRC)." *NRC: Design Certification Pre-Application Review - ACR-700*. U.S. NRC, 26 Sept. 2002. Web. 20 July 2009. <http://www.nrc.gov/reactors/new-licensing/design-cert/acr-700.html>.

Ahmad, S. Y. "Axial Distribution of Bulk Temperature and Void Fraction in Heated Channel with Inlet Subcooling." *Journal of Heat Transfer* (1970): 595-609. Print.

Brown, M. J., S. M. Petoukhov, and P. M. Mathew. "Influence of Coolant Phase Separation on Event Timing During a Severe Core Damage Accident in a Generic CANDU 6 Plant." *OECD Nuclear Energy Agency*. NEA, 22 May 2006. Web. 07 Aug. 2009. <http://www.nea.fr/html/nsd/reports/2007/nea6053/Session-IV-Applications-to-Uncertainty-Assessment-in-Level-2-PSA/>.

Carey, Van P. *Liquid Vapor Phase Change Phenomena An Introduction to the Thermophysics of Vaporization and Condensation Processes in Heat Transfer Equipment*. Dallas: Taylor & Francis, 2007. Print.

Chexal, B., and G. Lellouche. *A Full-Range Drift-Flux Correlation for Vertical Flows*. Tech. no. EPRI NP-3989-SR. Palo Alto, California: Electric Power Research Institute, 1985. Print.

Collier, John G., and John R. Thome. *Convective Boiling and Condensation*. 3rd ed. Vol. 39. Oxford UP, USA, 2001. Print.

Doria, F. J. "CANDU Safety #13: Small Loss of Coolant Accidents." Atomic Energy of Canada Limited, 21 May 2001. Web. 20 July 2009.

Gauntt, R. O., R. K. Cole, R. D. Gasser, S. B. Rodriguez, M. F. Young, Scott Ashbaugh, Mark Leonard, and Adam Hill. *MELCOR Computer Code Manuals: Demonstration Problems*. Rep. no. NUGREG/CR-6119 (SAND2001-0929P). Vol. 3. Albuquerque, NM: Sandia National Laboratories, 2001. Print.

Haaland, S. E. "Simple and Explicit Formulas for the Friction Factor in Turbulent Pipe Flow." *Journal of Fluids Engineering* 105 (1983): 89-90. Print.

Harrow, F. H., and J. E. Welch. "Numerical Calculation of Time-Dependent Viscous Incompressible Flow of Fluid with Free Surface." *Phys. Fluids* 8 (1965): 2182. Print.

Hussein, F. M. "Consequences of a Single Feeder Break Accident in CANDU Power Reactors." *J. King Saud Univ.* 1 (1989): 179-98. Print.

INTERNATIONAL ATOMIC ENERGY AGENCY. *Procedures for Conducting Probabilistic Safety Assessment of Nuclear Power Plants*. Rep. Vienna: IAEA, 1996. Print. Safety Report Ser. No. 50.

INTERNATIONAL ATOMIC ENERGY AGENCY. *Procedures for Conducting Probabilistic Safety Assessment of Nuclear Power Plants*. Rep. Vienna: IAEA, 1996. Print. 50-P-856.

INTERNATIONAL ATOMIC ENERGY AGENCY. *Accident Analysis for Nuclear Power Plants*. Rep. Vienna: IAEA, 2001. Print. Safety Report Ser. No. 23.

INTERNATIONAL ATOMIC ENERGY AGENCY. *Accident Analysis for Pressurized Water Reactors*. Rep. Vienna: IAEA, 2003. Print. Safety Report Ser. No. 29.

INTERNATIONAL ATOMIC ENERGY AGENCY. *Implementation of Accident Management Programmes in Nuclear Power Plants*. Rep. Vienna: IAEA, 2004. Print. Safety Report Ser. No. 32.

INTERNATIONAL ATOMIC ENERGY AGENCY. *Analysis of Severe Accidents in Pressurized Heavy Water Reactors*. Rep. no. IAEA-TECDOC-1594. Vienna: IAEA, 2008. Print.

INTERNATIONAL ATOMIC ENERGY AGENCY. *Approaches and Tools of Severe Accident Analysis*. Rep. Vienna: IAEA, 2008. Print. Safety Report Ser. No. 56.

INTERNATIONAL ATOMIC ENERGY AGENCY. *Best Estimate Safety Analysis for Nuclear Power Plants - Uncertainty Evaluation*. Rep. Vienna: IAEA, 2008. Print. Safety Report Ser. No. 52.

Ishii, Mamoru, and Takashi Hibiki. *Thermo-fluid Dynamics of Two-Phase Flow.* New York: Springer, 2005. Print.

Luxat, J. C., R. G. Huget, D. K. Lau, and F. Tran. *Development and Application of Ontario Power Generation's Best Estimate Nuclear Safety Analysis Methodology.* Proc. of Proceedings for International Meeting on ?Best-Estimate? Methods in Nuclear Installation Safety Analysis, Washington DC. Washington DC, 2000. Print.

Luxat, J. C. *Thermalhydraulic Aspects of Progression to Severe Accidents in CANDU Reactors.* Proc. of Proceedings for the 12th International Topical Meeting on Nuclear Reactor Thermalhydraulics (NURETH-12). Pittsburgh, Pennsylvania, 2007. Print.

Luxat, John C. "RE: 33rd Annual CNS-CNA Student Conference." Message to the author. 30 Mar. 2009. E-mail.

Massoud, Mahmoud. *Engineering Thermofluids Thermodynamics, Fluid Mechanics, and Heat Transfer.* New York: Springer, 2005. Print.

Mathew, P. M., T. Nitheanandan, and S. Bushby. *Severe Core Damage Progression within a CANDU 6 Calandria Vessel.* Proc. of ERMSAR 2008, Nesseber, Bulgaria. 2008. Print.

Mladin, Mirea, Daniel Dupleac, and Ilie Prisecaru. *Two New Models in SCDAP for Fuel Channel under Severe Accidents.* Proc. of Proc. of TOPSAFE, Dubrovnick, Croatia. 2008. A1-031.1-1-031.15. Print.

Mladin, M., D. Dupleac, and I. Prisecaru. "Modifications in SCDAP code for early phase degradation in a CANDU fuel channel." *Annals of Nuclear Energy* 36 (2009): 634-40. Print.

Mladin, M., D. Dupleac, and I. Prisecaru. "SCAP/RELAP5 application to CANDU 6 fuel channel analysis under postulated LLOCA/LOECC conditions." *Nuclear Engineering and Design* (2009): 353-64. Print.

Nguyen, T., R. Jaitly, K. Dinnie, R. Henry, D. Sinclair, D. Wilson, and M. O'Neill. "Development of severe accident management guidance (SAMG) for the Canadian CANDU 6 nuclear power plants." *Nuclear Engineering and Design* 238 (2008): 1093-099. Print.

Patankar, S. V., and D. B. Spalding. "A Calculation Procedure for Heat, Mass and Momentum Transfer in Three-Dimensional Parabolic Flows." *Int. J. Heat Mass Transfer* 15 (1972): 1787. Print.

Patankar, Suhas V. *Numerical heat transfer and fluid flow*. [S.l.]: Taylor & Francis, 1980. Print.

Peric, M., R. Kessler, and G. Scheuerer. "Comparison of Finite-Volume Numerical Methods with Staggered and Co-located Grids." *Computers & Fluids* 13.4 (1988): 389-403. Print.

Pohl, Daniel J. Raw data and input files for SCDAP/RELAP5 and MELCOR models. 28 Sept. 2009. Raw data. Prof. John C. Luxat, JHE/A315-McMaster University, Hamilton, Ontario, Canada.

Reyes, Jr., Jose N. "GOVERNING EQUATIONS IN TWO-PHASE FLUID NATURAL CIRCULATION FLOWS." IAEA. Web. 20 July 2009. <www.iaea.or.at/OurWork/ST/NE/...NC.../Annexes/Annex_06.doc>.

SCDAP/RELAP5-3D© Code Development Team. *SCDAP/RELAP5-3D© CODE MANUAL VOLUME 2: MODELING OF REACTOR CORE AND VESSEL BEHAVIOR DURING SEVERE ACCIDENTS.* Rep. no. INEEL/EXT-02-00589. Vol. 2. Idaho Falls, Idaho: Idaho National Engineering and Environmental Laboratory, 2003. Print.

SCDAP/RELAP5-3D© Code Development Team. *SCDAP/RELAP5-3D© CODE MANUAL VOLUME 3: USER?S GUIDE AND INPUT MANUAL.* Rep. no. INEEL/EXT-02-00589. Vol. 3. Idaho Falls, Idaho: Idaho National Engineering and Environmental Laboratory, 2003. Print.

SCDAP/RELAP5-3D© Code Development Team. *SCDAP/RELAP5-3D© CODE MANUAL VOLUME 4: MATPRO - A LIBRARY OF MATERIALS PROPERTIES FOR LIGHT-WATER-REACTOR ACCIDENT ANALYSIS.* Rep. no. INEEL/EXT-02-00589. Vol. 4. Idaho Falls, Idaho: Idaho National Engineering and Environmental Laboratory, 2003. Print.

SCDAP/RELAP5-3D© Code Development Team. *SCDAP/RELAP5-3D© CODE MANUAL VOLUME 5: ASSESSMENT OF MODELING OF REACTOR CORE BEHAVIOR DURING SEVERE ACCIDENTS.* Rep. no. INEEL/EXT-02-00589. Vol. 5. Idaho Falls, Idaho: Idaho National Engineering and Environmental Laboratory, 2003. Print.

SCDAP/RELAP5-3D© Code Development Team. *SCDAP/RELAP5-3D© CODE MANUALVOLUME 1: CODE ARCHITECTURE AND INTERFACE OF THERMAL HYDRAULIC AND CORE BEHAVIOR MODELS.* Rep. no. INEEL/EXT-02-00589. Vol. 1. Idaho Falls, Idaho: Idaho National Engineering and Environmental Laboratory, 2003. Print.

Shaughnessy, Edward J., Ira M. Katz, and James P. Schaffer. *Introduction to Fluid Mechanics includes CD.* New York: Oxford UP, USA, 2004. Print.

Summers, R. M., R. K. Cole, Jr., R. C. Smith, D. S. Stuart, S. L. Thompson, S. A. Hodge, C. R. Hyman, and R. L. Sanders. *MELCOR Computer Code Manuals: Primer and User's Guides.* Rep. no. NUGREG/CR-6119 (SAND93-2185). Vol. 1. Albuquerque, NM: Sandia National Laboratories, 1995. Print.

Summers, R. M., R. K. Cole, Jr., R. C. Smith, D. S. Stuart, S. L. Thompson, S. A. Hodge, C. R. Hyman, and R. L. Sanders. *MELCOR Computer Code Manuals: Reference Manuals.* Rep. no. NUGREG/CR-6119 (SAND93-2185). Vol. 2. Albuquerque, NM: Sandia National Laboratories, 1995. Print.

Van Doormaal, J. P., and G. D. Raithby. "Enhancements of the SIMPLE Method for Predicting Incompressible Fluid Flow." *Numerical Heat Transfer* 7 (1984): 147-63. Print.

Wren, J. C., J. M. Ball, and K. Liric. "An updated model for iodine behaviour in the presence of organic impurities." *Rad. Phys. Chem.* 60 (2001): 577. Print.

Zeng, M., and W. Q. Tao. "A comparison study of the convergence characteristics and robustness for four variants of SIMPLE-family at fine grids." *Engineering Computations* 20.3 (2003): 320-40. Print.

Zuber, P., and P. Saha. "Point of net vapor generation and vapor void fraction in subcooled boiling." Proc. of Proceedings of the Fifth International Heat Transfer Conference. Tokyo: Japan Society of Mechanical Engineers, 1974. 175-79. Print.

Appendix: Severe Accident Experimental Facilities

The following are brief descriptions of the main experimental facilities in Canada which are defined in the IAEA-TECDOC-1594. These facilities are used to elucidate severe accident phenomena for severe accidents in pressurized heavy water reactors (PHWRs), including CANDU nuclear reactors, and to provide data for the development and validation of computer codes to model severe accident behaviour.

A.1 RD-14M Test Loop Facility

The RD-14M test loop facility is located at AECL Whiteshell laboratories. Experiments conducted in the RD-14M facility are used to gain an improved understanding of thermalhydraulic behaviour of a PHWR during loss of coolant accidents, under forced and natural circulation conditions during shutdown scenarios. The test loop is show in Figure 77 below.

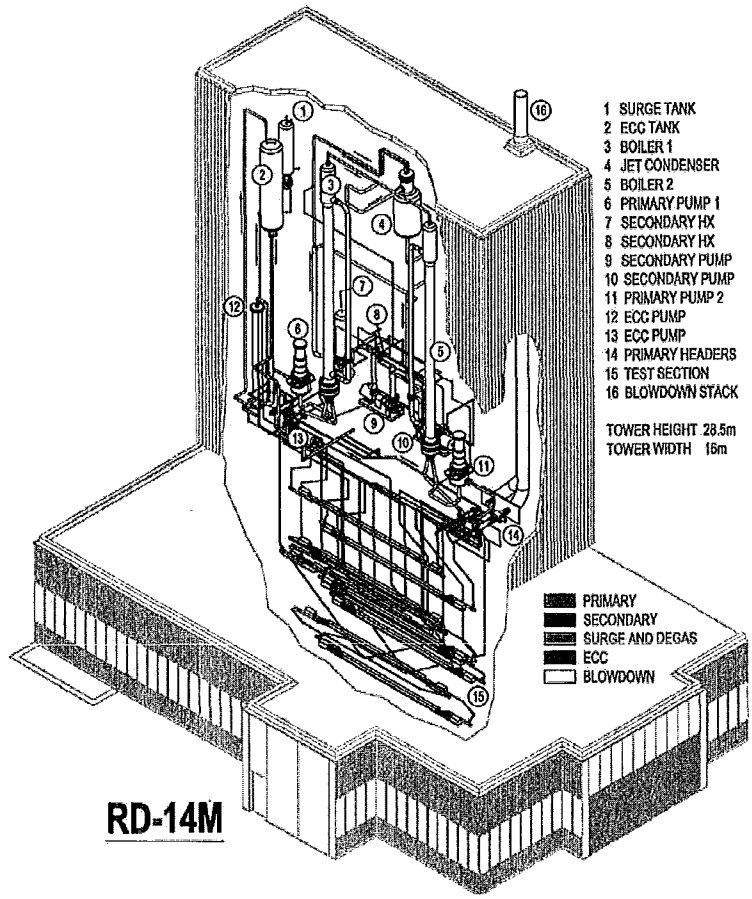

Figure 77: Schematic diagram of RD-14M test loop facility

(IAEA-TECDOC-1594, 2008)

RD-14M is an 11 MW, full-elevation scaled representation of PHWR primary heat transport system. The reactor core is simulated by ten 6 m long, horizontal channels each of which contains seven electrically heated fuel element simulators. Each of the channels has end fitting simulators that are connected to headers by full length feeder pipes. This facility also includes full height steam generators and heat transport system pumps. The components are arranged in the standard figure-of-eight geometry. The facility operates up to a pressure of 10

MPa and up to temperatures of 310 °C, which are typical system values. The data collected from this facility are used to identify and examine phenomena observed in the heat transport system and forms a database for developing and validating thermalhydraulic computer codes used to predict PHWR behaviour.

A.2 High Temperature Heat Transfer Laboratory

The high temperature heat transfer laboratory is located at AECL Chalk River Laboratories. It is used to investigate the integrated thermal-chemical-mechanical response of a CANDU fuel channel under accident conditions.

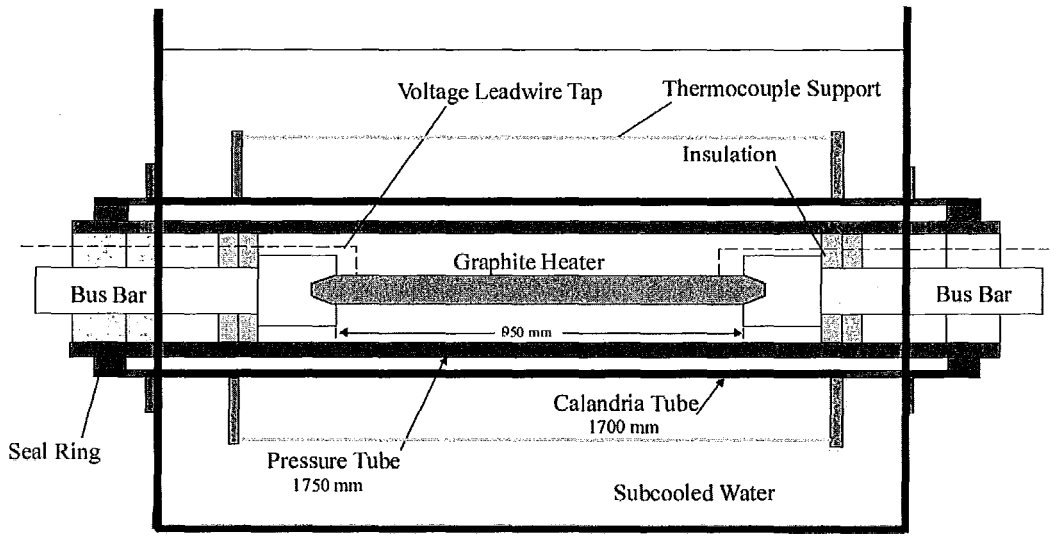

Figure 78: Schematic diagram of thermal-mechanical fuel channel apparatus

(IAEA-TECDOC-1594, 2008)

The apparatus is capable of performing high temperature (~1700 °C) and high pressure (~10 MPa) transient heat transfer experiments. This facility can handle pressure tubes that are 1.5 to 2.5 m long. This is shown in the Figure 78 above. The facility uses graphite heaters or fuel element simulators where the

fuel elements influence fuel channel behaviour. For instance, fuel element to pressure tube contact can be studied. Superheated steam can be flowed through the pressure tubes and the calandria tube which are submerged in a water tank. This simulates the moderator conditions. It is also equipped with instrumentation for pressure, mass flow and temperature measurements, deformation of the pressure tube and calandria tube, and hydrogen production. Test series have been performed to investigate heat transfer phenomena and to establish the conditions under which a pressure tube and calandria tube may fail.

A.3 Large Scale Vented Combustion Test Facility

The large scale vented combustion test facility is located at AECL Whiteshell laboratories. The facility simulates a wide range of thermodynamic conditions that are relevant to the containment atmosphere after an accident. It was originally designed to quantify effects of key thermodynamic and geometric parameters affecting pressure development during vented combustion under conditions relevant to ignition. This facility is seen in the Figure 79 below.

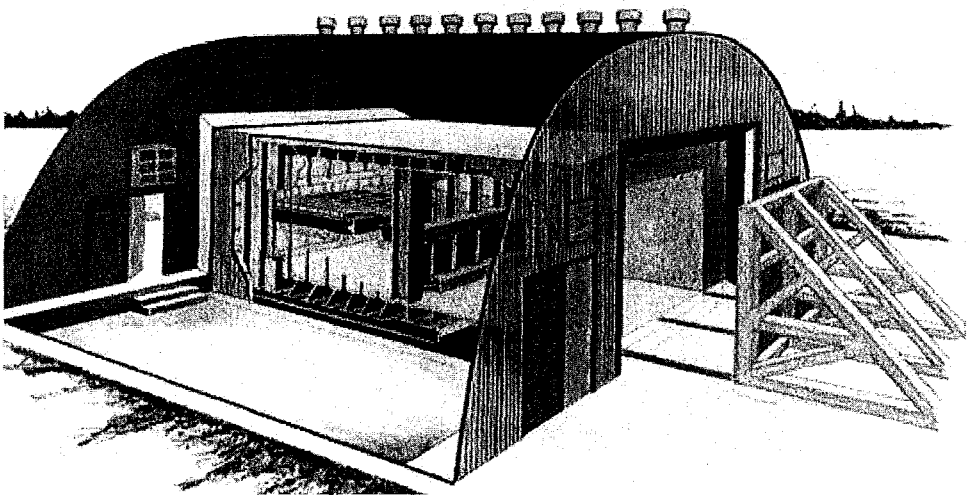

Figure 79: Schematic diagram of large scale vented combustion test facility (IAEA-TECDOC-1594, 2008)

The large scale vented combustion test facility is 10 m long, 4 m wide, and 3 m high, which accounts for a total volume of 120 m^3. It has a rectangular structural steel building designed to withstand an internal impulse pressure of 600 kPa and an internal static pressure 300 kPa. The building is insulated and electrically heated up to 120 °C. The end panels of the building are designed to provide a variable vent area from 0.4 to 7.2 m^2. Internally, the building has three separate gas addition systems for steam, hydrogen and inert gases. Hydraulic fans inside the test chamber are used to mix the gases and can be used to provide turbulent conditions during combustion. Instrumentation includes pressure transducers, thermocouples, and gas sampling by a mass spectrometer, at various locations inside the test chamber. The facility has good control of initial thermodynamic conditions, is sufficiently large to capture the effects of scale and is geometrically similar to rooms within the nuclear power plant.

A.4 Large Scale Gas-Mixing Facility

The large scale gas mixing facility as shown in Figure 80 below was located at AECL Whiteshell laboratories. It was used to study containment thermalhydraulics, in particular the behaviour of steam and air mixed with helium (i.e. to simulate hydrogen). The facility was used to study mixing, buoyancy induced flows, stratification, condensation, and effects of containment partitions and has provided data for use in validation of containment thermalhydraulic codes and predictions of hydrogen distributions.

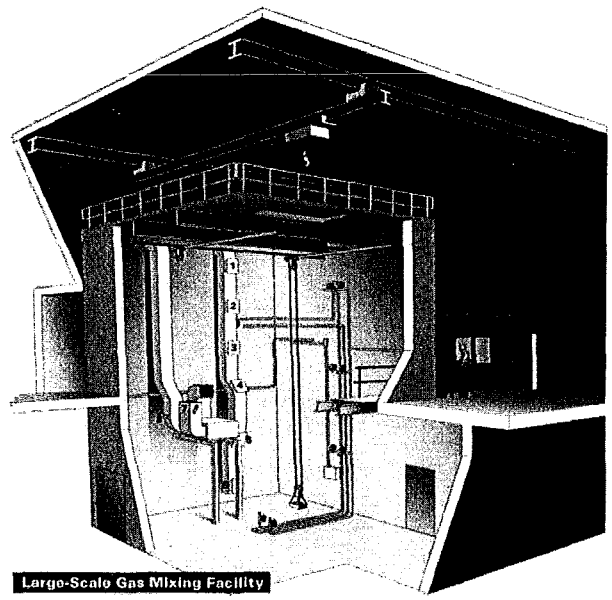

Figure 80: Schematic diagram of large scale gas mixing facility

(IAEA IAEA-TECDOC-1594, 2008)

The facility was 1000 m^3 in volume and was insulated and had injection points for steam and helium. Partitions were used to simulate subcompartments within the structure. Instrumentation included temperature measurements, condensate collection and gas phase sampling. The large scale gas mixing facility

was closed in 2001, and has been replaced by the large scale containment facility at the AECL Chalk River laboratories.

A.5 Radioiodine Test Facility

The radioiodine test facility was located at AECL Whiteshell laboratories from 1988 to 1999. The radioiodine test facility provided many potential reaction combinations (i.e. gas phase, aqueous phase and a variety of surfaces) and conditions (i.e. pH, temperature, radiation, various initial concentrations and initial speciation of iodine) to simulate the containment building following an accident. The schematic diagram of the radioiodine test facility is shown in Figure 81 below.

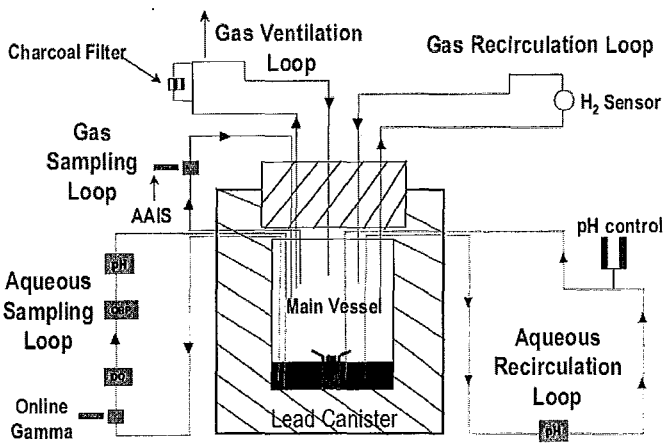

Figure 81: Schematic flow diagram of radioiodine test facility

(IAEA-TECDOC-1594, 2008)

A.6 Molten Fuel Moderator Interaction Facility

The molten fuel moderator interaction facility is located at AECL Chalk River laboratories. The purpose of this facility is to investigate the high pressure

ejection of corium melt into the moderator. The facility is shown in Figure 82 below.

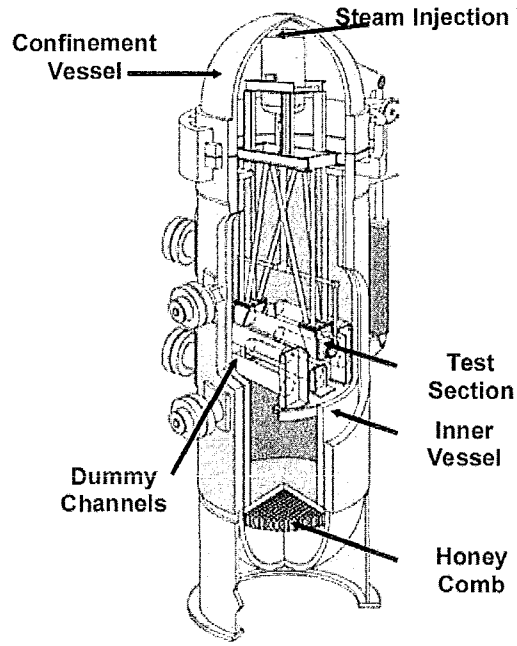

Figure 82: Schematic diagram of molten fuel moderator interaction facility (IAEA-TECDOC-1594, 2008)

The experiments involve of heating up a mixture of UO_2, Zr, and ZrO_2. This mixture is the molten material expected in a fuel channel, inside a short length of pressure tube during a severe accident. Once the molten material has reached the desired temperature (~2400 °C), the pressure inside the tube is set to 10 MPa. The pressure tube then fails at a pre-machined flaw and releases the molten material into the surrounding tank of water. The experiments that are planned will cover two different amounts of molten material, and will investigate

the effects of the material interacting with tubes representing neighbouring fuel channels.

A.7 Blowdown Test Facility

The blowdown test facility is part of the NRU reactor located at the AECL Chalk River laboratories. Four blowdown test facility experiments were performed inside the NRU reactor to improve the understanding of PHWR fuel and fission product behaviour under accident conditions and to provide data for use in reactor safety code validation. The facility is seen in Figure 83 below.

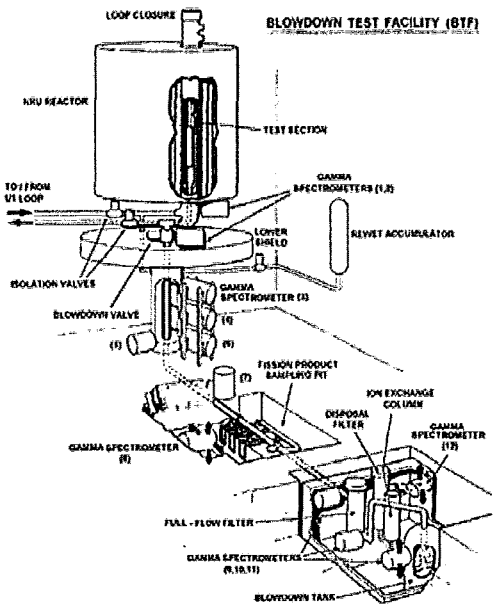

Figure 83: Schematic diagram of blowdown test facility in the NRU reactor

(IAEA-TECDOC-1594, 2008)

A.8 Core Disassembly Facility

The core disassembly facility is located at AECL Chalk River laboratories and is used to investigate the core disassembly process. The progression of a severe core damage accident in a PHWR is characterized by moderator boil off

and sequential failure of fuel channels as they become uncovered. It is based on a facility with 1/5 scale fuel channels, heated by individual tungsten heaters to simulate fuel bundles. An array of 4 channels can be subjected to a transient to investigate the formation of suspended debris through the interaction of failed channels with lower intact channels. Figure 84 shows the results of a typical test.

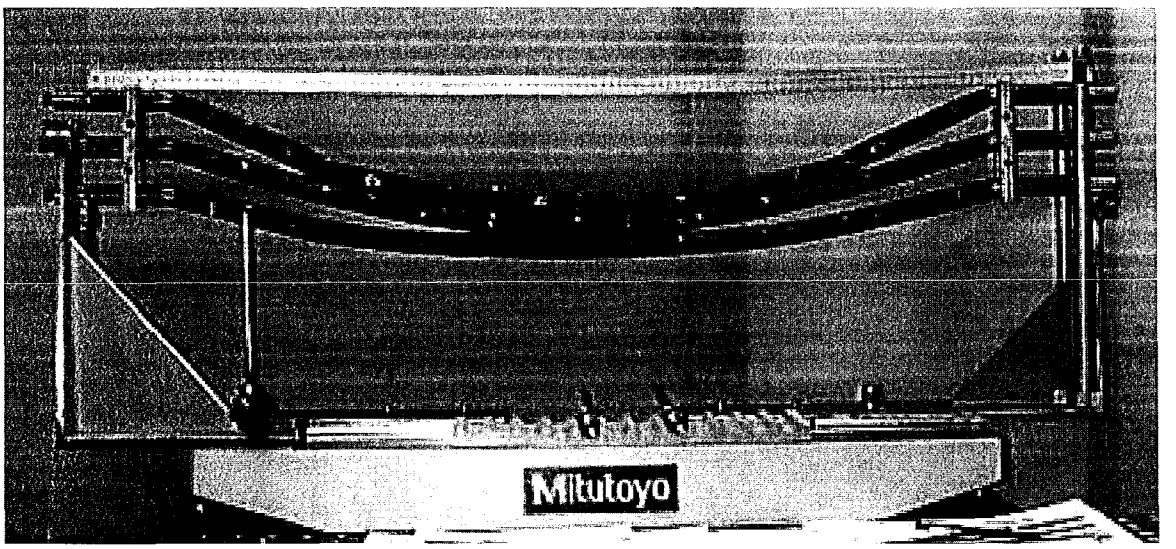

Figure 84: Post-test view of core-disassembly test (IAEA-TECDOC-1594, 2008)